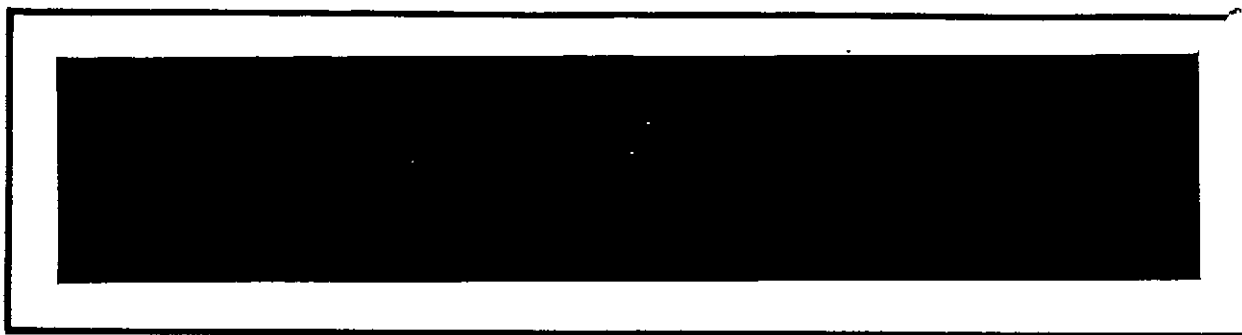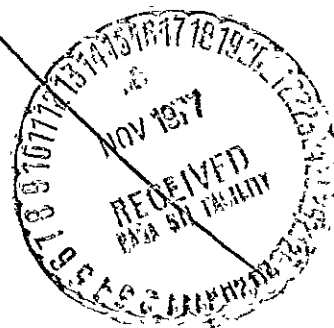NASA CR·
151539

▰ Axiomatix

Marina del Rey ● California

INVESTIGATION AND EVALUATION OF SHUTTLE/GPS

NAVIGATION SYSTEM

FINAL REPORT

Contract No. NAS 9-15387

Prepared for

NASA Lyndon B. Johnson Space Center
Houston, Texas 77058

Prepared by

Peter W. Nilsen

Axiomatix
13900 Panay Way, Suite 110M
Marina del Rey, California 90291

Axiomatix Report No. R7710-3
October 15, 1977

TABLE OF CONTENTS

Attachment

SHUTTLE GPS RECEIVER DEFINITION AND PERFORMANCE STUDY
(LinCom Corporation under Subcontract AX770801GH)

LIST OF TABLES

LIST OF FIGURES

1.0   INTRODUCTION

In late 1976, NASA Management decided that the NAVSTAR Global
Positioning System (GPS) being developed by the DOD should be investi-
gated as a potential Shuttle navigation system. The GPS navigation
system has the potential for increasing the Shuttle navigation accuracy
while at the same time consolidating several separate navigation systems
functions into one system. This has the potential for a net decrease
in Shuttle avionics weight and power consumption. Furthermore, it is
possible that a Shuttle GPS navigation system could result in a large
decrease in ground data processing, i.e., a net cost savings.

In light of the Shuttle's fast-paced development schedule, Shuttle
Management decided that a panel of NASA, DOD, and industry experts
should be formed to quickly determine the feasibility of incorporating
GPS onboard the Shuttle. This panel was to be charged with the respon-
sibility of answering the key questions of "What system?" "How well will
it perform?" "How much will it cost?" and "How soon can it operate on
the Shuttle?" Axiomatix was chosen as a panel member because of its
deep involvement in Shuttle communications and tracking and its expertise
in GPS systems analysis. Thus, the task of Shuttle/GPS systems analysis
was assigned to Axiomatix. This task was performed in close conjunction
and with the support of the other panel members. These members are NASA
JSC and NASA Goddard, the GPS Joint Program Office (SAMSO), Rockwell
International, LinCom (under subcontract to Axiomatix), Magnavox, TASC,
and Intermetrics.

The results of the Axiomatix study effort for the first phase
of this investigation are complete and documented herein. This study
is to continue in FY'78 and, at the end of this period, a detailed
system design and performance analysis will be completed.

2.0 SUMMARY

The system performance analysis for two Shuttle/GPS navigation system configurations has been completed. These configurations are preliminary configurations and will not represent the final operational configuration. The analysis of these configurations has been an iterative procedure. The close cooperation between Axiomatix and the other panel members has been highly instrumental in developing a system configuration having good system performance.

The first system considered was designed strictly as an early OFT experimental system. However, this system was rejected in favor of a more sophisticated system having much greater performance capability. The bulk of the results presented in this report pertain to the latter system, sometimes referred to as the "baseline" system.

The most significant result of the performance analysis is that the GPS system can provide on-orbit navigation accuracy an order of magnitude better than the baseline system, with very adequate link margins. The worst-case link margin is 4.3 dB. This link margin accounts for Shuttle RF circuit losses which were carefully minimized by Rockwell under the constraints of program schedule and environmental limitations. Also implicit in the link analyses are the location trade-offs for preamplifiers and antennas.

A preliminary analysis of the potential TACAN interference to the Shuttle GPS performance was performed due to the magnitude of the TACAN pulse (60 dBm) and the frequency proximity to the L2 GPS signal. The preliminary analysis indicates that the interference is highly dependent on the TACAN pulse shape and transmitter filtering. For a Gaussian shaped pulse, there is no interference. For a square pulse, there is a serious problem. Since the TACAN pulse is more of a Gaussian pulse than a square pulse, it would seem the problem is not as serious as the preliminary analysis for a square pulse indicates. Certain detailed analyses were performed by LinCom under subcontract to Axiomatix and are documented in their report, which is included as part of this report.

3.0   SHUTTLE NAVIGATION REQUIREMENTS

The baseline Shuttle navigation systems will provide the required navigation accuracy for the Shuttle to leave earth, orbit, and return safely. However, in the area of mission support, the substantially increased accuracy of a Shuttle/GPS navigation system will provide more flexible mission capability and a great cost savings due to the substantial reduction in ground processing costs for reduction of payload data. Furthermore, the GPS system will allow the Shuttle to meet current DOD requirements for accuracy, security, and autonomy. The Shuttle navigation requirements, as reflected by NASA experiment accuracy requirements, are tabulated in Table 3-1. The Shuttle navigation requirements as reflected by Air Force requirements are tabulated in Table 3-2. A plot of the position and velocity errors expected from TDRSS, as shown in Figures 3-1 and 3-2, illustrates that these requirements may not be met. On the other hand, a plot of the position and velocity errors predicted for Shuttle navigation with Phase I GPS (limited satellite constellation deployment), as shown in Figures 3-3 and 3-4, illustrates that the Shuttle/GPS navigation system will quite adequately satisfy the NASA and Air Force requirements.

Representative on-orbit maximum signal dynamics for the Shuttle/ GPS link are given in Table 3-3.

Table 3-1. NASA Experiment Shuttle Navigation Requirements

o Laser Ground Tracking (1983)

   o   10M required for reasonable amount of ground processing
   o   30M is upper limit to avoid extensive ground processing
   o   Current expectations of 100M result in extensive and
       very costly ground processing

o LANDSAT and Earth Resources

   o   3M required for reasonable amount of ground processing
   o   10M is upper limit to avoid extensive ground processing
   o   Current expectation of 150M results in extensive and
       very costly ground processing

o EVAL (Gimbaled from Shuttle)

   o   Requires 10-15M

NOTE: Ground processing increases as the square of the
       navigation error

Table 3-2. Air Force Shuttle Mission Navigation Requirements

o Navigation Accuracies (40 min after insertion)

Satellite Deployment (3σ)

	Position (nm)			Velocity (ft/sec)		
	Tang.	Nor.	Rad.	Tang.	Nor.	Rad.
Baseline	±20	±10	±2	±20	±100	±90
Growth	± 1	± 1	±1	± 4	± 4	± 3

o On-Orbit Navigation (3)

Growth	±0.3	±0.3	±0.3	±1.0	±1.0	±1.0

Table 3-3. Representative Maximum On-Orbit Signal Dynamics
for Shuttle/GPS Link

Range Rate (ft/sec)	2.9×10^4
Range Acceleration (ft/sec^2)	5.0×10^2
Range Jerk (ft/sec^3)	6.5×10^{-2}
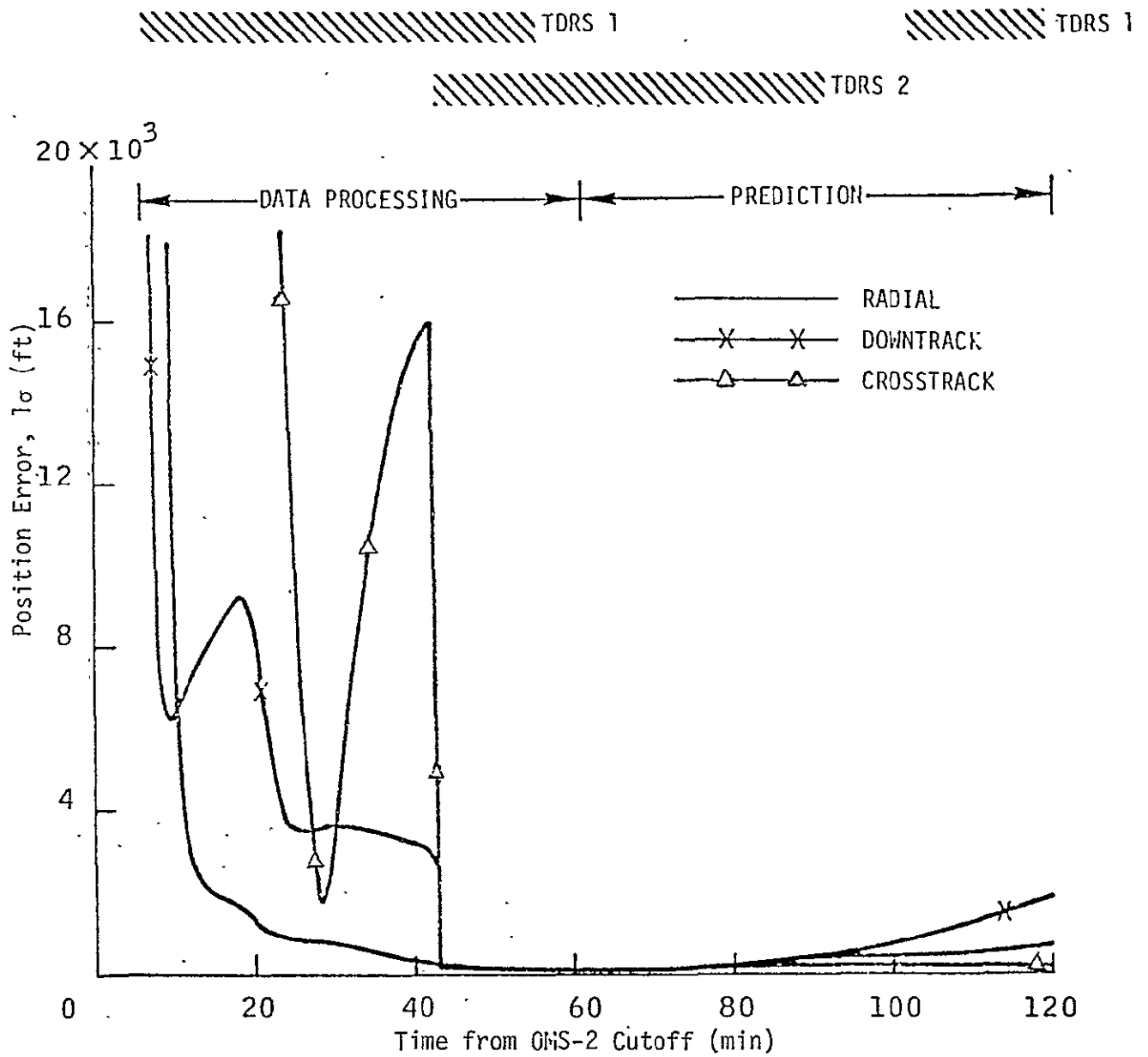
Figure 3-1. Navigation Position Accuracy with TDRS
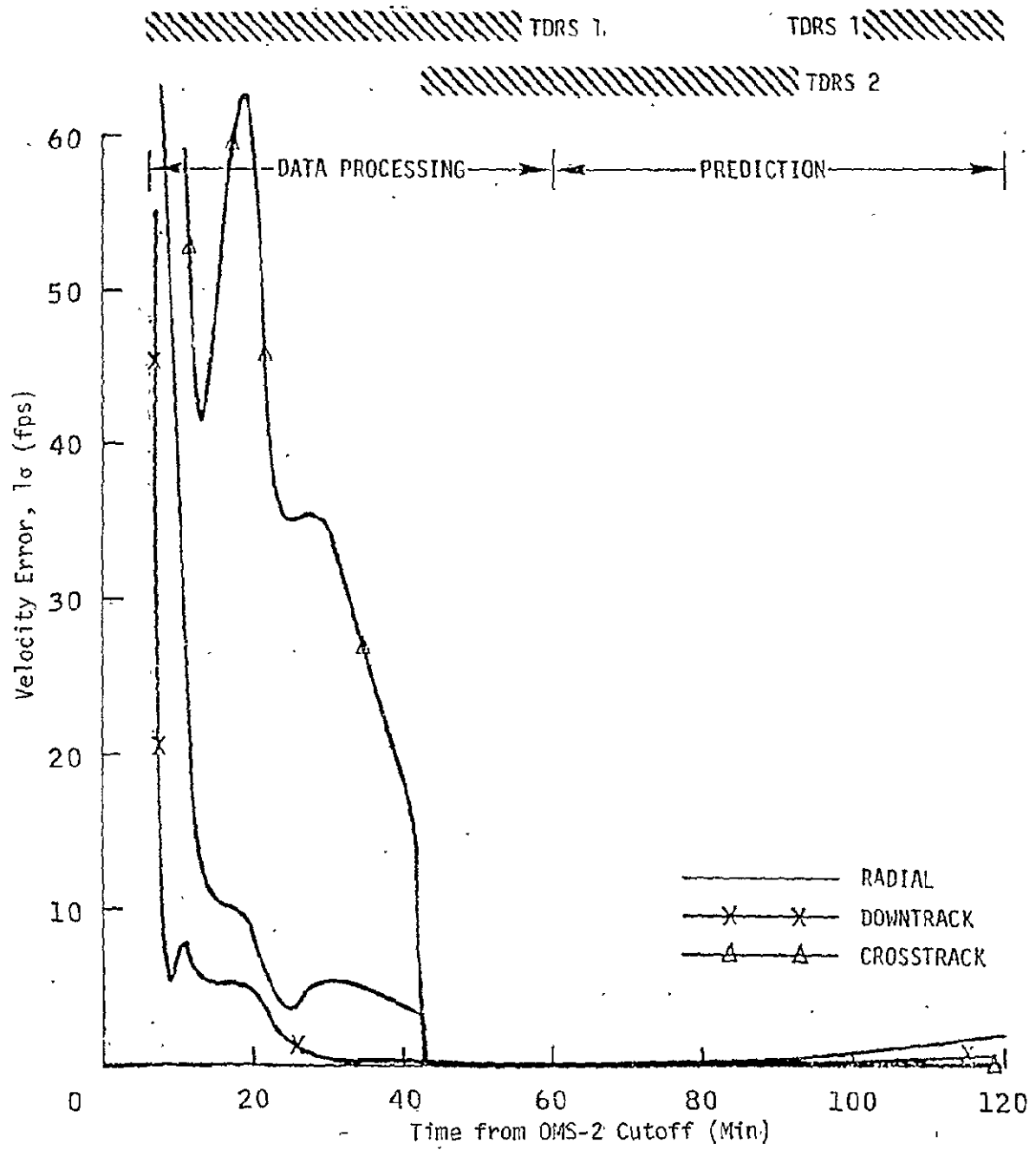
Figure 3-2.   Navigation Velocity Accuracy with TDRS
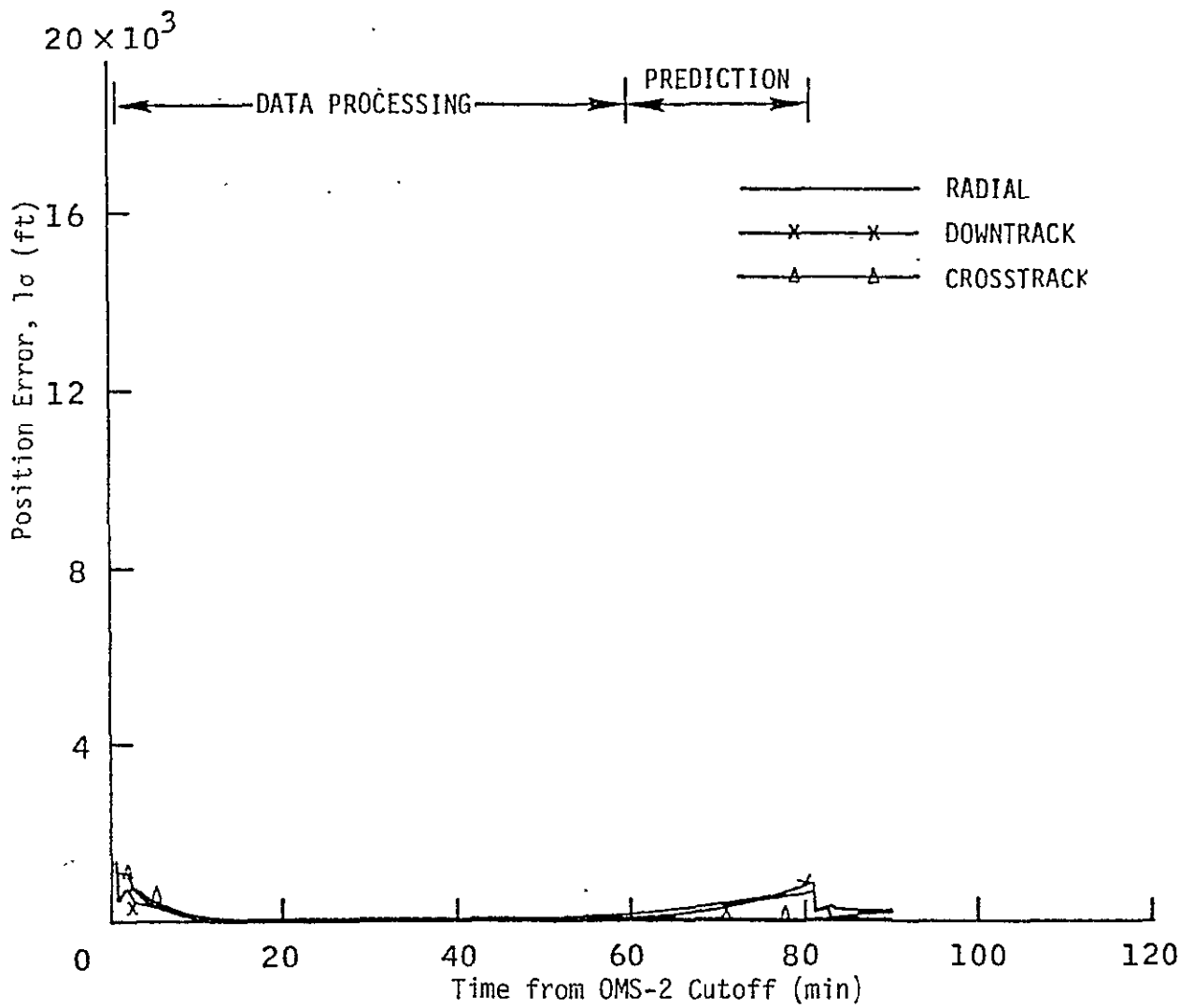
Figure 3-3. Phase I GPS Orbital Navigation RMS Position Errors
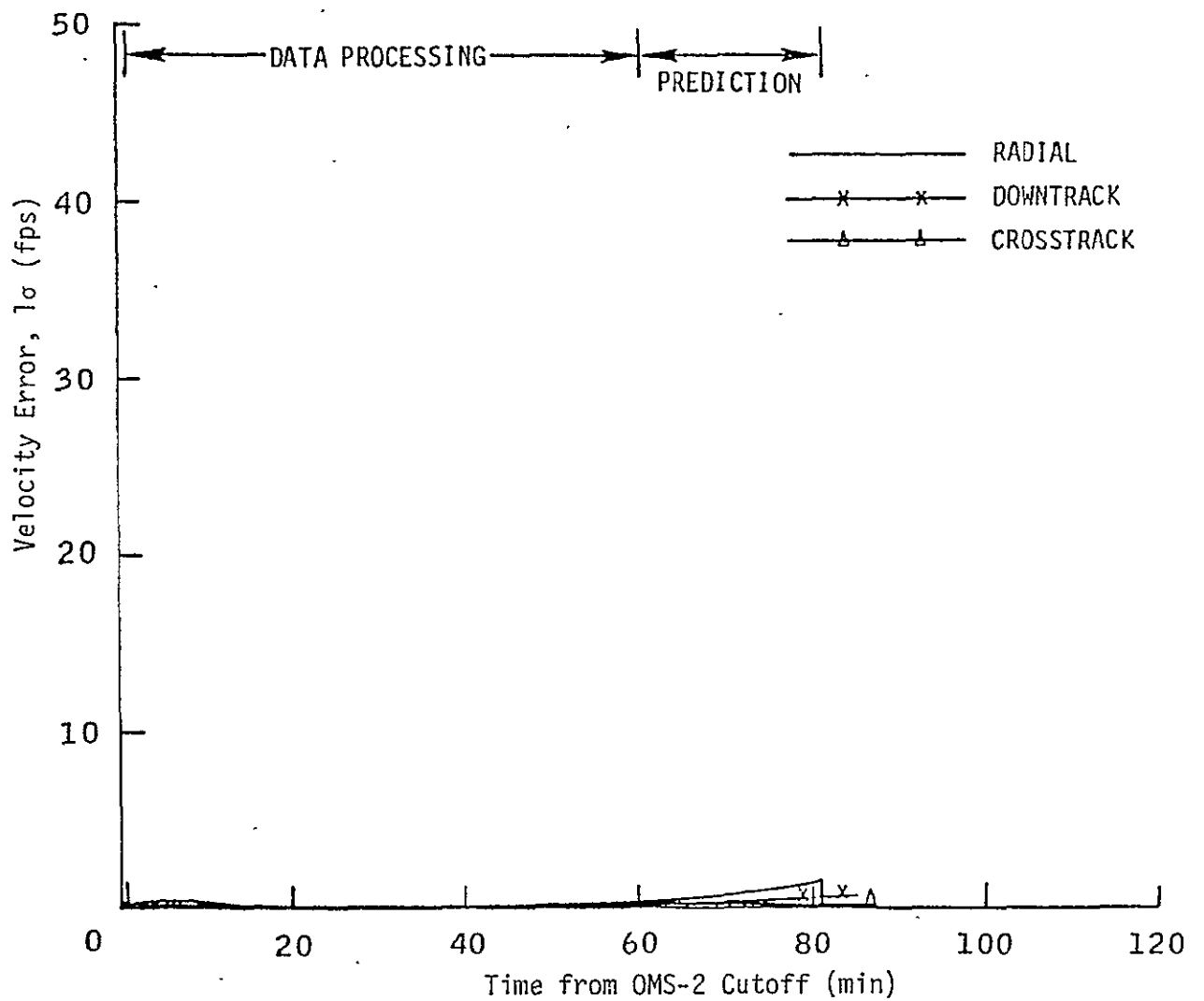
Figure 3-4.   Phase I - GPS Orbital Navigation RMS Velocity Errors

4.0 GPS NAVIGATION PRINCIPLES

The GPS system is being developed by the DOD to provide a high-precision position and velocity determination capability to a variety of users located anywhere in the world. Table 4-1 indicates the navigation accuracy that is predicted for the fully operational system in 1984 and Figure 4-1 shows the GPS development schedule with the Shuttle program milestones also indicated. A general systems block diagram for the overall GPS system, indicating the interaction between all elements, is shown in Figure 4-2.

Table 4-1. GPS System Accuracy

	Accuracy	
Usage	Horizontal	Vertical
50% of Time	5 m	7 m
90% of Time	8 m	10 m

The GPS system is a passive system, meaning that a user only receives the continuously transmitted satellite signals. Since only the satellites transmit signals, an unlimited number of users can use the system at any time. Another advantage of the system is that all users will develop their navigation information in a common GPS coordinate system. The following sections explain the principles of position fixing with the GPS and the principles of operation of the GPS receivers.

4.1 Position Fixing Principles

The principles by which the GPS system derives navigation fixes are best understood by considering a two-dimensional position-determining scenario, such as depicted in Figure 4-3 and expanding the example to the GPS case. The user, which we shall assume has a means for accurately determining time, measures his range to the two transmitters. These ranges are related to the user's position by

$$R_1 = [(X_u - X_1)^2 + (Y_u - Y_1)^2]^{1/2} \tag{4-1}$$

$$R_2 = [(X_u - X_2)^2 + (Y_u - Y_2)^2]^{1/2}, \tag{4-2}$$
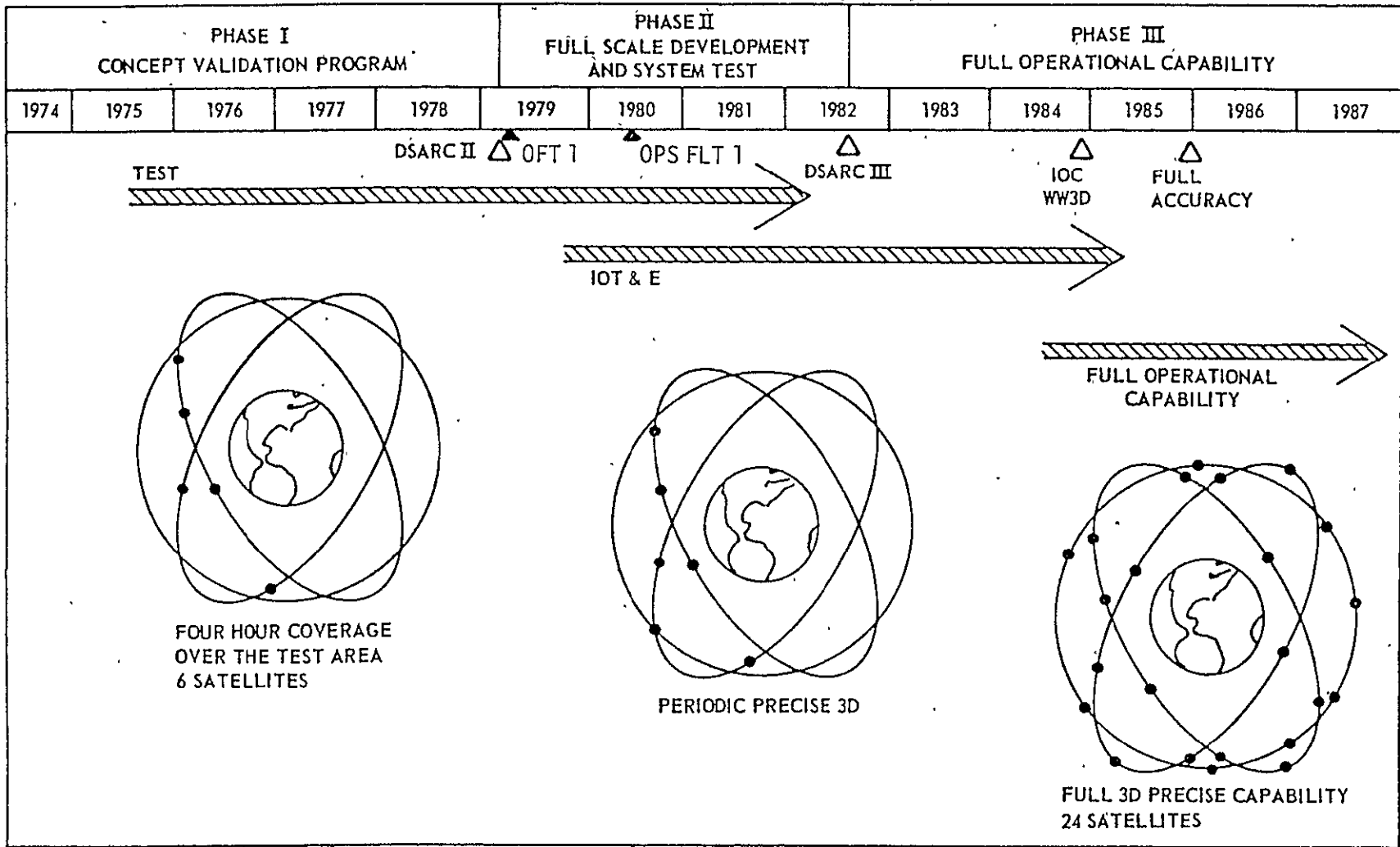
Figure 4-1. NAVSTAR Global Positioning System Schedule
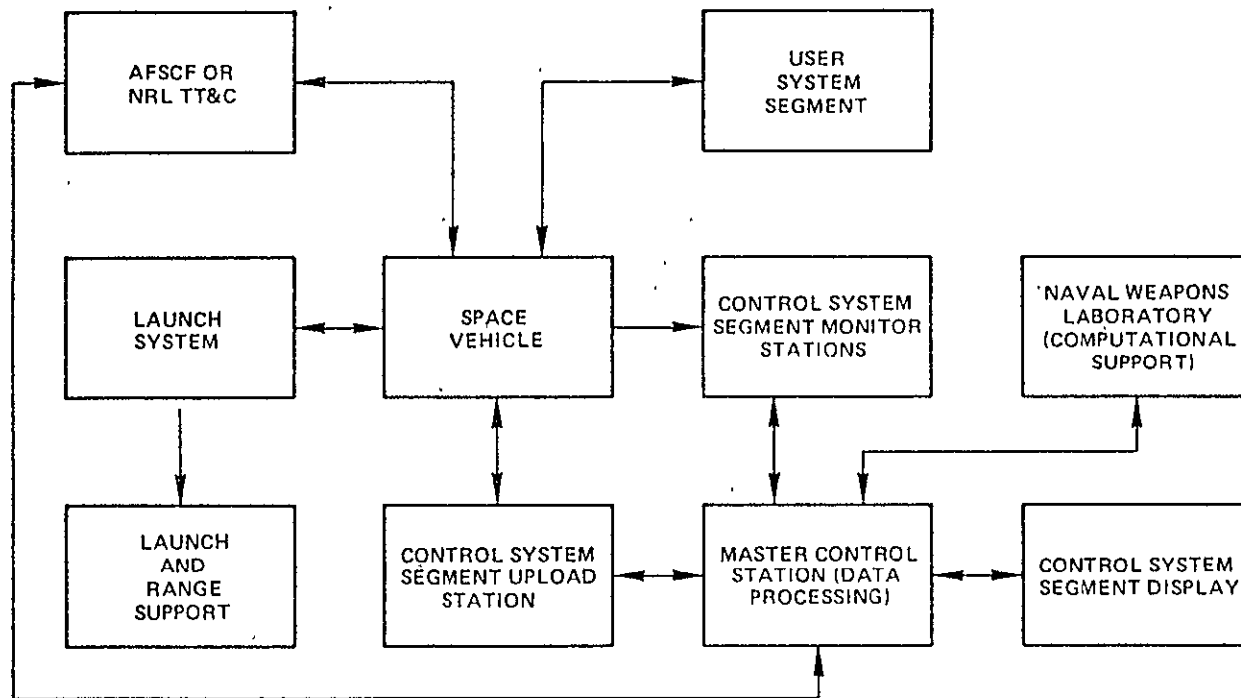
Figure 4-2. GPS System Overall Block Diagram
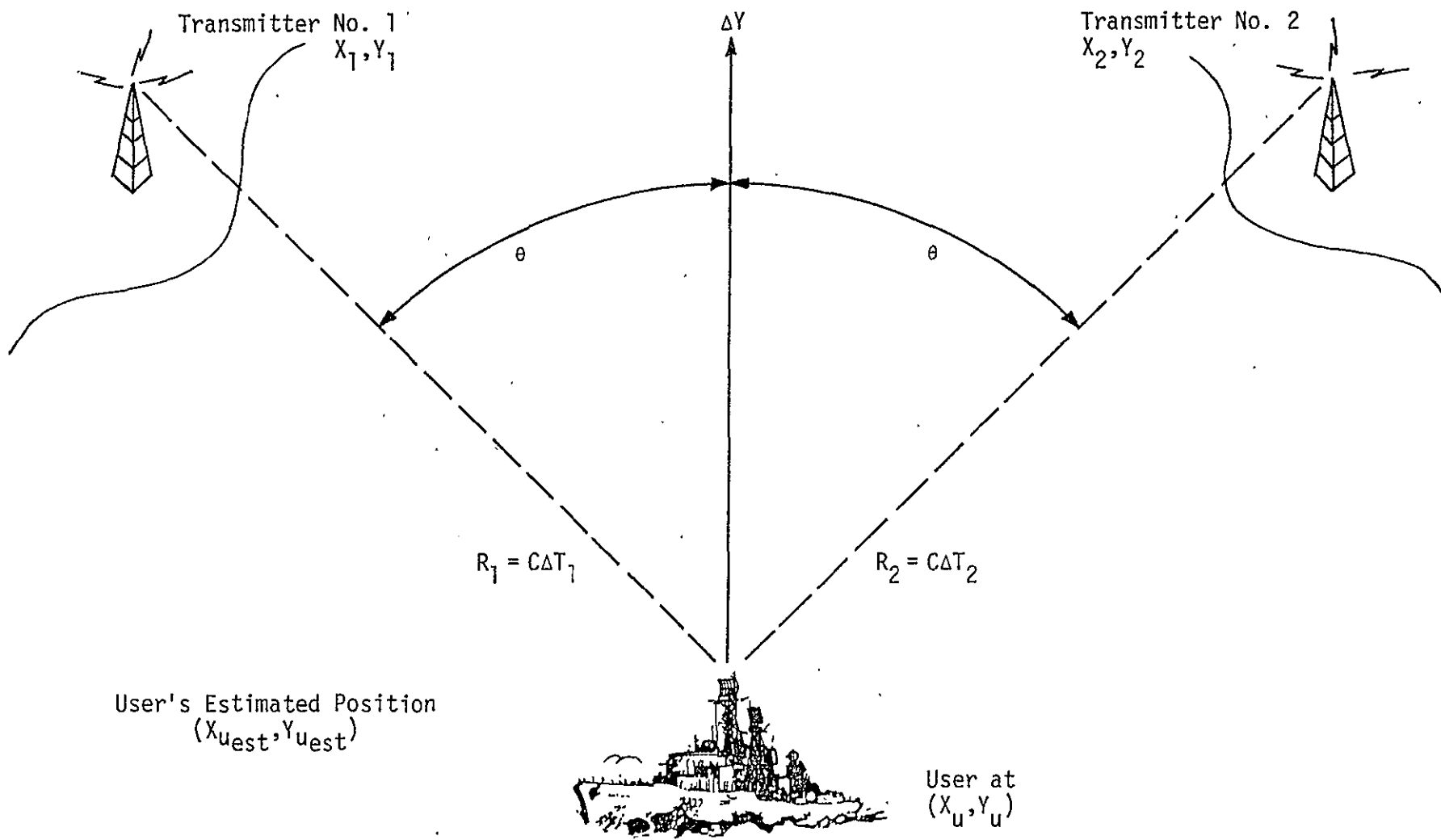
Figure 4-3. Example of Two-Dimensional Position Determination Scenario

Transmitter No. 1
X_1, Y_1

ΔY

Transmitter No. 2
X_2, Y_2

θ

θ

$R_1 = C\Delta T_1$

$R_2 = C\Delta T_2$

User's Estimated Position
$(X_{u_{est}}, Y_{u_{est}})$

User at
(X_u, Y_u)

where

X_u = user's X coordinate

Y_u = user's Y coordinate

X_1 = transmitter No. 1 X coordinate, precisely known

X_2 = transmitter No. 2 X coordinate, precisely known

Y_1 = transmitter No. 1 Y coordinate, precisely known

Y_2 = transmitter No. 2 Y coordinate, precisely known .

The range expressions are expanded in a Taylor series expansion to get

$$\Delta R_1 = C\Delta T_1 - [(X_{u_{est}} - X_1)^2 + (Y_{u_{est}} - Y_1)^2]^{1/2}$$

$$= \frac{\partial R_1}{\partial X_u} \Delta X + \frac{\partial R_1}{\partial Y_u} \Delta Y + u_1 \qquad (4\text{-}3)$$

where

$X_{u_{est}}$ = user's estimated X coordinate

$Y_{u_{est}}$ = user's estimated Y coordinate .

In terms of the angle θ of Figure 4-3, this can be written as

$$\Delta R_1 = \sin \theta \Delta X + \cos \theta \Delta Y + u_1 \qquad (4\text{-}4)$$

$$\Delta R_2 = \sin \theta \Delta X + \cos \theta \Delta Y + u_2, \qquad (4\text{-}5)$$

where we define

$$Q = u_1^2 + u_2^2 \qquad (4\text{-}6)$$

and we wish to minimize Q by setting

$$\frac{\partial Q}{\partial \Delta X} = 0$$

$$\frac{\partial Q}{\partial \Delta Y} = 0 \qquad (4\text{-}7)$$

and solve for ΔX and ΔY. Thus, we obtain

$$\Delta X_{Best} = \frac{1}{2 \sin \theta} (\Delta R_1 - \Delta R_2) \qquad (4\text{-}8)$$

$$\Delta Y_{Best} = \frac{1}{2 \cos \theta} (\Delta R_1 + \Delta R_2) . \qquad (4\text{-}9)$$

The determination of the user's position is obviously an iterative pro-
cedure which starts with an initial estimate and uses the iterative
operations

$$X_{u_{new}} = X_{u_{old}} + X_{Best} \tag{4-10}$$

$$Y_{u_{new}} = Y_{u_{old}} + Y_{Best} \tag{4-11}$$

to converge on a precise estimate of position. This is illustrated by
the example in Figure 4-4. The expansion of this simple illustrative
example to the GPS three-dimensional case is obtained merely by writing
the range equation for the range between the user's unknown X_u, Y_u, and
Z_u position and four GPS satellites; thus,

$$(X_1 - X_u)^2 + (Y_1 - Y_u)^2 + (Z_1 - Z_u)^2 = (r_1 - b)^2 \tag{4-12}$$

$$(X_2 - X_u)^2 + (Y_2 - Y_u)^2 + (Z_2 - Z_u)^2 = (r_2 - b)^2 \tag{4-13}$$

$$(X_3 - Y_u)^2 + (Y_3 - Y_u)^2 + (Z_3 - Z_u)^2 = (r_3 - b)^2 \tag{4-14}$$

$$(X_4 - Y_u)^2 + (Y_4 - Y_u)^2 + (Z_4 - Z_u)^2 = (r_4 - b)^2, \tag{4-15}$$

where b is the range error due to the user's time uncertainty. In the
case of the two-dimensional example, we had two unknowns and two equa-
tions. However, with the GPS case, there are four unknowns—X_u, Y_u,
Z_u, and b. Thus, four equations are used, which necessitates the four
measurements to four satellites. It should be noted that, if the user
knows his altitude, say, through use of another sensor, then only three
equations and three satellites are required. The details of the solu-
tion of the four equations can be done in a number of ways but, in general,
it is an iterative procedure similar to the two-dimensional example.
A block diagram of a typical receiver solution process is given in
Figure 4-5.

4.2   PN Receiver Principles

The GPS signal transmitted from the satellite is a pseudo-noise
(PN) modulated carrier at 1227 MHz (L2) and 1575 MHz (L1). The PN
modulation consists of a 10.23 megachips per second code (P code) and
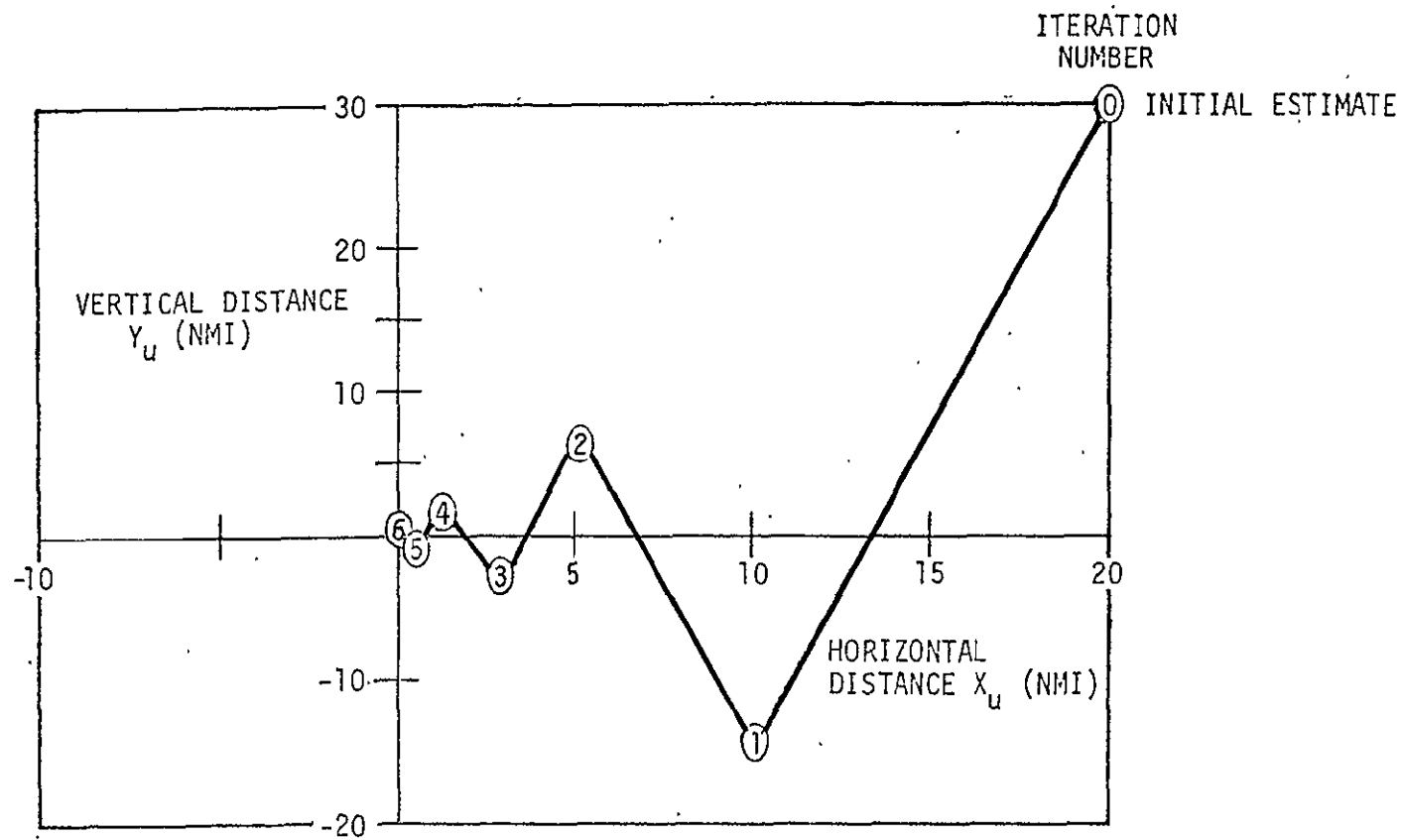
Figure 4-4. Example of Iterative Nature of Two-Dimension Position Solution
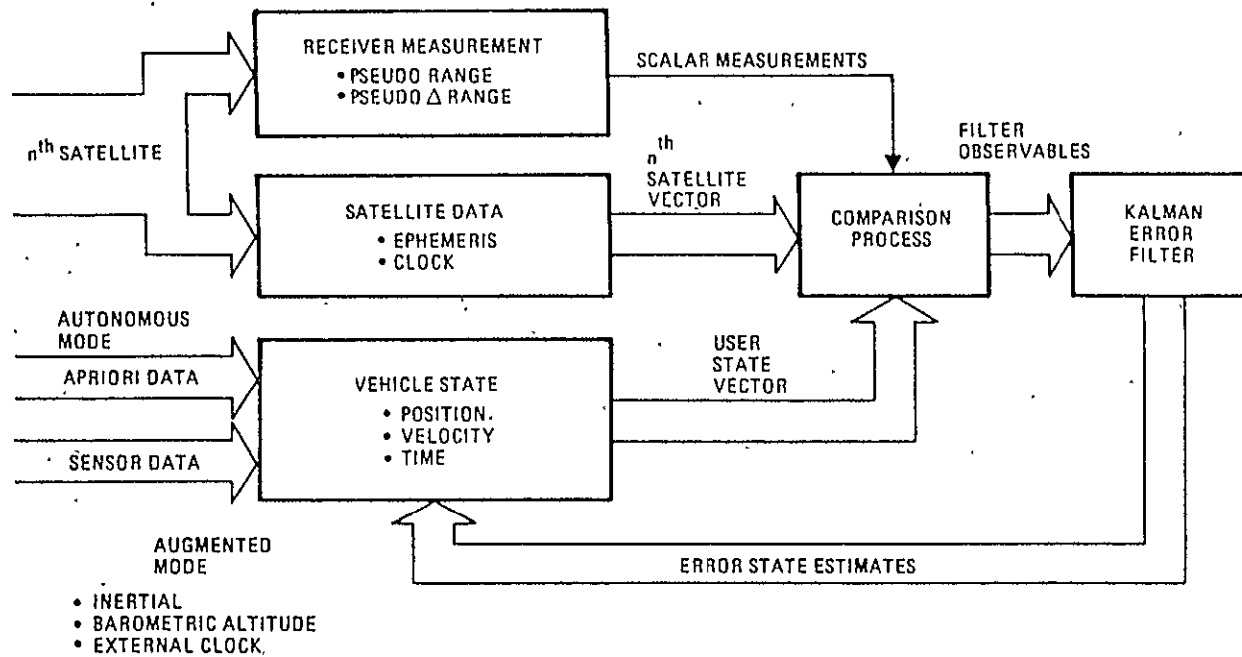
Figure 4-5. Flow Diagram for GPS Solution of Position and Velocity

a 1.023 megachips per second C/A code. Both codes are bi-phase modulated by the 50 bps NRZ satellite data. The modulation index of both codes is chosen so that they share the total signal power with the C/A code signal having three dB more power than the P code signal. An elementary block diagram of a basic PN transmitter is shown in Figure 4-6 and a block diagram of an elementary PN receiver is shown in Figure 4-7.

The spectrum of the transmitted GPS signal is shown in Figure 4-8. The predominant feature of this spectrum is its wide bandwidth, i.e., the P signal occupies a 20 MHz bandwidth between its first nulls and the C/A signal occupies a 2 MHz bandwidth between its first nulls. When the Fourier transform of the spectrum is taken, the autocorrelation function for the PN code is obtained, as shown in Figure 4-9. The most significant feature of this autocorrelation function is that, when the reference code is separated by ±1 chips from the received code, i.e., when the code tracking function in Figure 4-7 is not in perfect synchronization, the output of the correlator is reduced by 1/N, where N is the number of bits in the code. The number of bits in the code is determined by the number of stages in the code generator, as shown in Figure 4-10, the block diagram for a maximal linear PN code generator For an n-stage PN generator, the number of bits is given by $N = 2^n-1$.

Modulation of data on the GPS signal is accomplished by bi-phase modulating the PN sequence with the binary data stream. This is accomplished by simply exclusive or-ing the binary data with the binary PN sequence, as depicted in Figure 4-11. The output of the exclusive "or" then modulates the carrier by means of a balanced modulator.

Several of the functions shown in the elementary PN receiver block diagram of Figure 4-7 merit further elaboration, since they are the key to the PN receiver performance. The first of these is the PN tracking function. The function of the PN tracking loop is to keep the receiver local PN generator in synchronization with the received PN code so that the maximum correlator output is obtained. Furthermore, the primary function of the GPS receiver is to measure range by estimating the phase of the received PN code. This is done by the PN code tracking function so that an improvement in the PN tracking accuracy is a direct improvement in the range measurement performance.

A straightforward and prevalent approach to tracking the phase of the incoming code is the so-called delay lock tracking loop. A
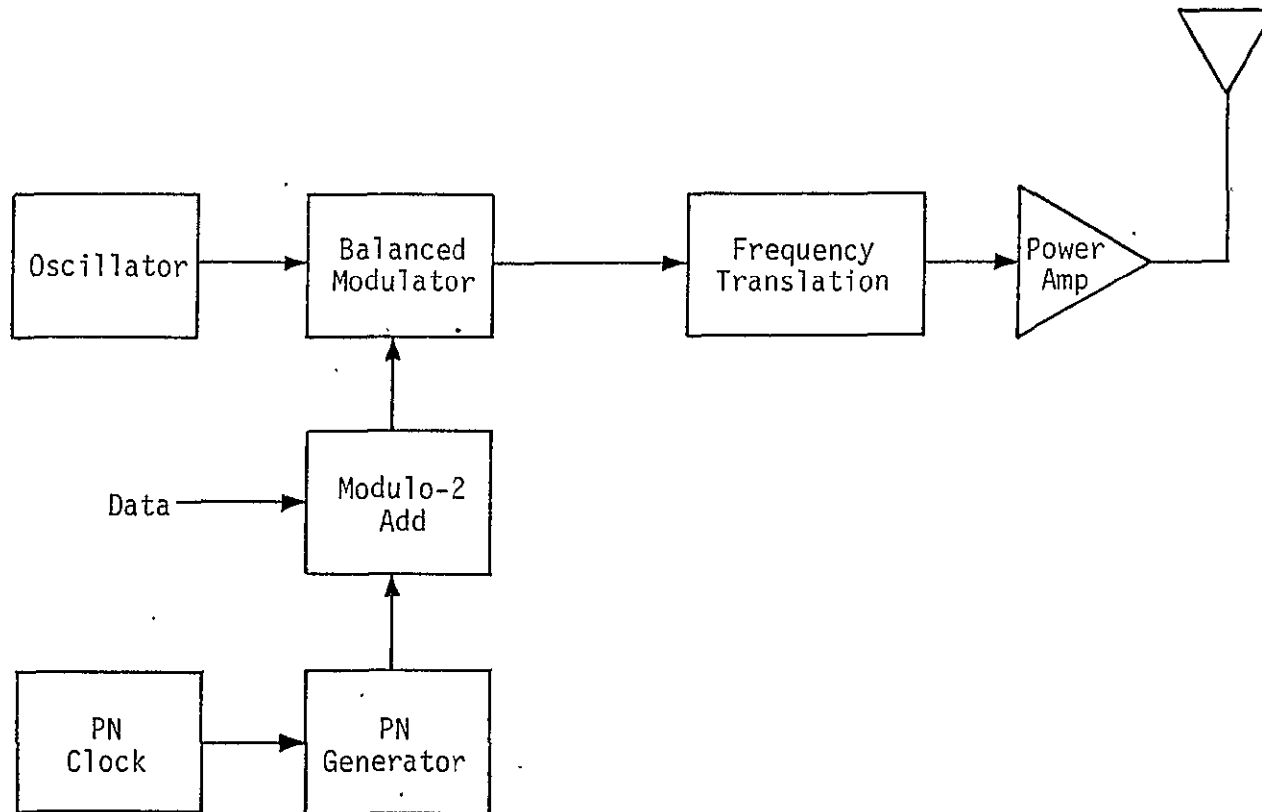
Figure 4-6.   Elementary PN Transmitter Block Diagram
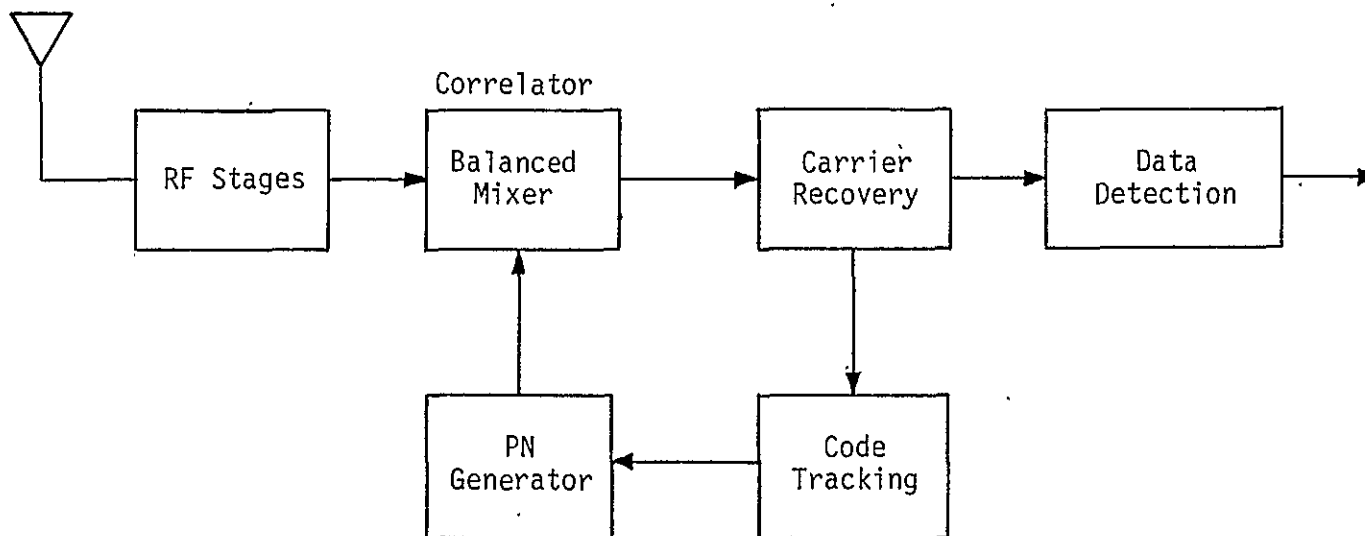
Figure 4-7. Elementary PN Receiver Block Diagram
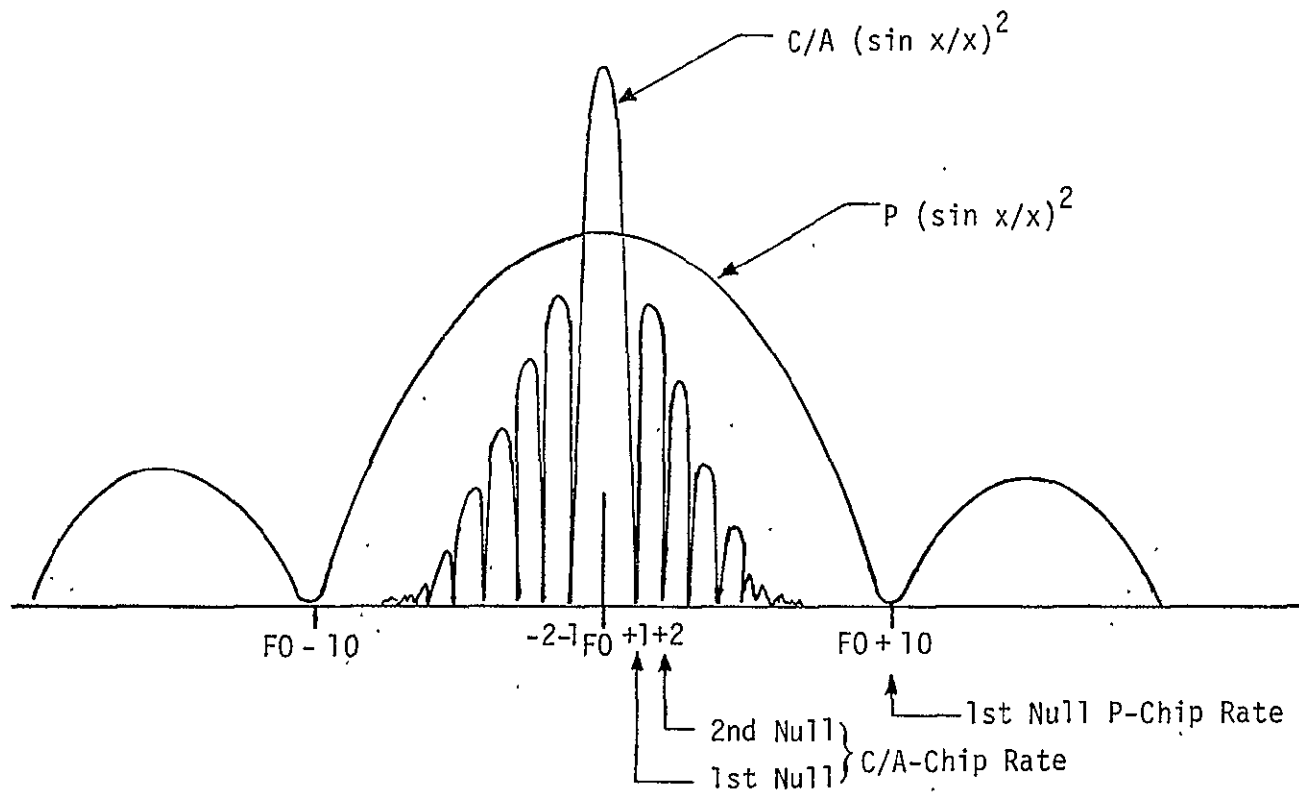
Figure 4-8. GPS Signal Spectrum
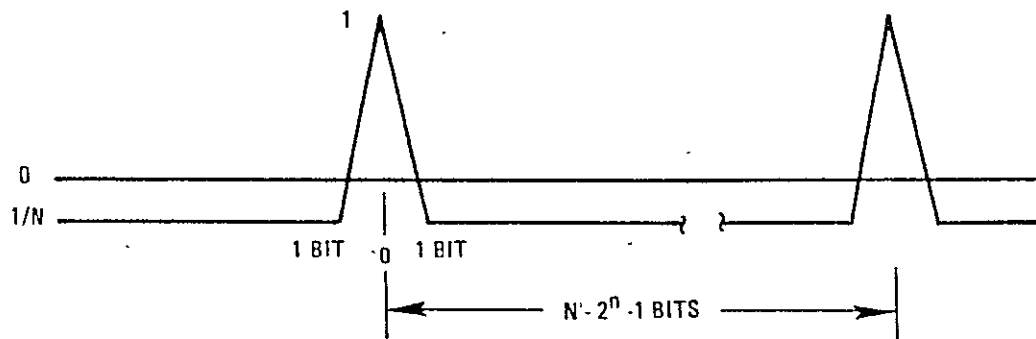
Figure 4-9. Normalized Autocorrelation Function
of Maximal Linear PN Code
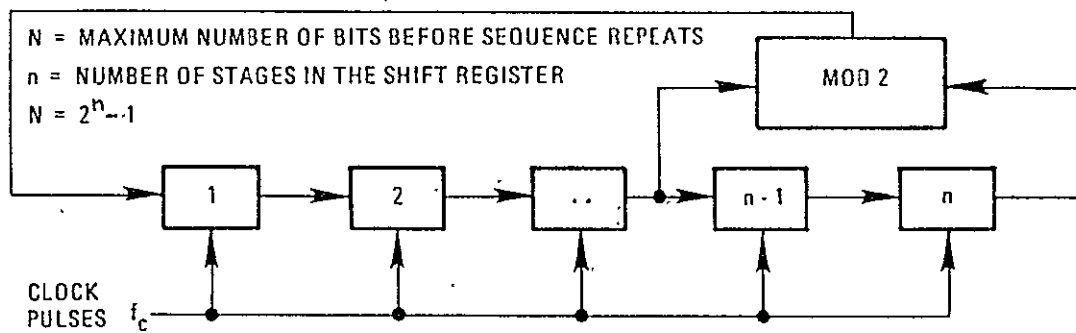
Figure 4-10. Maximal Linear PN Code Generator
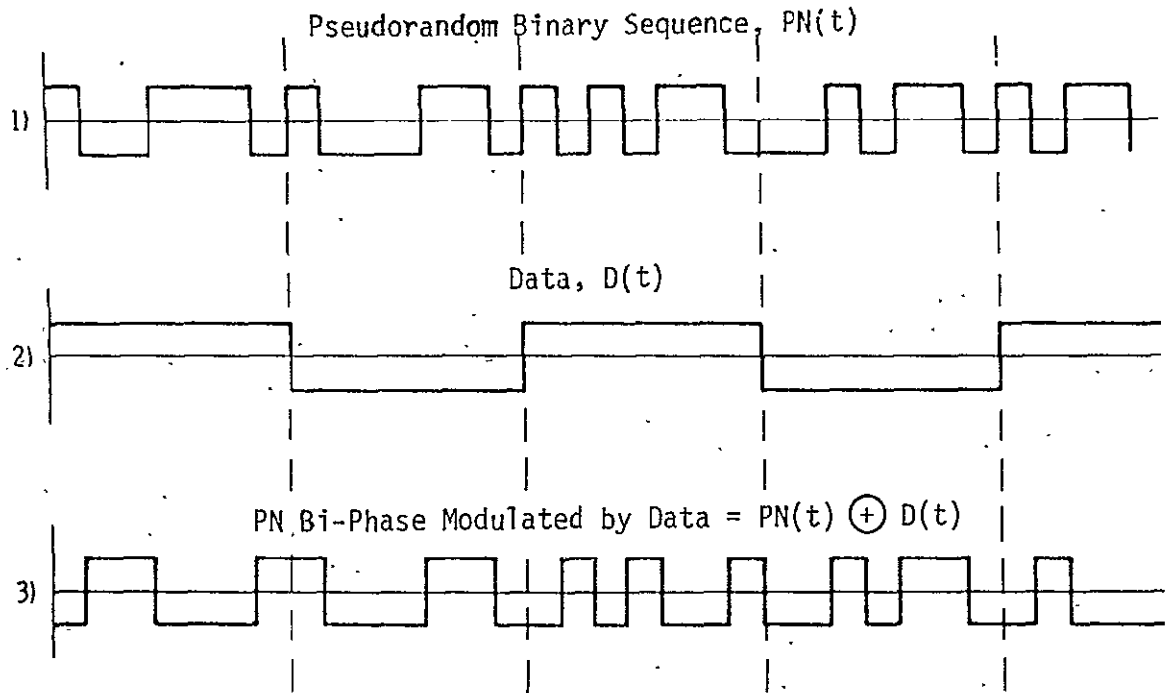
Figure 4-11. Data Modulation of Pseudorandom Sequence

block diagram of the basic delay lock discriminator is shown in Figure 4-12. Note that it is illustrated in a basic form to simplify discussion. An actual loop would most likely operate at an IF frequency so that the LPFs would become bandpass filters with the IF frequency either being removed at the output of the BPF or at the input of the loop filter. Note also that, if data is present, it may be removed at the input of the loop by a data estimate, or following the LPF in each channel by a squaring or absolute value device, as illustrated in Figure 4-12 by dashed lines.

The incoming code is multiplied by the reference code which is advanced by a chip duration (T) and by the reference code delayed by the same amount, in the upper and lower multiplier, respectively. Creating the advanced and delayed versions of the reference code is easily accomplished by tapping off of two adjacent storage cells in the PN generator. If the delay is to be different from the chip duration, a more complicated device would be required to achieve the delay and advance (such as a fraction of T). The result of these multiplications are two functions of ε (the code phase error) at the input of the summer. The function into the plus input of the summer is the code correlation function advanced by T and the function into the minus input is the code correlation function delayed by T. The output gives the discriminator function,which is the difference of the two correlation functions and is shown in Figure 4-13. The output of the summer drives a voltage controlled oscillator (VCO) which, in turn, clocks the PN code generator.

Also shown in Figure 4-12 are the acquisition control inputs. The input before the VCO is used to sweep the clock to the correct frequency or to delay or advance the phase of the code.

As discussed previously, the delay lock tracking loop requires two identical processing channels. These channels must be identical so that the error function will be symmetrical and without bias. If the gains of both channels are not perfectly matched, a distorted discriminator characteristic and, consequently, poor system performance will result. To circumvent these problems, it is possible to utilize one channel and time-multiplex it between the -T reference and the +T reference. This system is called a time-shared loop or, more commonly, it is known as the tau jitter tracking loop. This loop is shown in
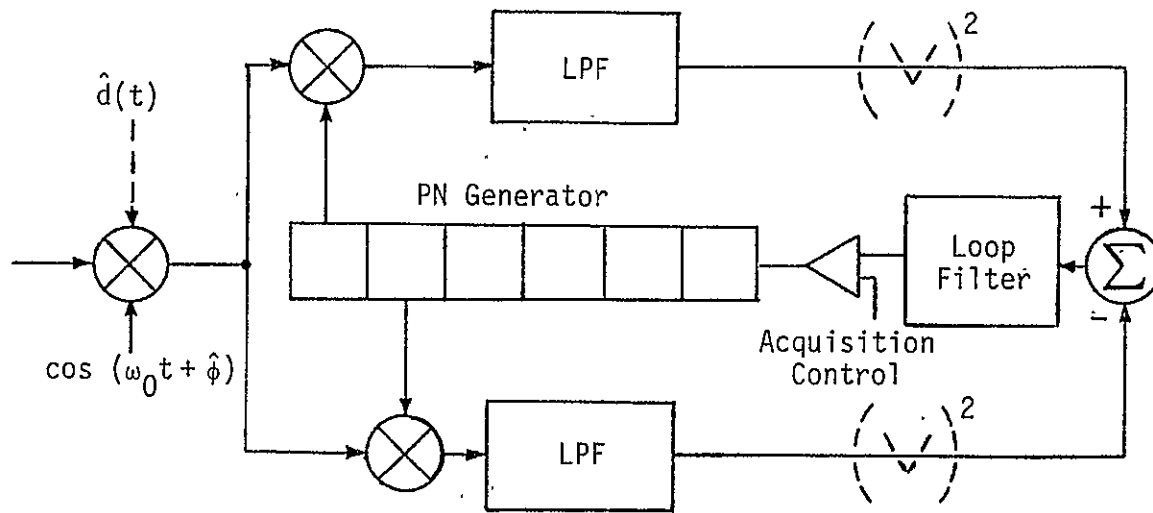
Dashed lines denote optional elements.

Figure 4-12.   Delay Lock Tracking Loop
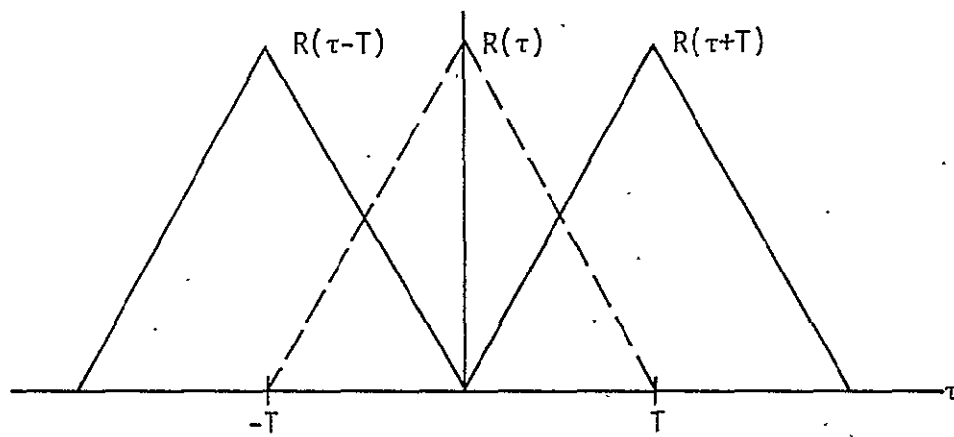
A. Delayed and Advanced Correlation Function
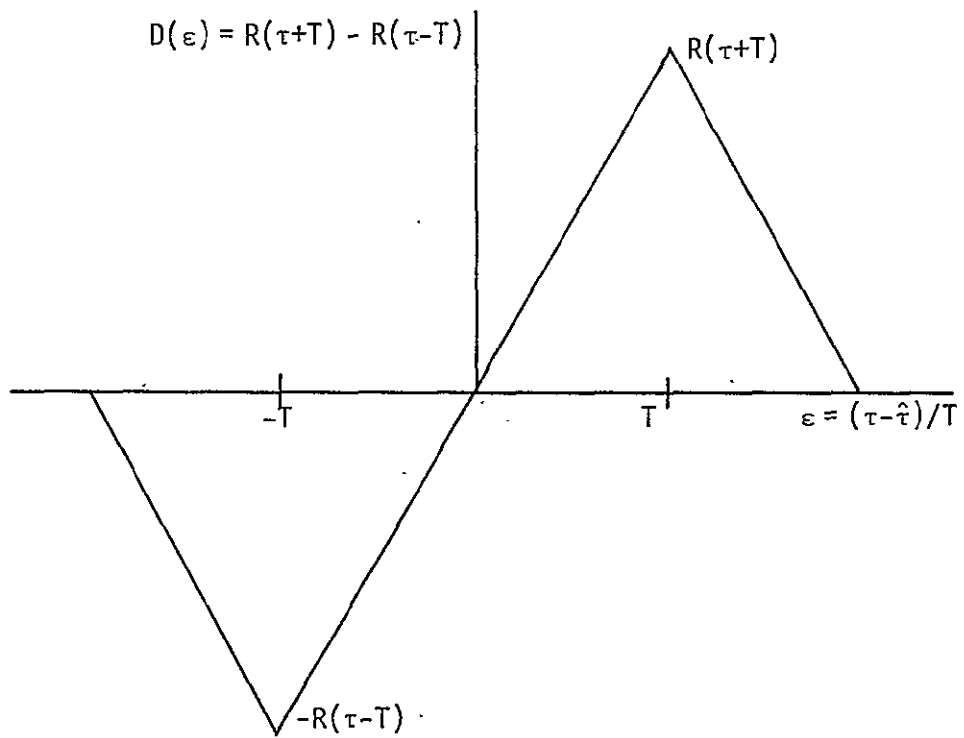
B. Discriminator Function for the Delay Lock Loop

Figure 4-13. Delay Lock Loop Discriminator Function

Figure 4-14. Time multiplexing of the channels is accomplished by a square wave which alternately advances and retards the phase of the reference code by T. This jittered reference code is then correlated with the incoming signal. The output of the correlator passes through a lowpass filter whose output contains a square wave with the error signal amplitude modulated onto it. The square wave is removed at the multiplier just before the loop filter. It can be shown that the mathematical model for this loop is equivalent to the one for the delay lock loop, except that the discriminator gain for the tau loop is 1/2 the gain of the delay lock loop discriminator, resulting in a 3 dB loss in loop SNR.

A detailed analysis of the delay lock code loop and tau dither code loop tracking performance is presented in Appendix B.

Another function shown in the generalized PN receiver block diagram of Figure 4-7 which is worthy of further explanation is the carrier receiver. Since the PN code bi-phase modulates the carrier with effectively random +1's and -1's, the average carrier component is zero. This is usually referred to as suppressed carrier modulation and it requires a receiver which is designed to recover the suppressed carrier. A squaring loop or Costas tracking loop is used to accomplish this function, with a Costas loop the implementation most generally chosen for GPS receiver design. Figure 4-15 shows a functional block diagram of a Costas loop. The loop filter bandwidth determines the Costas loop performance with a narrow bandwidth desirable from the desire to minimize noise caused phase error jitter and a wide loop filter desirable to minimize the tracking error due to link dynamics, i.e., range acceleration and jerk. The noise performance for the Costas loop is discussed in Section 7.1 and the selection of loop bandwidth that minimizes noise jitter and dynamic tracking errors is discussed in Appendix C.

$\hat{d}(t)$

$\cos (\omega_0 t + \hat{\phi})$

LPF

Loop
Filter

m(t)

Square Wave
Oscillator

PN Code
Generator

Gated Advance
Delay, τ_d

VCO
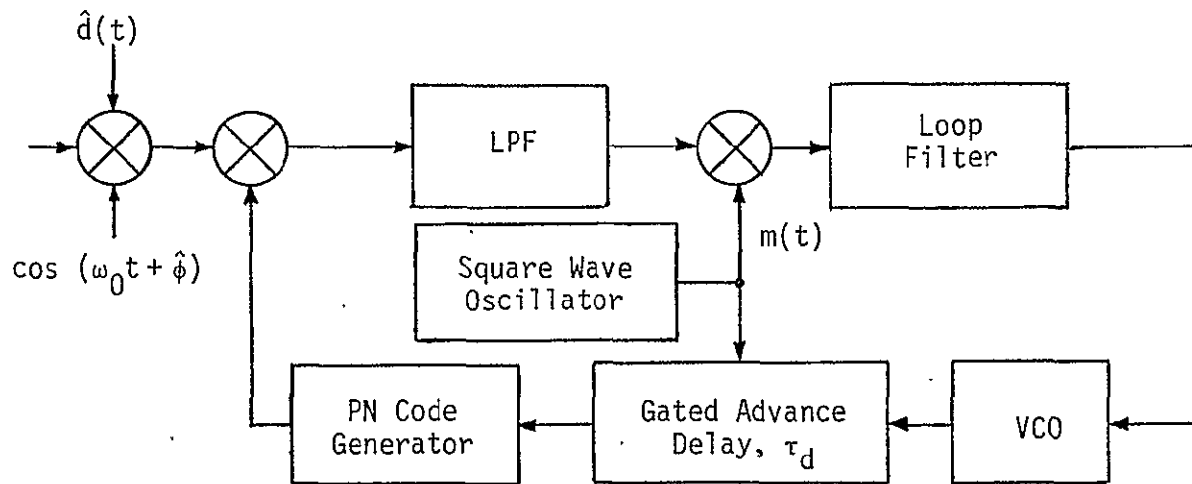
Acquisition control not shown.

Figure 4-14.   Time-Shared (Tau) Tracking Loop
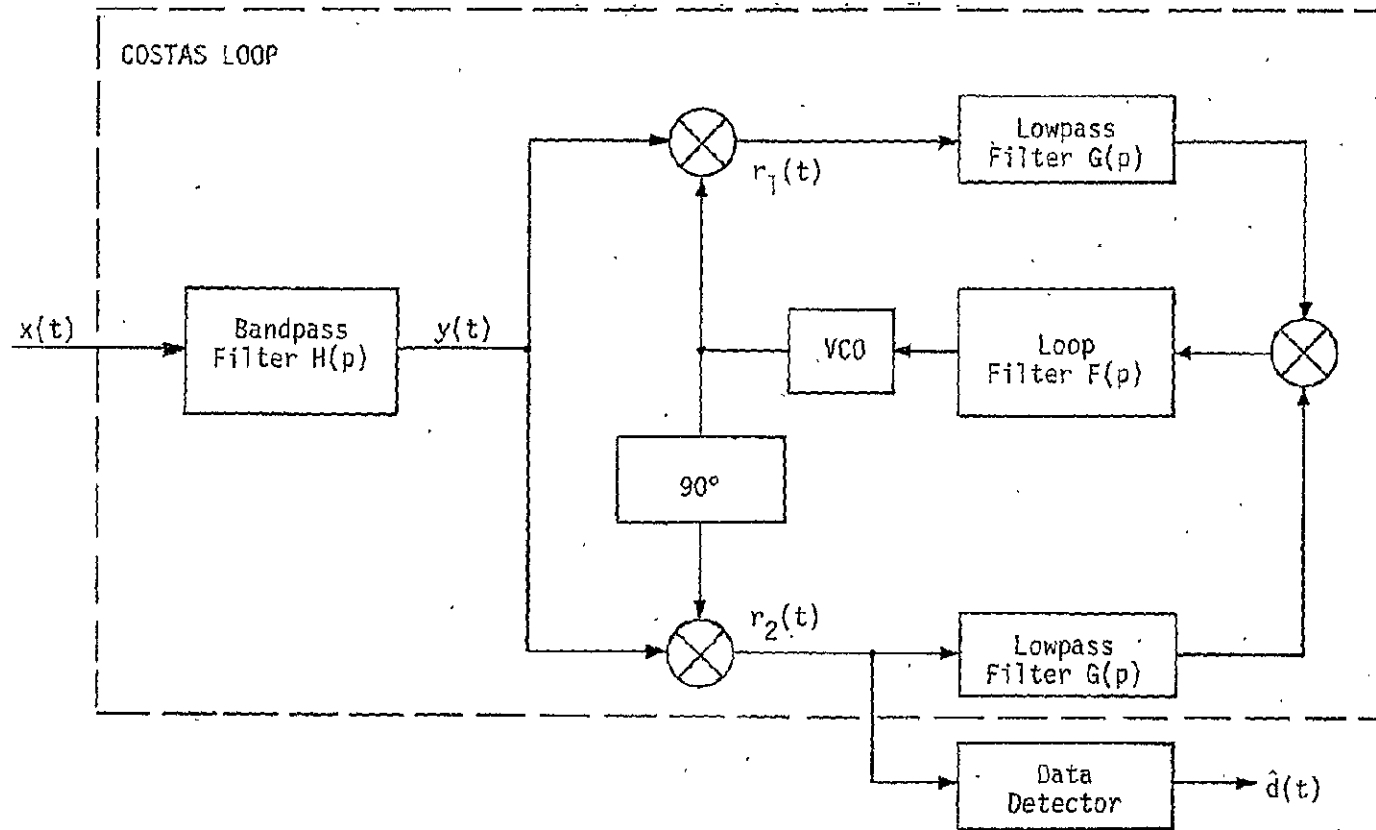
Figure 4-15. Costas Loop Receiver

5.0 GPS USER EQUIPMENT SURVEY

5.1 Receivers

There are a number of GPS navigation receivers that are presently under development or that have completed development as part of the GPS Phase I effort. These receivers have been examined as possible candidates for the Shuttle GPS navigation function. The obvious intention is to find an existing receiver that is capable of operating within the Shuttle environmental constraints while providing the necessary navigation performance. There are two basic constraints that strongly influence the selection of candidate receivers. These are signal dynamics and environmental factors, such as temperature. Table 5-1 lists those receivers being developed under Phase I which are considered to be the most likely candidates for a Shuttle/GPS receiver.

Table 5-2 lists several other receivers which were also evaluated. These receivers are being developed for space and missile applications. Of the receivers evaluated in Table 5-1, the X set most nearly meets the Shuttle requirements. However, its rather large size, $0.156 \ m^3$, makes it difficult to mount in the Shuttle avionics bay and, since it is designed for ambient environment, it cannot be located in the payload bay. The Z set, on the other hand, is compact ($0.013 \ m^3$) and is designed to physically replace standard TACAN sets. However, since it does not operate with a P code, its range measurement accuracy is 10 times worse than that of the X set. However, in the FY'78 study, the overall Shuttle navigation accuracy which results from the 15 meter range measurement error will be evaluated. A more serious limitation of the Z set is its limited signal dynamics capability and lack of IMU aiding provisions. During FY'78 fiscal efforts, the implications of adding an IMU aiding interface will be examined.

From Table 5-2, it is seen that the GPSPAC receiver is space-rated (in fact, the only GPS receiver currently under development that is space-rated). Its signal dynamics capabilities are satisfactory as far as the velocity capability, since it is designed for orbital operation. However, the acceleration and jerk capabilities, although satisfactory for on-orbit operation, will not enable the receiver to track the GPS signal during the entire Shuttle entry and landing phase. This could be changed by the addition of IMU aiding, or possibly by using two GPSPAC

Table 5-1. Phase I GPS Receiver Performance Requirements

	X	Y	Z
Operating Frequency	L1,L2	L1,L2	L1
Signals	P,C/A	P,C/A	C/A
Provisions for IMU Aiding	Yes	Yes	No
TTFF (sec)	80	225	200
Required Pseudo Range Accuracy, 1σ Error (meters)			
P	1.5	1.5	--
C/A	15	15	15
Range Rate Accuracy, 1σ Error (m/sec)			
P	0.006	0.006	---
C/A	0.006	0.006	0.006
Maximum User Vehicle Dynamics			
Velocity (m/s)	900	600	600
Acceleration (m/s^2)	50	20	20
Jerk (m/s^3)	100	100——	50
Size (m^3)	0.156	0.156	0.013
Weight (kg)	106	106	16
Power (w)	940		166
Environment	Ambient	Ambient	Ambient

Table 5-2. GPS Development Receivers for Space and Missile Applications

	GPSPAC	MBRS	M
Operating Frequency	L1,L2		
Signals	P,C/A	P,C/A	P
Provisions for IMU Aiding	No	No	Yes
Required Pseudo Range Accuracy, 1 Error (meters)			
P	1.5	1.35	
C/A	15	13.5	
Range Rate Accuracy, 1 Error (m/sec)			
P	0.006	0.012	
C/A	0.006	0.012	
Maximum User Vehicle Dynamics			
Velocity (km/s)	9	7.7	
Acceleration (m/s^2)	16	98	
Jerk (m/s^3)	0.02	9	
Size (m^3)	0.026	0.064	
Weight (kg)	16.8	35	
Environment	-20°C to +50°C Space-Rated	60°F to 175°F Ambient	Ambient

receivers and increasing the dwell time for each satellite (the GPSPAC is a sequential track receiver). During the course of the study, the GPSPAC receiver was recommended as the best candidate GPS receiver to implement an early OFT test and demonstration capability. The reasons for this recommendation are summarized in Table 5-3.

In the context of existing receivers (or receiver developments) to be used as an operational Shuttle GPS receiver, three possibilities exist: a repackaged X set (with IMU aiding), a Z set with IMU aiding added, and a GPSPAC receiver (or receivers) with IMU aiding added. Repackaging the X set into a smaller volume may well represent a major new development in itself, since packaging represents a significant portion of avionics development cost. However, with microprocessor technology evolving so fast, this route merits investigation. The Z set, adapted for IMU aiding, is an attractive alternate because of its TACAN package configuration. Finally, the GPSPAC receiver, since it is space-rated, is an obvious alternate to study.

5.2   Antennas

The design and integration studies of GPS antennas suitable for Shuttle Orbiter use were largely the responsibility of RI. However, Axiomatix worked closely with RI in these matters from the aspect that antenna performance strongly affects the GPS/Shuttle link performance. The RI baseline antenna design is a classical cavity-backed slot or dipole antenna, shown conceptually in Figure 5-1, that would provide approximately -1 dB gain (RHCP) over a solid angle of half cone angle of 50 to 60 degrees. Due to the limited number of GPS satellites available during the early Shuttle flights; it was of great interest to investigate new-technology antenna developments that might provide greater usable viewing angle. The antenna technology investigated by Axiomatix was the microstrip antenna which has been under development by Ball Brothers of Boulder, Colorado. Of special interest was the fact that Ball Brothers has developed and delivered several operational GPS antennas. Figure 5-2 shows a picture of the Ball Brothers GPS antenna designed for mounting on a high performance aircraft. It can be seen from the figure that the antenna is relatively small, especially the thickness dimension. The performance for this antenna (cross-slot) is indicated in the gain versus elevation plots given in Figures 5-3 and 5-4 for L1 and L2

Table 5-3. Applicability of Existing or Planned Hardware to an
Early OFT GPS Test/Demonstration

o Many GPS user sets available or planned for various applications

  o High Performance Aircraft Set (X-set)

    o Ambient environment only

    o Large volume/weight

  o Tactical Missile Set (M-set)

    o Ambient environment only

    o Requires initialization from external GPS receiver

    o No data demodulation capability

  o Man Pack Set

    o Ambient environment only

    o Not capable of orbital/signal dynamics

  o Minuteman Missile Receiver (MBRS)

o GPSPAC closest to meeting Shuttle requirements

  o Space-qualified; operates in payload bay environment

  o Schedule compatible with OFT-1

  o Compatible with Orbiter signal dynamics on-orbit

RADOME

2.50 SQ APERTURE

FEED CABLES

1.90

CONNECTOR

CROSSED DIPOLE

STRIPLINE ASSEMBLY

RADOME REMOVED FOR CLARITY

HOUSING

3.00
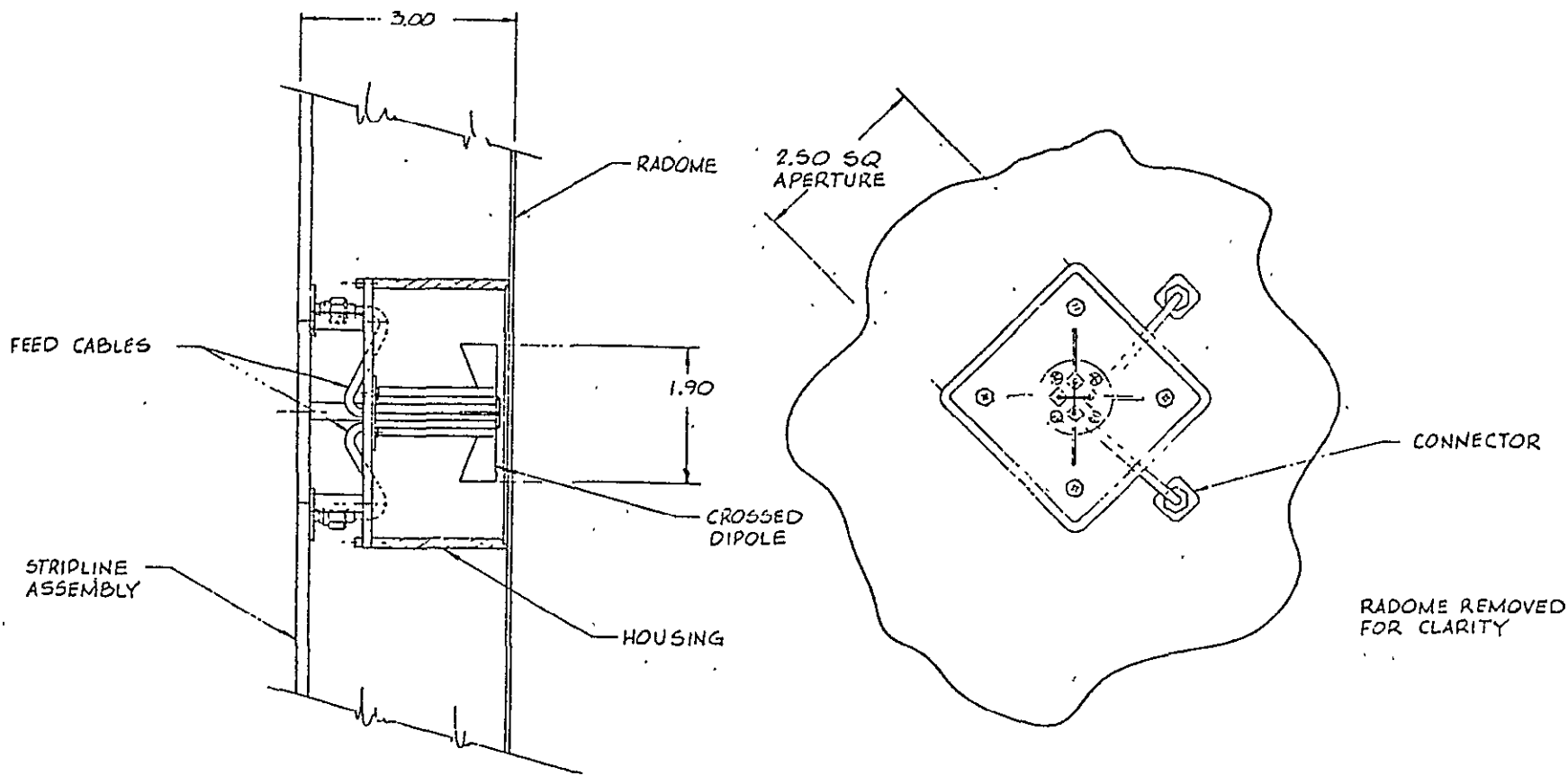
Figure 5-1. Crossed-Dipole Antenna Element (S-Band)
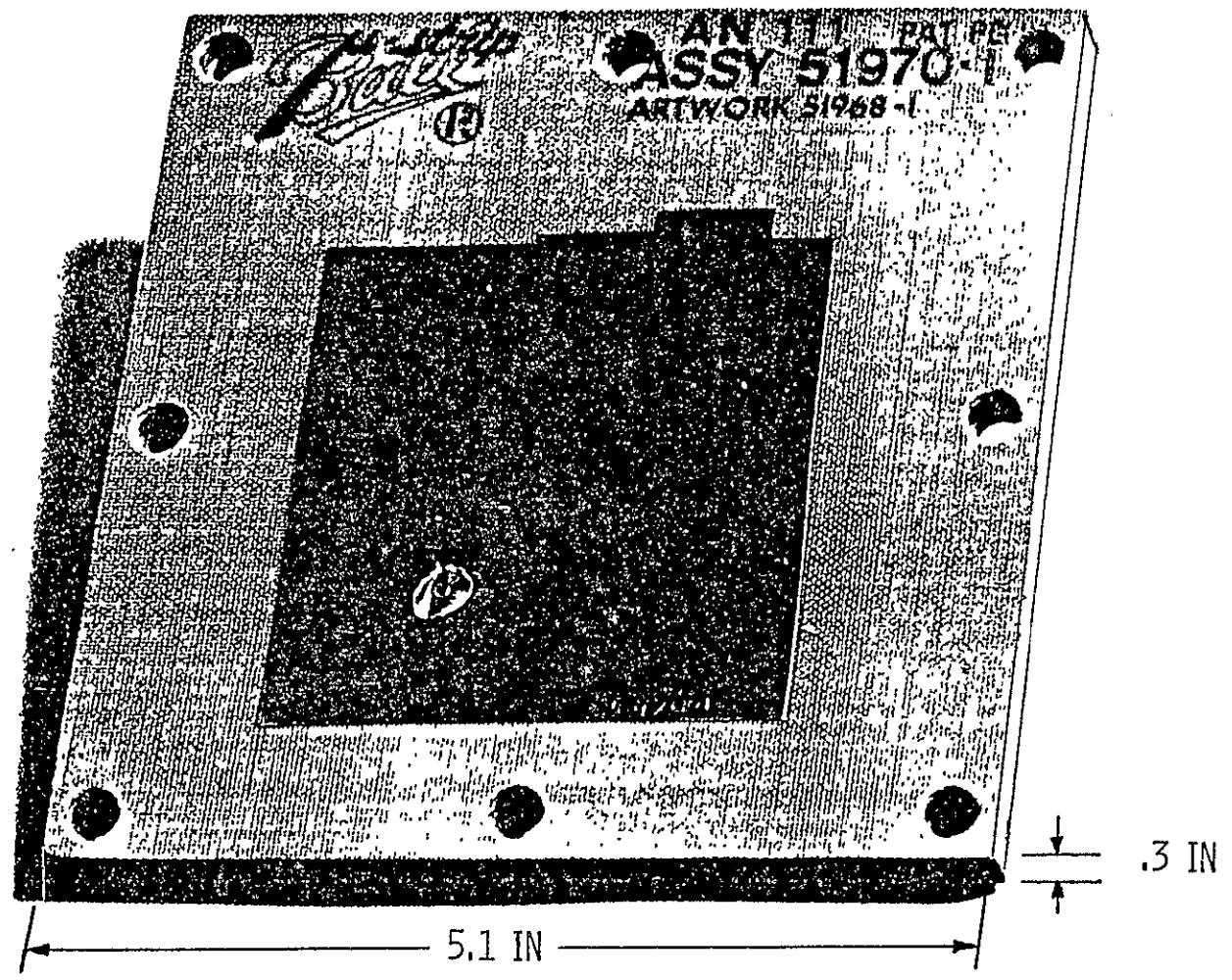
Figure 5-2.   Ball Brothers GPS Cross Slot Microstrip Antenna

36
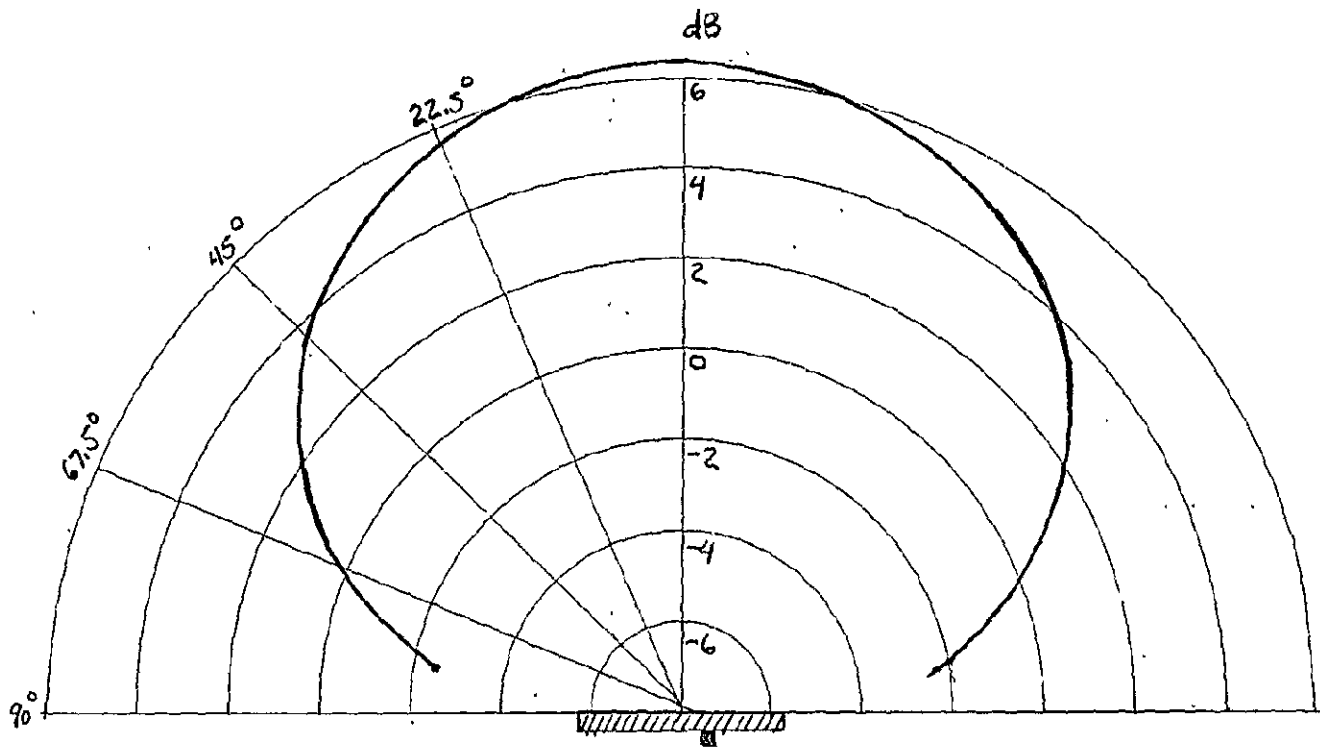
Figure 5-3. Ball Brothers GPS Antenna Coverage Cross Slot
(1575.4 MHz Gain (RHCP) vs. Elevation Angle)
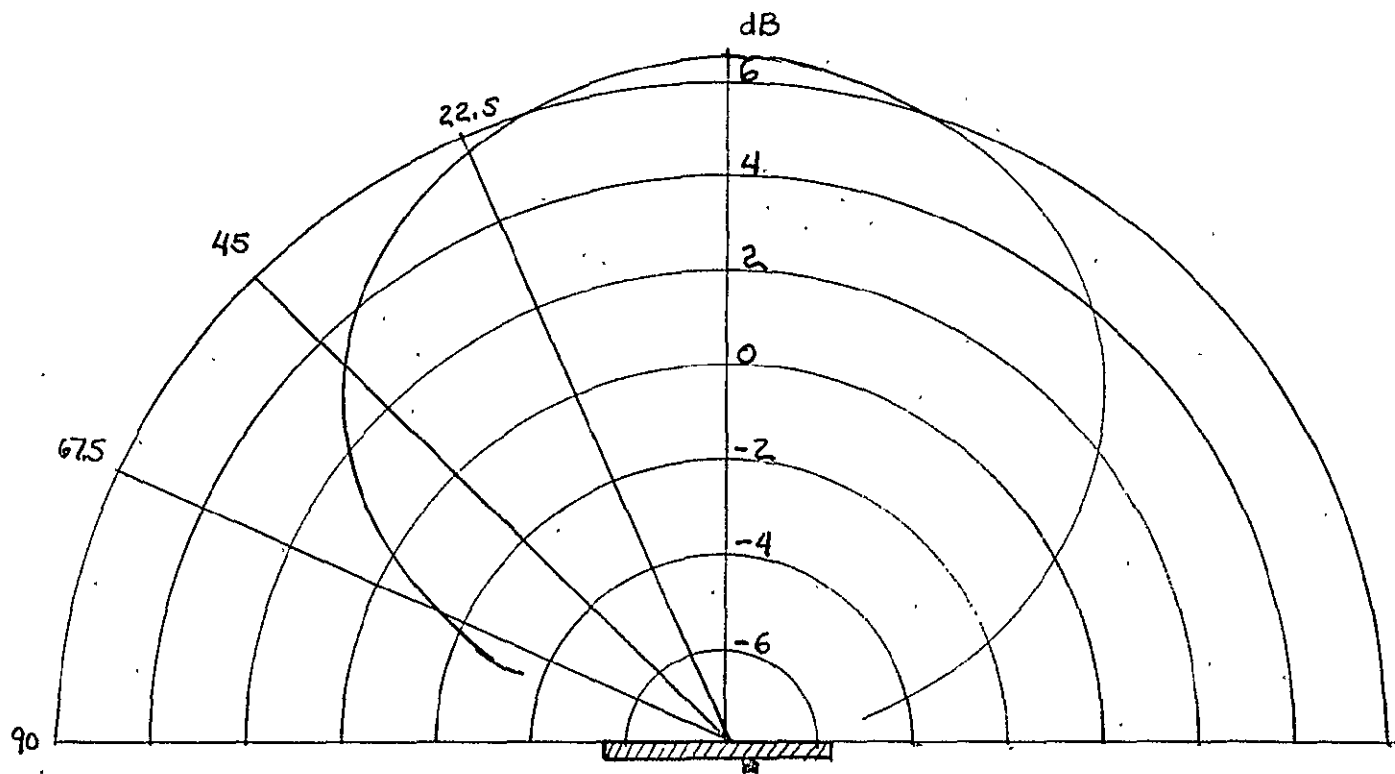
Figure 5-4. Ball Brothers GPS Antenna Coverage Cross Slot
(1227.6 MHz Gain (RHCP) vs. Elevation Angle)

frequencies, respectively. The antenna provides -1 dB (RHCP) of gain at approximately 75° at L1 and at 67° at L2. In order to get a greater gain distribution at the larger angles, an annular slot antenna was also developed. The gain plots for this antenna are shown in Figures 5-5 and 5-6. It can be seen that the gain peaks around 60° for this antenna and, allowing for the 3 dB polarization loss (the annular slot is a linearly polarized antenna), the peak gain is approximately +2 dB (RHCP) at 60° and -3 dB (RHCP) at approximately 80°.

Although the Ball Brothers microstrip antennas exhibit good performance characteristics, further investigation of the thermal environmental resistance is recommended. This can be understood by considering their typical construction technique as shown in Figure 5-7. The copper strip, which is a result of etching away the copper cladding on the dielectric material, can be sensitive to extreme temperature changes, such as those that could be encountered during Orbiter entry.
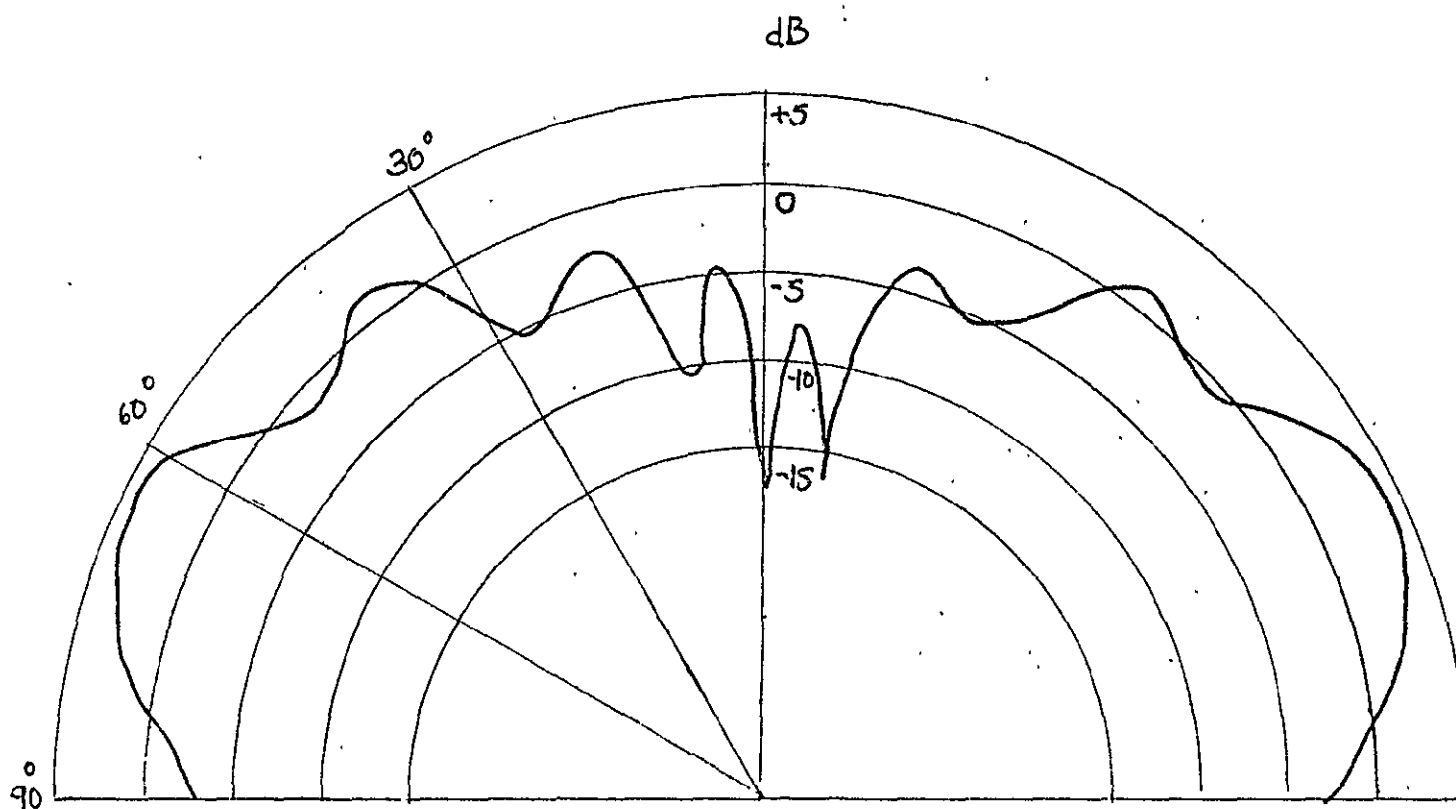
Figure 5-5. Ball Brothers GPS Antenna Coverage Annular Slot
(1575.4 MHz Gain (Linear Polarization) vs. Elevation Angle)
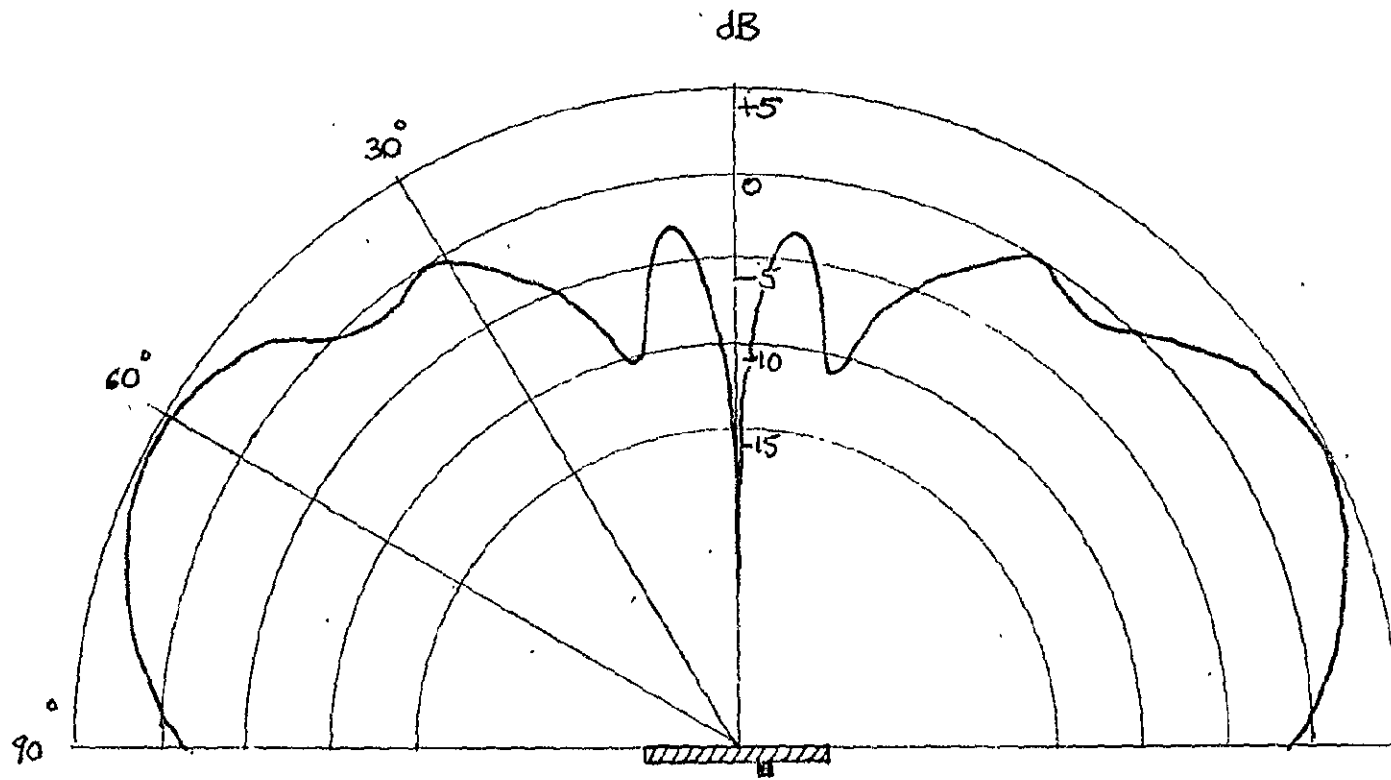
Figure 5-6. Ball Brothers GPS Antenna Coverage Annular Slot
(1227.6 MHz Gain (Linear Polarization) vs. Elevation Angle)
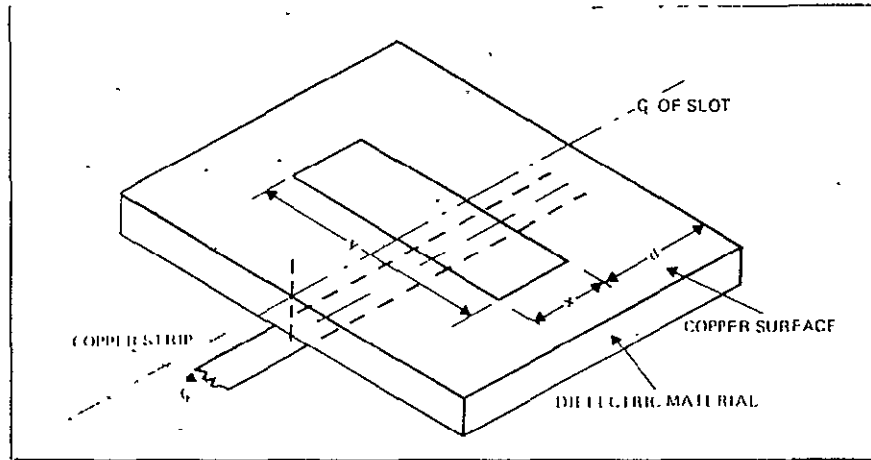
Figure 5-7. Sketch of a Single Slot Fed by a Microstrip Line

6.0   SHUTTLE/GPS SYSTEM DESCRIPTION

The development of a Shuttle GPS navigation capability was origi-
nally conceived at the start of the study as a phased development. The
first phase was to be a test/demonstration system that could be imple-
mented in a minimum time period and would be flown on OFT-1. An interim
phase would follow that would provide increased mission coverage and.
redundancy. This would lead to an operational phase in which triple
redundancy, full on-board processing and display, redundancy management,
and total mission capability would be implemented. The link performance
for the first two phases was analyzed in detail during the study and
the results are reported in Section 7.0. Since NASA Management has
recommended eliminating the first two phases, no further work will be
done on them. During the FY'78 study, the third phase—Operational—
will be extensively studied. A description of each configuration follows.

6.1   Test/Demonstration System

The test/demonstration system was conceived as the quickest,
least expensive route to get a GPS navigation capability on-board the
Shuttle. As such, the system had severe performance limitations. A
block diagram of this system is shown in Figure 6-1. The dominant
feature of this system, as seen from the block diagram, was the single
antenna and single receiver. The antenna was to be the GPS antenna
being developed by APL for SEASAT and other satellites. This antenna
was to be integrally mounted with the SEASAT preamp on a nondeployable
boom in the payload bay, as shown in Figure 6-2. A sketch of this
antenna and its gain-versus-elevation performance are shown in Figures
6-3 and 6-4, respectively. Although the antenna had excellent free ·
space gain characteristics, the viewing angle was limited by the Orbiter
structure and it would provide GPS coverage for only the upper hemi-
sphere. A more severe limitation was the fact that once the payload
bays are closed, the antenna would be nonoperable, thus limiting the
mission coverage to strictly on-orbit.

The receiver to be used for the test/demonstration system was
the GPSPAC receiver, under development by Magnavox for the SEASAT (the
SEASAT will not fly with the GPSPAC receiver due to schedule delays in
the GPSPAC development). A functional block diagram of this receiver
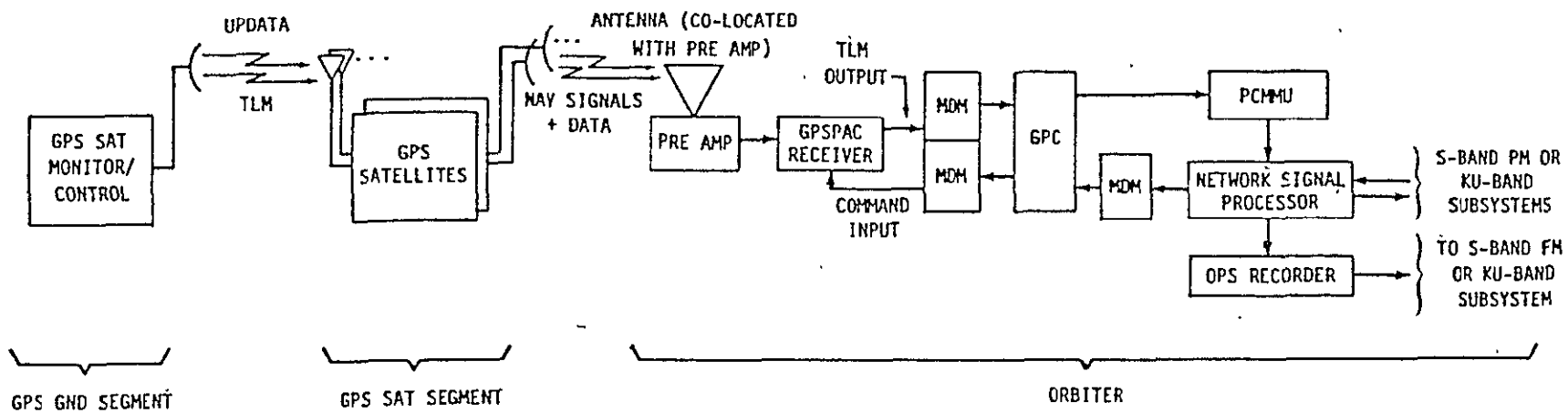
Figure 6-1. Functional Block Diagram of OFT Test/Demonstration System (Phase I)

PAYLOAD BAY LOCATION

ANTENNA AT   X = 1087
Y = 44
Z = 482.6

DFI CONT NO. 1

DFI CONT NO. 3

IECM

STACKED ANTENNA

PREAMP UNIT

BOOM SUPPORT
STRUCTURE

DFI CONT NO. 2

FWD

DFI PALLET
STRUCTURE

SUPPORT PNL

HONEY COMB PNL

GPS PACKAGE

Yo 0.0

DFI PALLET INSTALLATION
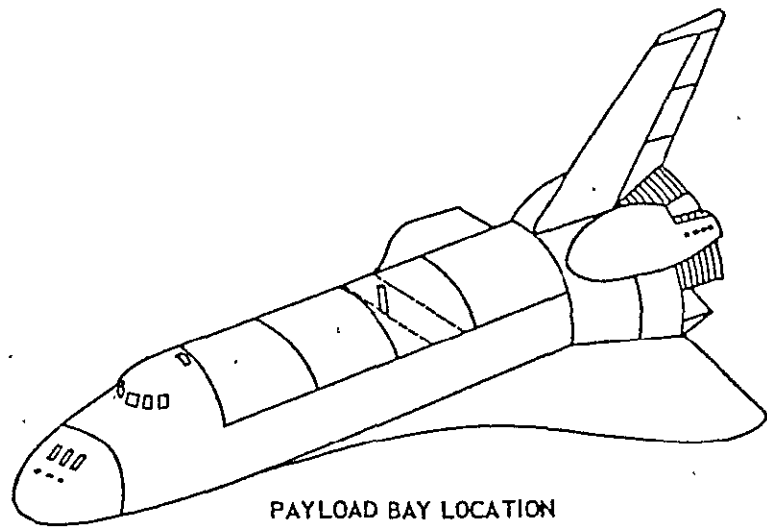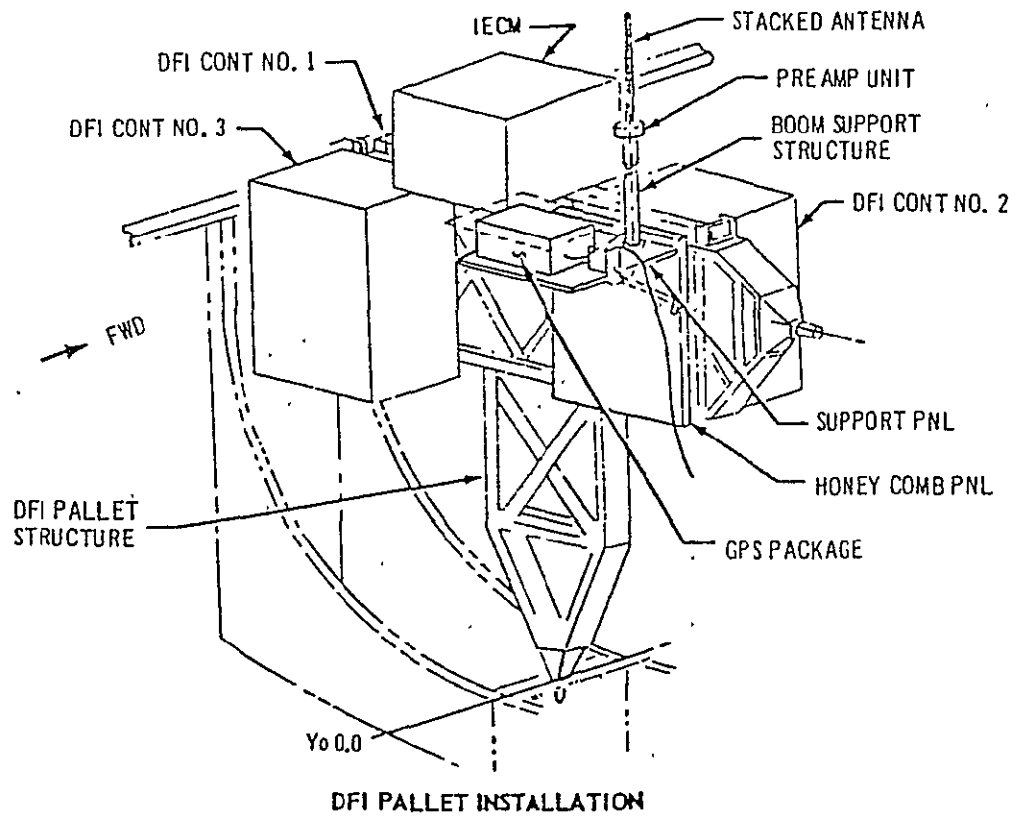
Figure 6-2.   OFT Test/Demonstration Installation Concept (Phase I)

Stacked Antenna
(15" x 1.16")

Directional Coupler
Housing (1")

Interface
Plate (LMSC)

Cable
Dispenser
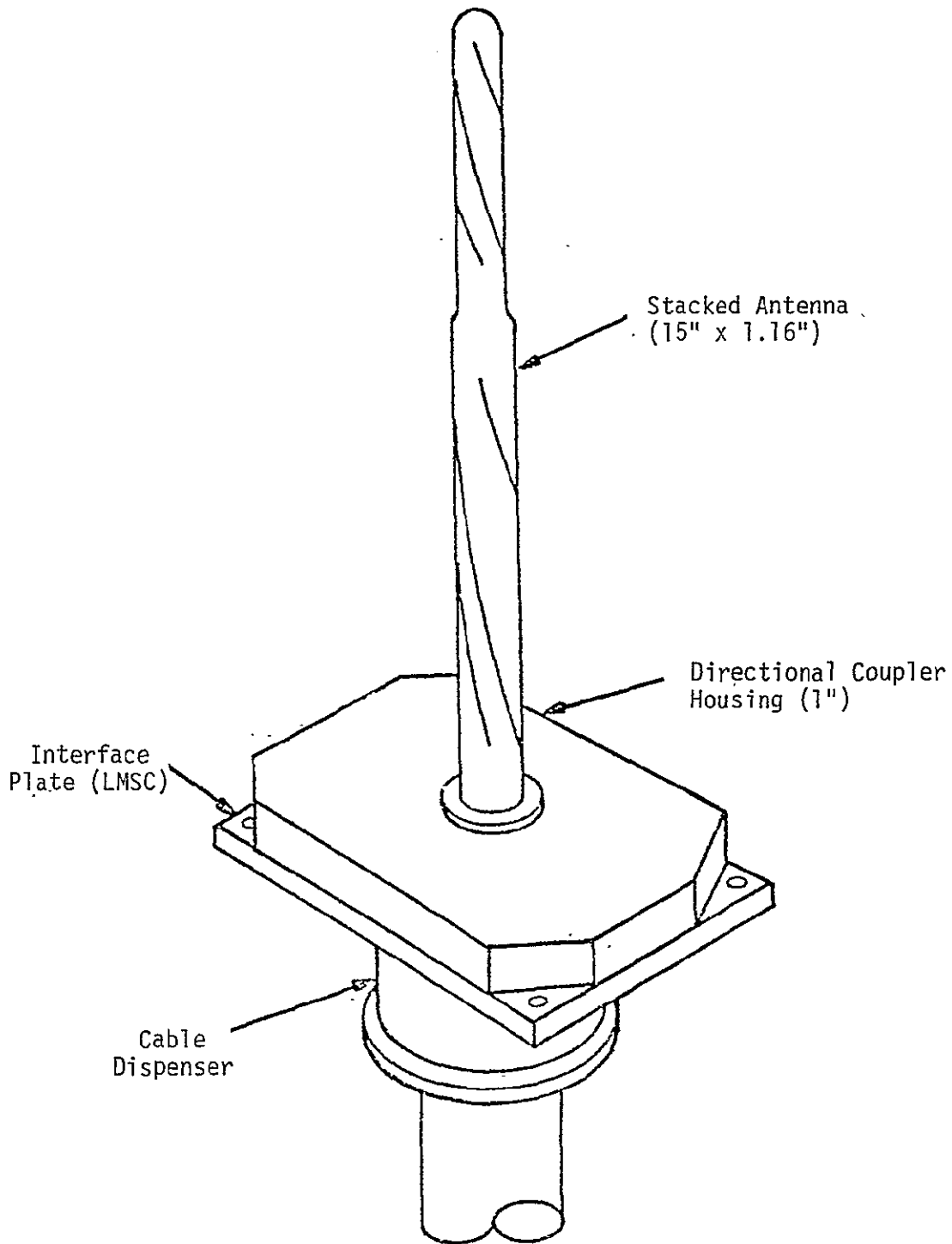
Figure 6-3. Payload Bay Antenna for Test/Demonstration System (Phase I)
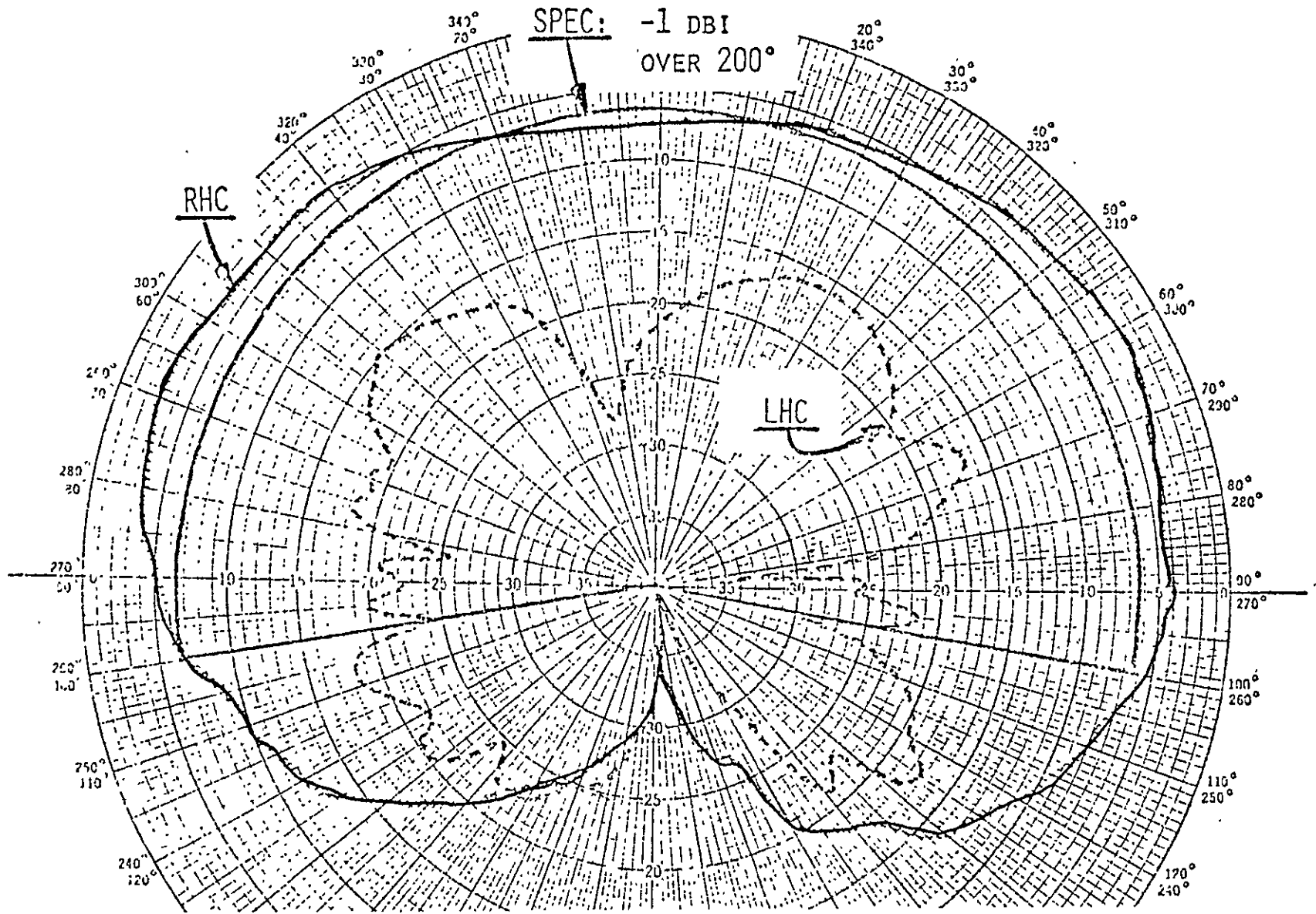
Figure 6-4. Gain vs. Elevation Angle for Test/Demonstration Antenna

is shown in Figure 6-5. This receiver was chosen because it was the only GPS receiver under development designed for space applications. One limitation of the receiver is that it is designed only for on-orbit signal dynamics. The key feature in obtaining the on-orbit tracking capability is that the receiver aids itself. It does this by taking the position estimates at the output of the navigation filter and computing doppler and doppler rate from them. These estimates are then used to aid the tracking loops. The pseudo-range estimate, which is used to pre-position the receiver code generator, is calculated from

$$R = \sqrt{(S_x - X)^2 + (S_y - Y)^2 + (S_z - Z)^2} + b,$$

where S_x = GPS satellite x coordinate

S_y = GPS satellite y coordinate

S_z = GPS satellite z coordinate

X,Y,Z = navigation filter estimate of GPSPAC coordinates

b = clock bias.

The pseudo range rate estimate is calculated from

$$\dot{R} = \left[\frac{S_x - X}{R - b}\right]\left[\dot{S}_x - \dot{X}\right] + \left[\frac{S_y - Y}{R - b}\right]\left[\dot{S}_y - \dot{Y}\right] + \left[\frac{S_z - Z}{R - b}\right]\left[\dot{S}_z - \dot{Z}\right] + \dot{b},$$

where the dots indicate the derivatives of the parameters discussed above. The extrapolated pseudo range rate is converted to a frequency offset, in Hz, and used to pre-position the receiver VCO frequency.

The preamp to be used for the first phase was the APL preamp developed for SEASAT. This preamp provides a worst-case noise figure of 4 dB and a worst-case gain of 30 dB at both L1 and L2. Examination of the preamp block diagram shown in Figure 6-6 shows that the preamp has two separate inputs, one from the L1 antenna element and one from the L2 antenna element. Each of these inputs is filtered and amplified separately in parallel channels and combined by a diplexer to form a single output. This configuration allows the NF and gain to be optimized for both L1 and L2 and represents a good approach for the operational system antenna preamp.
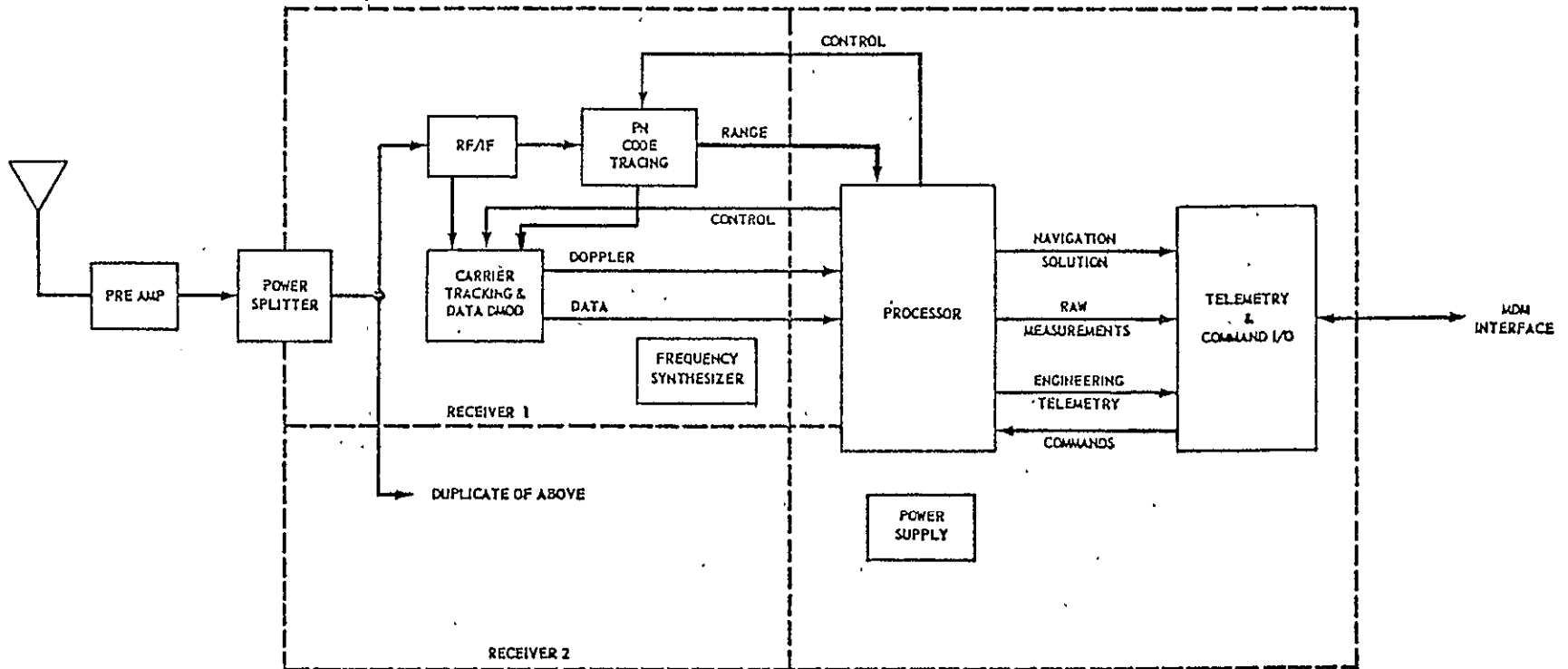
Figure 6-5. GPSPAC Receiver Functional Block Diagram
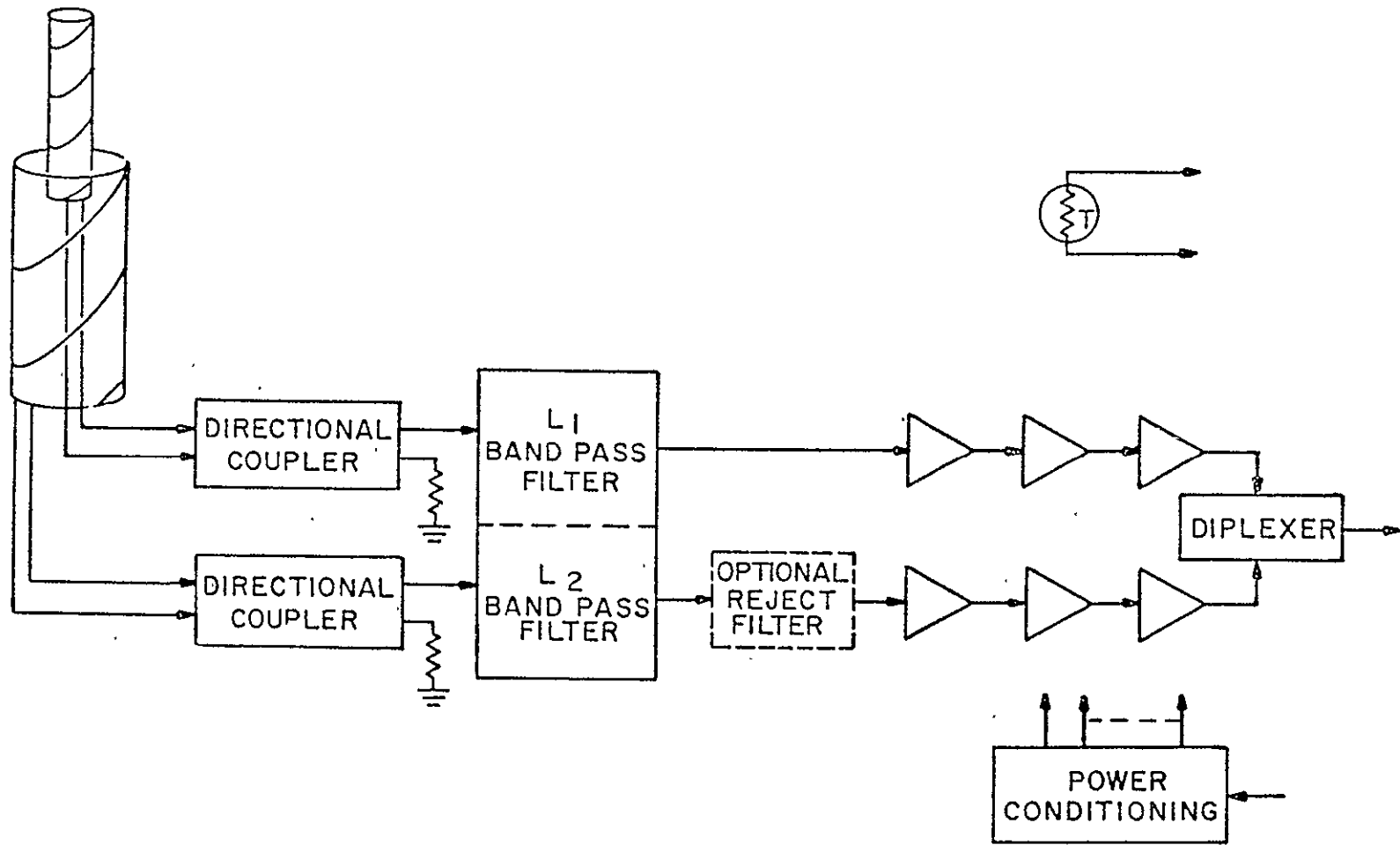
Figure 6-6. GPSPAC Antenna/Preamp Block Diagram

6.2   Interim (Baseline) System Configuration

The interim Shuttle/GPS system was configured to provide GPS coverage which is mostly independent of the Orbiter attitude and to provide a de-orbit navigation capability. Furthermore, the system was configured to provide redundancy for the electronic elements, i.e., preamps and receivers. A functional block diagram of the system is shown in Figure 6-7. The receivers and preamps were to be the same as those discussed in Section 6.1 for the Phase 1 system. The receivers were also to be mounted in the payload bay. The antennas were to be a conventional cavity backed crossed dipole, flush-mounted in the upper and lower hemi plates. This antenna has been discussed in Section 5.2. As part of the Phase 2 system, IMU aiding of the GPSPAC receivers was to be investigated with the intention being to provide a complete descent navigation capability.

6.3   Operational System

The operational Shuttle/GPS system is to be designed by RI and will be analyzed and designed, with contributions from Axiomatix, in FY'78. Consequently, it is premature for this report to discuss this system. However, a potential system configuration is shown in the functional block diagram of Figure 6-8.
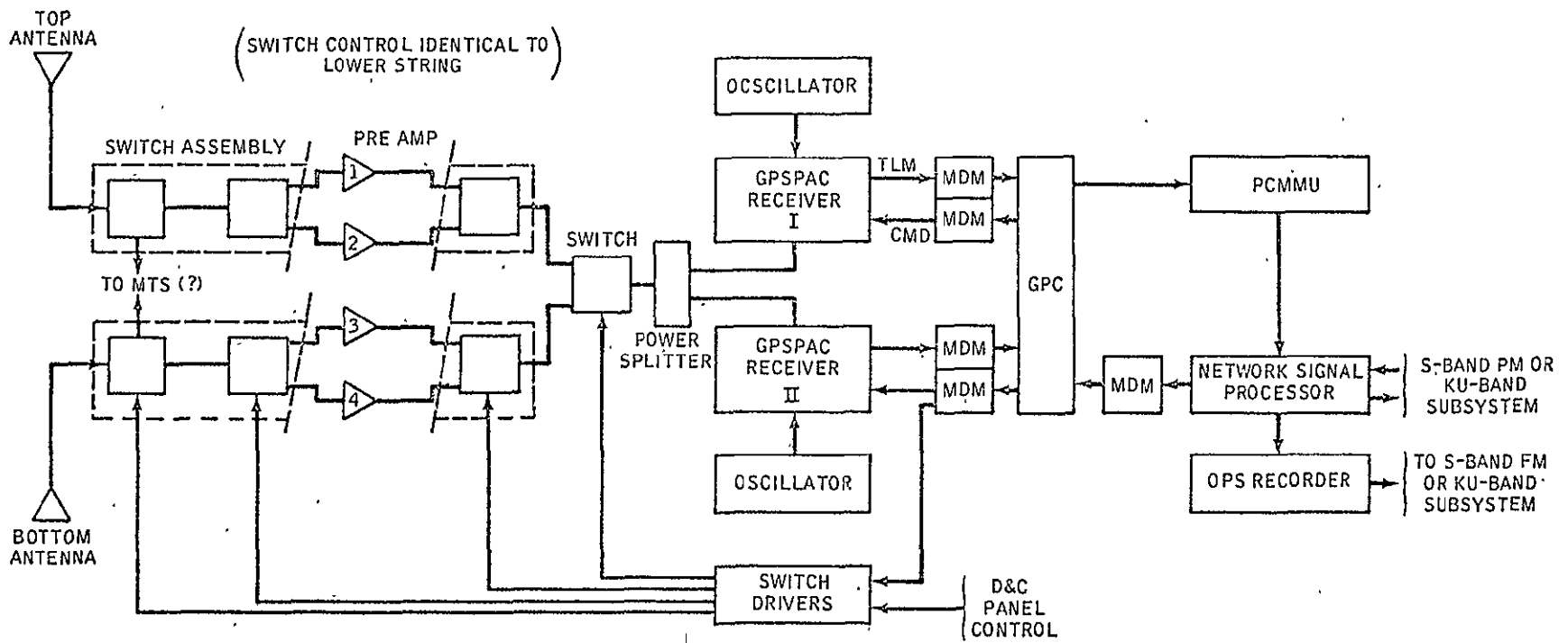
Figure 6-7. Baseline Initial GPS NAV System Block Diagram (Phase 2)
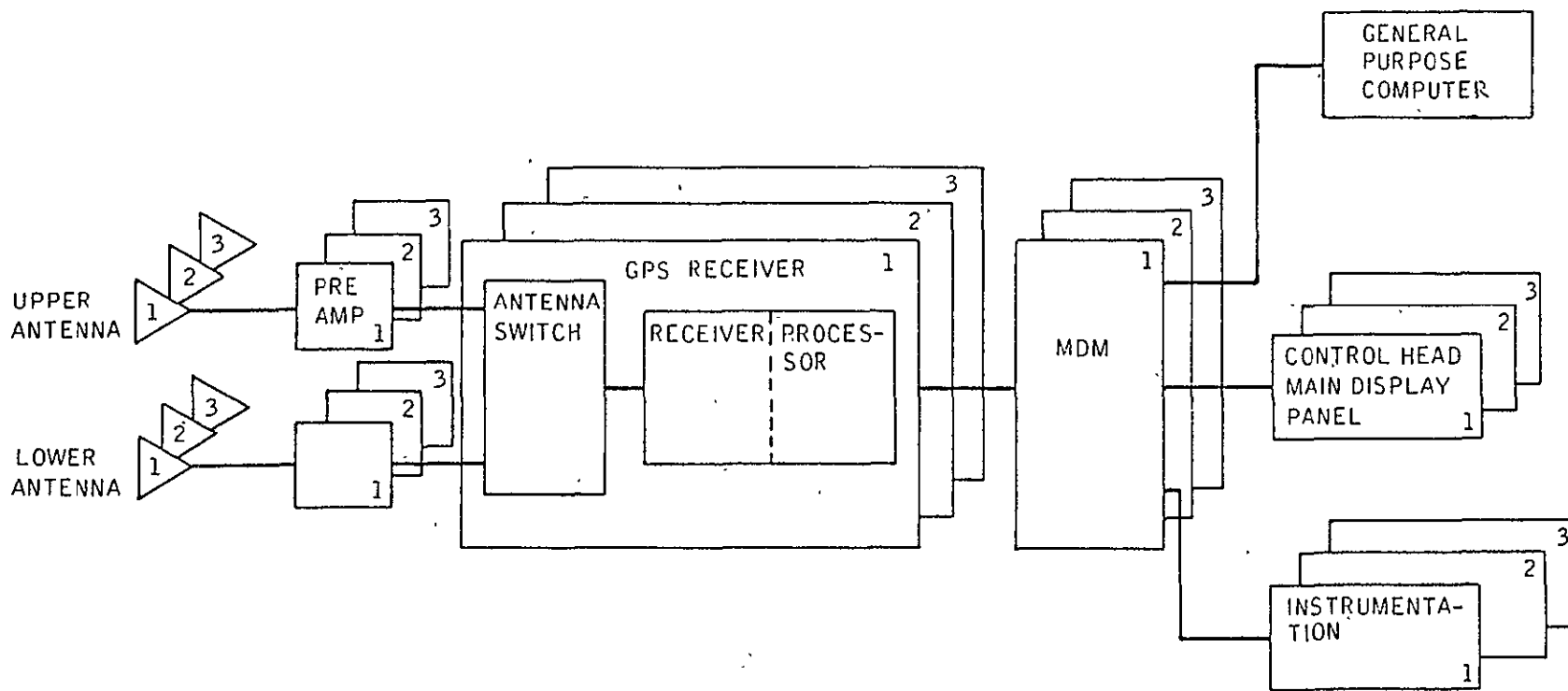
Figure 6-8. Candidate Operational GPS System Block Diagram

7.0   PERFORMANCE ANALYSES

7.1   Code Tracking, Carrier Tracking and Data Detection
       C/N_0 Requirements

This section establishes the received signal power over noise
density requirements for the three receiver functions that are essential
to extracting navigation measurements, i.e., PN code tracking (range
measurement), RF carrier tracking (range rate measurement), and data
detection. The values of C/N_0 which are calculated here are steady-
state tracking values and are not meant to be considered the require-
ments for acquisition. Acquisition performance and loss of lock perform-
ance are to be dealt with during the FY'78 study effort.

The required C/N_0 for PN code tracking depends on the required
code tracking accuracy and the receiver implementation. A reasonable
code tracking accuracy requirement is a one-sigma error of 5 ft. It
should be noted that this corresponds very closely to the 1.5 meter
requirement for the X, Y, and Z GPS receivers.

The receiver implementation can be either a delay lock tracking
loop or a tau dither tracking loop with either coherent or noncoherent
demodulation. A simplified functional block diagram of each type of
receiver is shown in Figure 7-1 to illustrate the difference of each
implementation.

The delay lock receiver is, in general, more costly to implement
but, on the other hand, it provides superior performance. Where high
performance is desired and where cost, weight and power consumption are
secondary considerations such as in the X set, a delay lock implemen-
tation is typically used. The difference in tracking performance can
be appreciated by considering the fact that the delay lock receiver
develops its error signal by correlating the advanced and retarded
reference codes with the same received PN chip, whereas the tau dither
receiver correlates against independent received chips. This results
in a 3 dB advantage for the delay lock loop due to the cancellation of
the noise samples. The delay lock loop rms tracking error for a receiver
with perfect coherent demodulation may be written as

$$\sigma_{\text{Delay Lock}} = \frac{1}{\sqrt{\frac{C}{2N_0 B_L}}} \frac{\sqrt{R(0)_{BL} - R(2\tau_d)_{BL}}}{2R'(\tau_d)_{BL}} \tag{7-1}$$
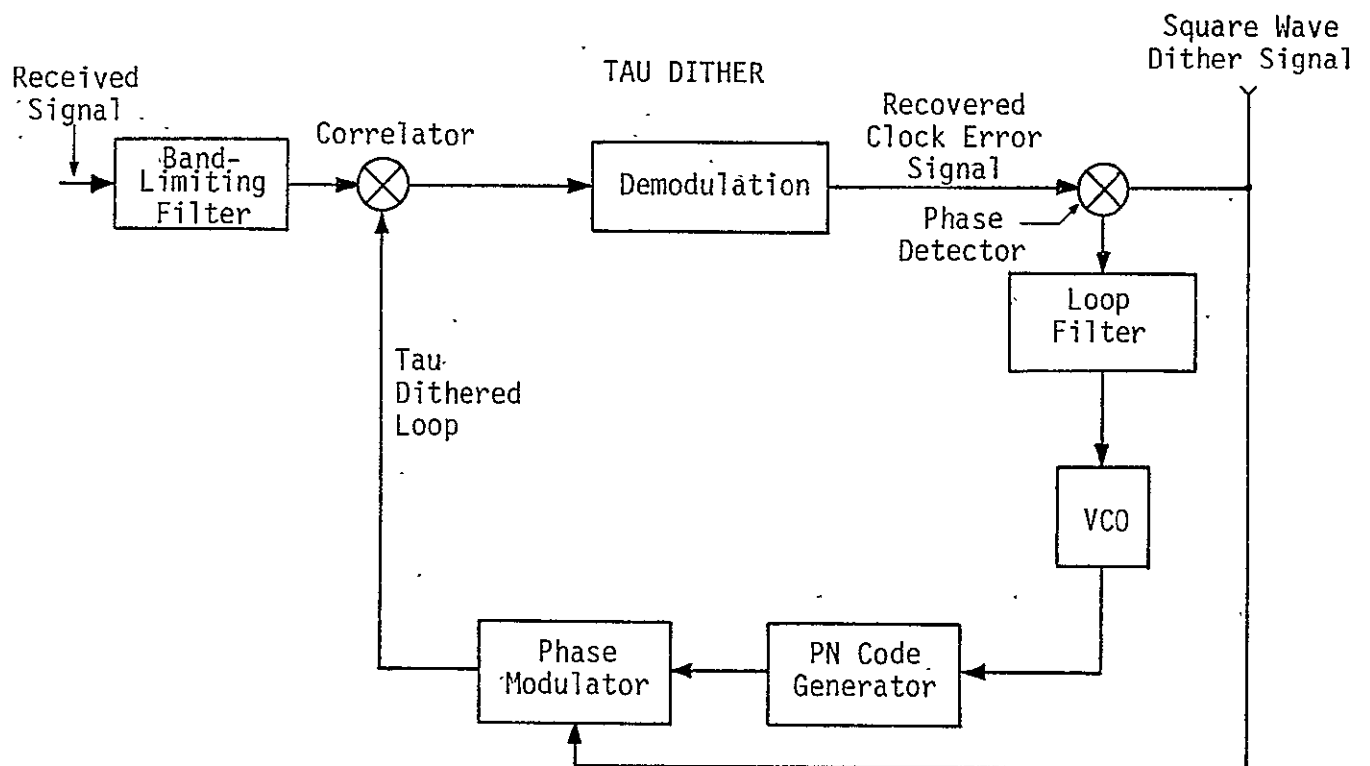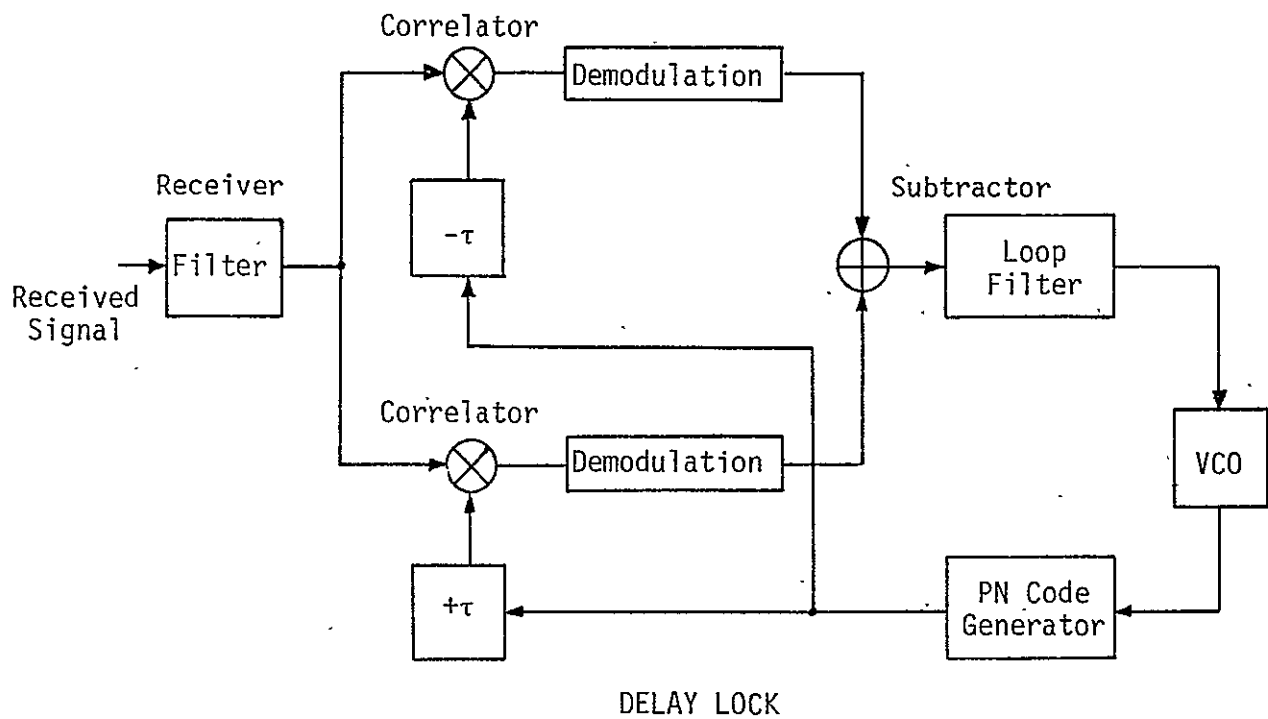
Figure 7-1. Functional Block Diagrams for Delay Lock and Tau Dither
PN Tracking Loops

where

B_L = one-sided loop noise bandwidth

$R(x)_{BL}$ = bandlimited (due to filtering) PN autocorrelation function evaluated at x

$R'(x)_{BL}$ = slope of $R(x)_{BL}$ at x

τ_d = delay lock spacing.

The equivalent expression for the tau dither loop is

$$\sigma_{\tau\ dither} = \frac{1}{\sqrt{\frac{C}{N_0 B_L}}} \frac{\sqrt{R(0)_{BL}}}{R'(\tau_d)_{BL}} \tag{7-2}$$

and taking the ratio of the two expressions, we get the delay lock advantage as

$$\begin{array}{l}\text{Delay Lock}\\\text{Advantage Over}\\\text{Tau Dither}\end{array} = \frac{\sqrt{2}}{2} \frac{\sqrt{R(0)_{BL} - R(2\tau_d)_{BL}}}{\sqrt{R(0)_{BL}}}. \tag{7-3}$$

For $\tau_d = 1/2$ chip, the mean square delay lock loop error is approximately 1/2 the tau dither, i.e., a 3 dB advantage for the delay lock. However, since considerations such as use of an existing receiver development for Shuttle may dictate the use of a tau dither tracking loop receiver, the C/N_0 requirements for code tracking (range measurement) will be determined by a tau dither loop.

Going one step further, it is appropriate at this point in the Shuttle/GPS study to base the requirements on a noncoherent tau dither tracking loop receiver. The rms tracking error for the noncoherent tau dither loop is given by

$$\sigma = \left\{ B_L \left[\frac{1}{C/N_0} + \frac{2B_{IF}}{(C/N_0)^2} \right] \right\}^{1/2} \quad \text{(chips)}, \tag{7-4}$$

where

B_L = one-sided loop noise bandwidth

B_{IF} = IF bandwidth.

This equation is plotted in Figure 7-2, where C/N_0 is shown plotted as a function of σ for the case of $B_L = 1.6$ Hz and $B_{IF} = 200$ Hz, the GPSPAC
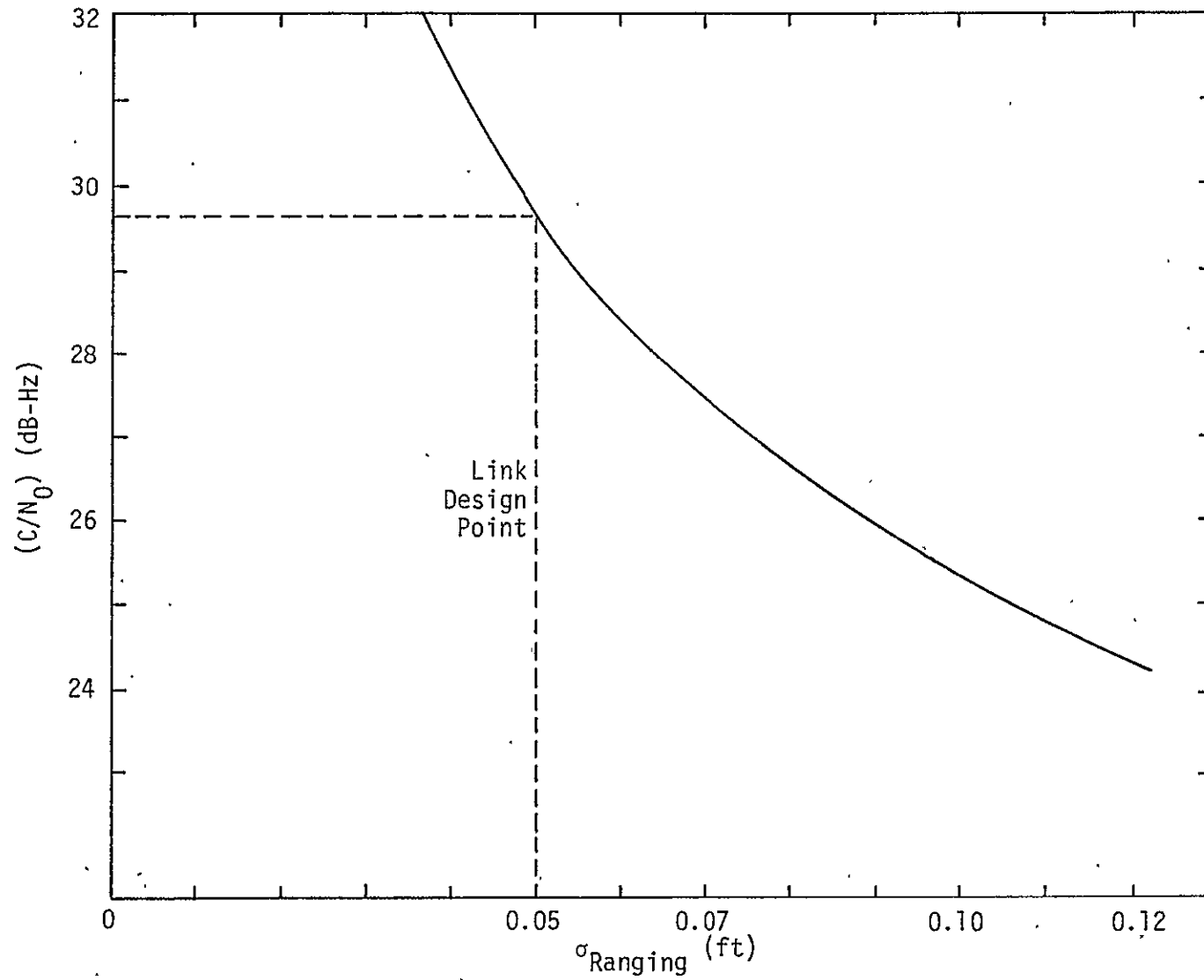
Figure 7-2.   Relationship Between GPS Ranging Error and Link C/N_0 for a Noncoherent
Tau-Dither GPS Receiver

receiver parameters. From this curve, C/N_0 required for PN tracking (range measurement) is found to be 29.6 dB.

The required C/N_0 for carrier tracking is determined from several considerations. These considerations are:

1. Allowable "noisy reference" degradation to data detection performance.
2. Required doppler measurement accuracy.
3. Link signal dynamics and receiver threshold requirements.

It is not the intention of this discussion to analyze each of these factors. However, previous analysis and experience with GPS-type receivers has indicated that a 15° rms (1. σ) phase error jitter is a reasonable requirement. This requirement will be examined in detail during the FY'78 study. The 15° jitter requirement can be related to C/N_0 from the equation

$$\sigma_\phi^2 = \frac{1}{C/N_0 \, B_L \, S_L} , \qquad (7-5)$$

where

B_L = one-sided Costas loop noise bandwidth (35 Hz for the GPSPAC receiver)

S_L = squaring loss due to the Costas loop third multiplier.

The squaring loss is determined by several factors and is given by

$$S_L = \frac{D_m}{K_D + K_L \dfrac{B_i/R_s}{2 R_d D_m}} , \qquad (7-6)$$

where

D_m = modulation distortion factor

B_i/R_s = ratio of two-sided filter bandwidth to data rate

K_L = 0.75 for a typical 2-pole Butterworth filter

R_d = data signal-to-noise ratio

K_d = constant related to data spectrum and filter type.

Fortunately, the squaring loss has been evaluated for a Costas loop with an RC arm filter and NRZ data, and is shown plotted in Figure 7-3
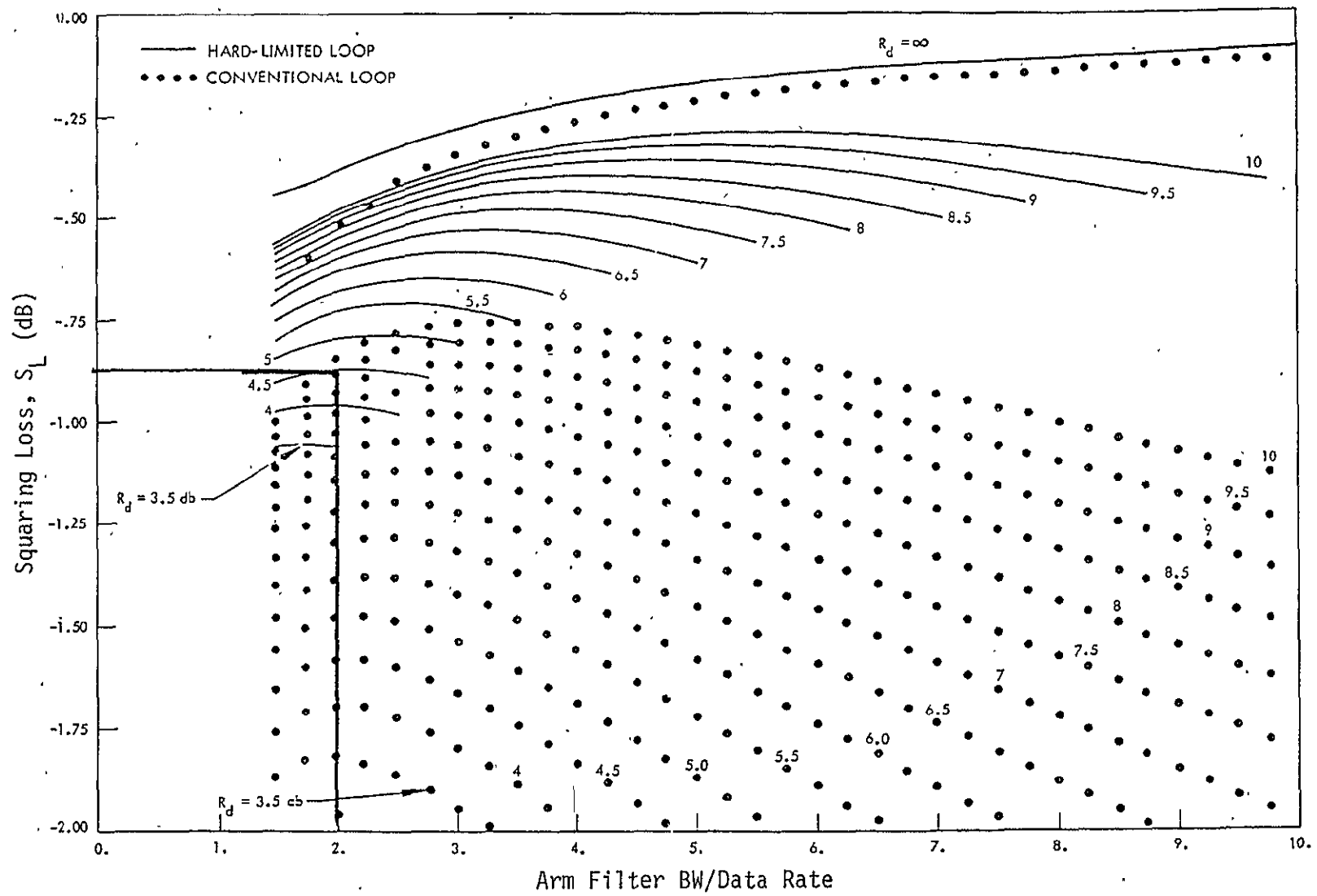
Figure 7-3. Costas Loop Squaring Loss as a Function of E_b/N_0 and Arm Filter Bandwidth

as a function of arm filter bandwidth and data signal-to-noise ratio. Thus, for $E_b/N_0 = 9.6$ dB $(BER = 10^{-5})$, $B_L = 35$ Hz, and a 15° allowable phase jitter, C/N_0 is found to be 28.0 dB. An implementation loss of 1.5 dB for PN losses brings the required C/N_0 for carrier tracking to 29.5 dB.

The C/N_0 required for data detection is based on desired bit error rate of 10^{-5}. The bit error rate versus E_b/N_0, or signal-to-noise ratio for PSK data modulation is given in Figure 7-4, and the required theoretical E_b/N_0 is seen to be 9.6 dB. To this value, the various. receiver implementation losses must be added to arrive at the actual signal-to-noise ratio. For a PN communication system operating with a C/N_0 of approximately 30 dB, the appropriate loss budget is presented in Table 7-1.

Table 7-1. Implementation Losses

Filter Loss	1.0 dB
PN Jitter Loss	0.5 dB
Noisy Reference Loss (Costas Jitter)	0.1 dB
Bit Synchronization Loss	0.2 dB
Carrier Reference Offset Loss (due to on-orbit static phase error)	0.2 dB
Total	2.0 dB

Thus, the actual required C/N_0 for data detection is

$$C/N_0 = 9.6 + 2.0 + 10 \log (50) = 28.6 \text{ dB} . \qquad (7-7)$$

7.2 Basic Link Budgets

The basic elements of the Shuttle/GPS RF link are depicted in Figure 7-5. This report will treat the GPS satellite primarily from a specified EIRP point of view, although some indication of the variation in EIRP that might be expected is given in Appendix A. Atmospheric loss has not been included as an element in the link for reasons which are explained in Section 7.8. The space loss value of -184.6 dB (L1) that is used in all the link calculations in this report is for the case where the line-of-sight path from the Orbiter to the GPS satellite is tangent to the orbit, as depicted in Figure 7-6. This is a reasonable
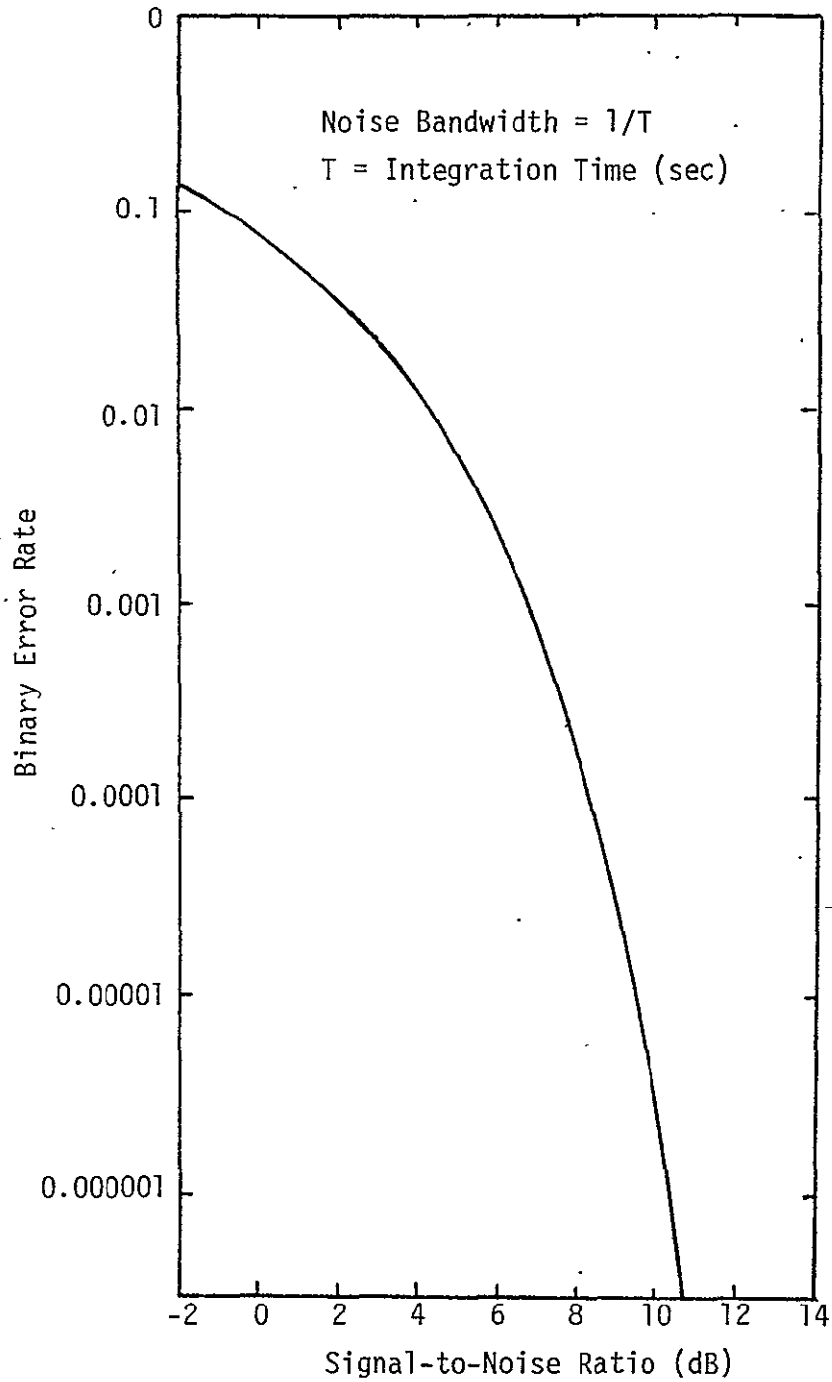
Figure 7-4. Error Rate Versus Signal-to-Noise Performance for Phase Shift System With Ideal Local Phase Reference

*Gain = -1 dB, Noise Temp = 125°K
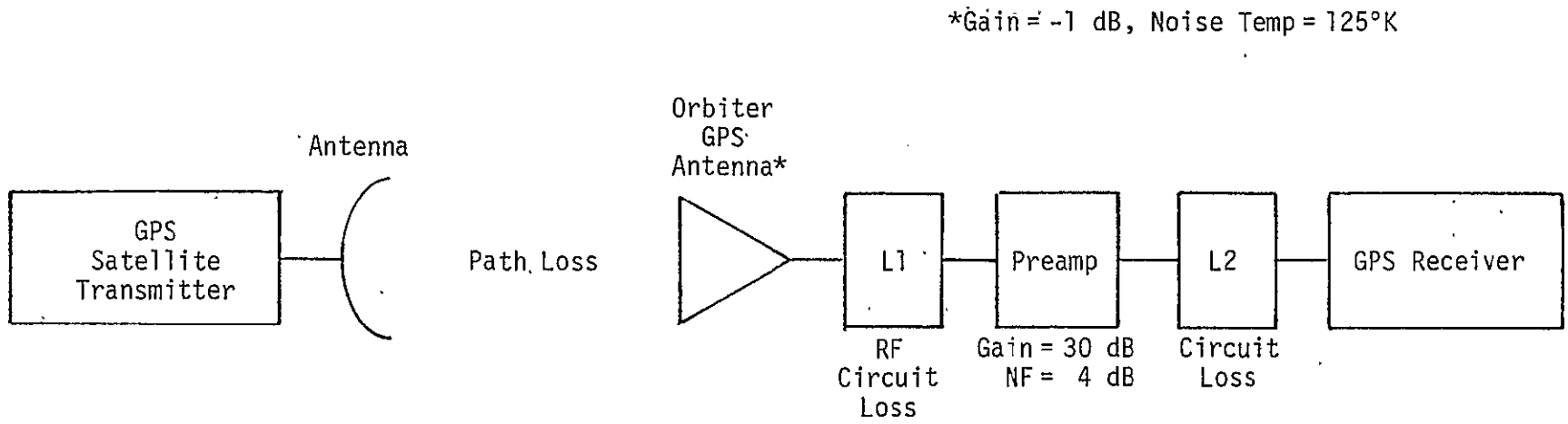
EIRP (Spec), dBw		
	L1	L2
P	23.8	19.1
C/A	26.8	19.1

Figure 7-5. Basic Elements of Shuttle/GPS RF Link
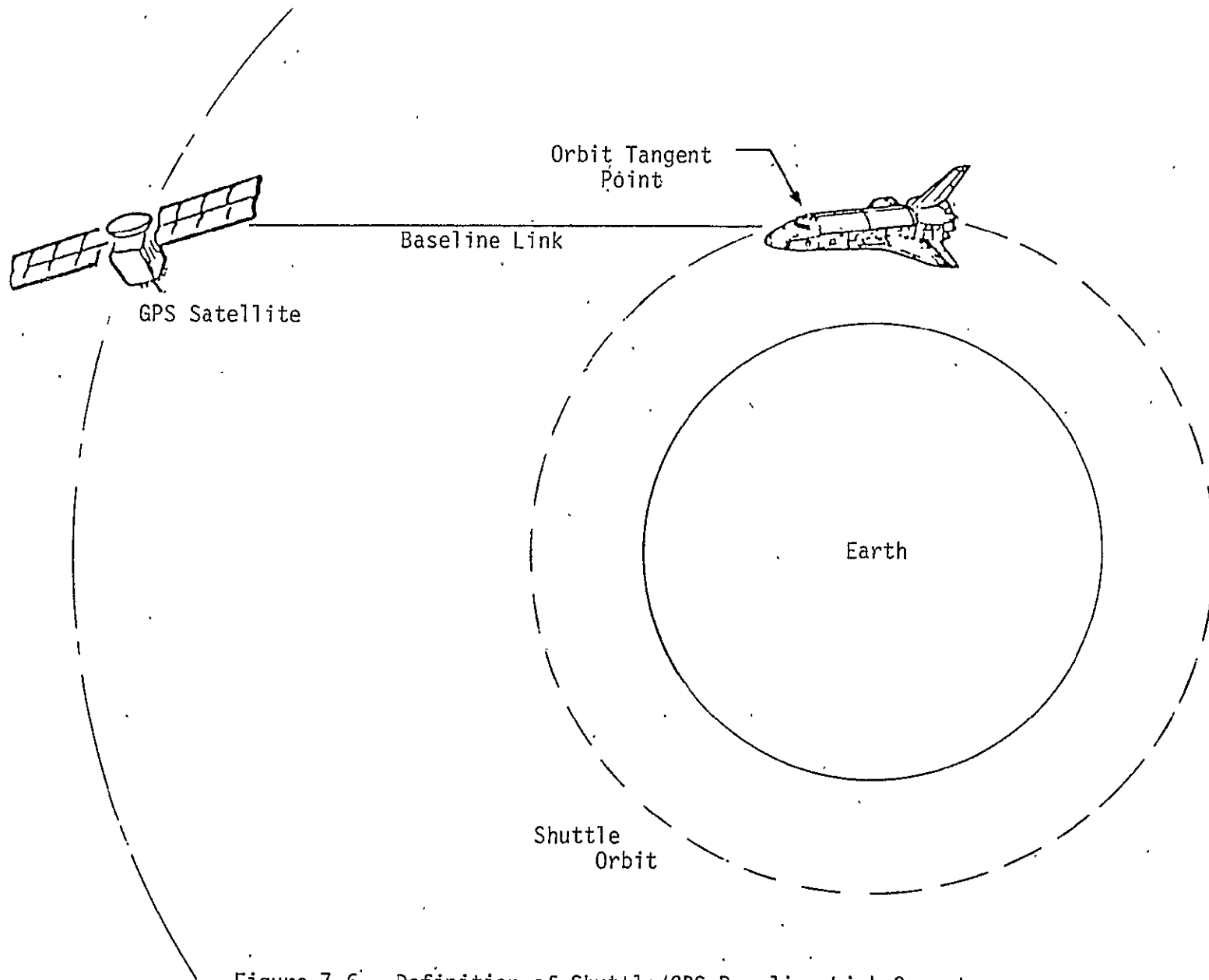
Figure 7-6. Definition of Shuttle/GPS Baseline Link Geometry

baseline and represents the same geometry for which the Shuttle on-orbit baseline telecommunication links have been calculated. The Orbiter antenna gain is given a value of -1 dB RHCP, as this has been found to be an achievable gain value (see Section 5.2). The RF circuit loss from the antenna to the preamp is more difficult to tie down at this point, since it depends strongly on.the specific system design, taking into account antenna location, preamp location, and redundancy configuration. The baseline system configuration analyzed for the study is shown in Figure 7-7. This configuration was developed jointly with RI and represents a perturbation to the configuration which RI identified as Configuration II in "GPS Orbiter Interface, Interim Operational Proposal," August 1, 1977. The perturbation is the elimination of the MTV/GPS switch, since the MTV function has been eliminated from consideration. RI has calculated the circuit loss between the upper antenna and the GPS preamp and between the lower antenna and GPS preamp to be the values shown in Table 7-2. It should be noted that this configuration provides an upper antenna and a lower antenna, but the coverage is less than 2π steradians, as indicated in Figure 7-8. Furthermore, this configuration is for location of the GPS receivers in the payload bay, a consideration which will be studied carefully during FY'78.

Table 7-2. RF Circuit Loss for Baseline Shuttle/GPS Configuration

	Loss (dB)			
	Upper Antenna		Lower Antenna	
Loss Source	L1	L2	L1	L2
Antenna to Preamp (L_A)	2.0	1.8	2.48	2.35
Effective Preamp to Receiver (LC)	0.14	0.12	0.12	0.10
Total	2.14	1.92	2.60	2.45

. Since the GPS preamp typically has a gain of about 30 dB and a noise figure of approximately 4 dB, the circuit loss between the preamp and the receivers does not generally contribute very much to
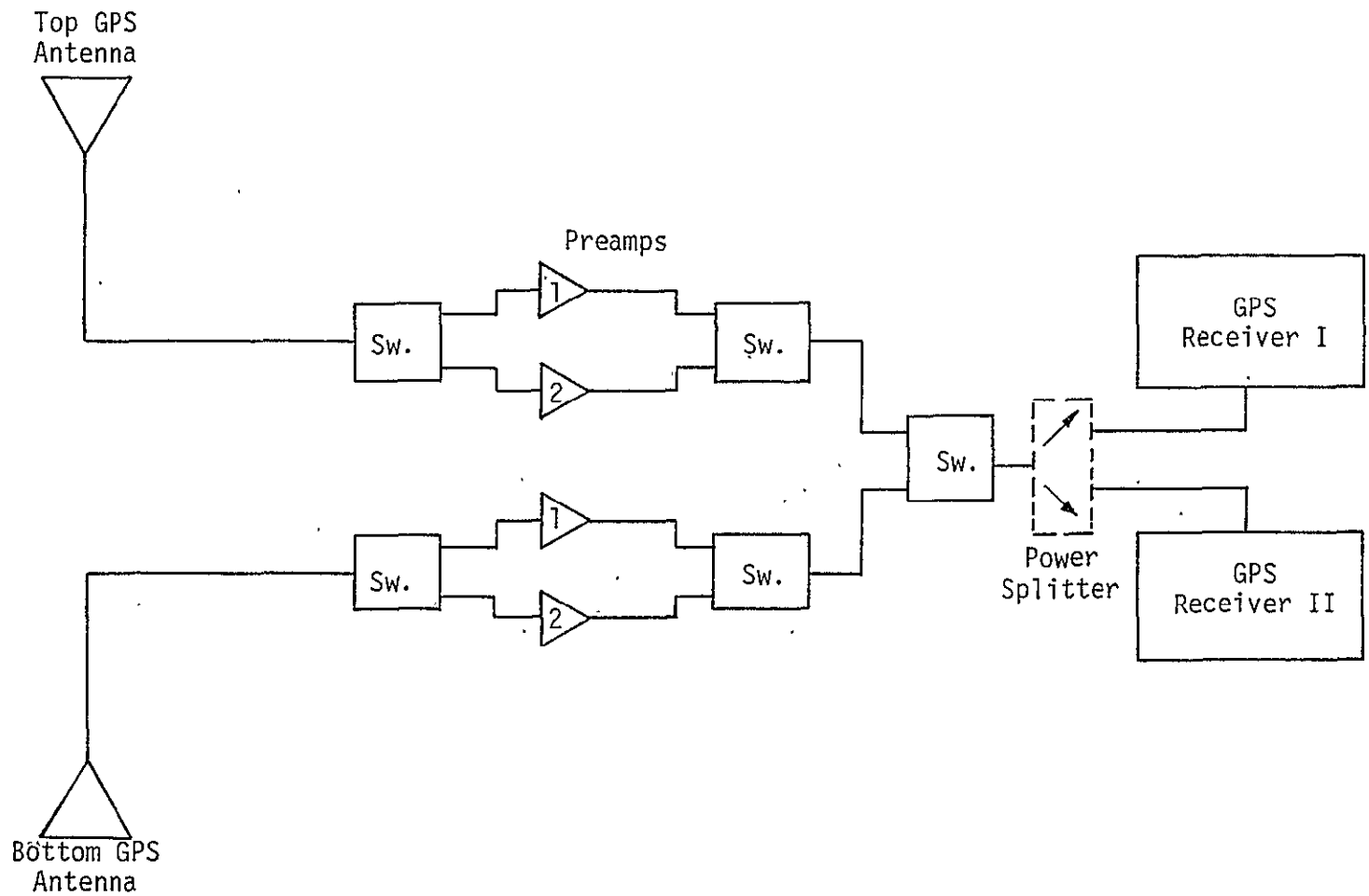
Figure 7-7. Baseline Shuttle/GPS System Configuration
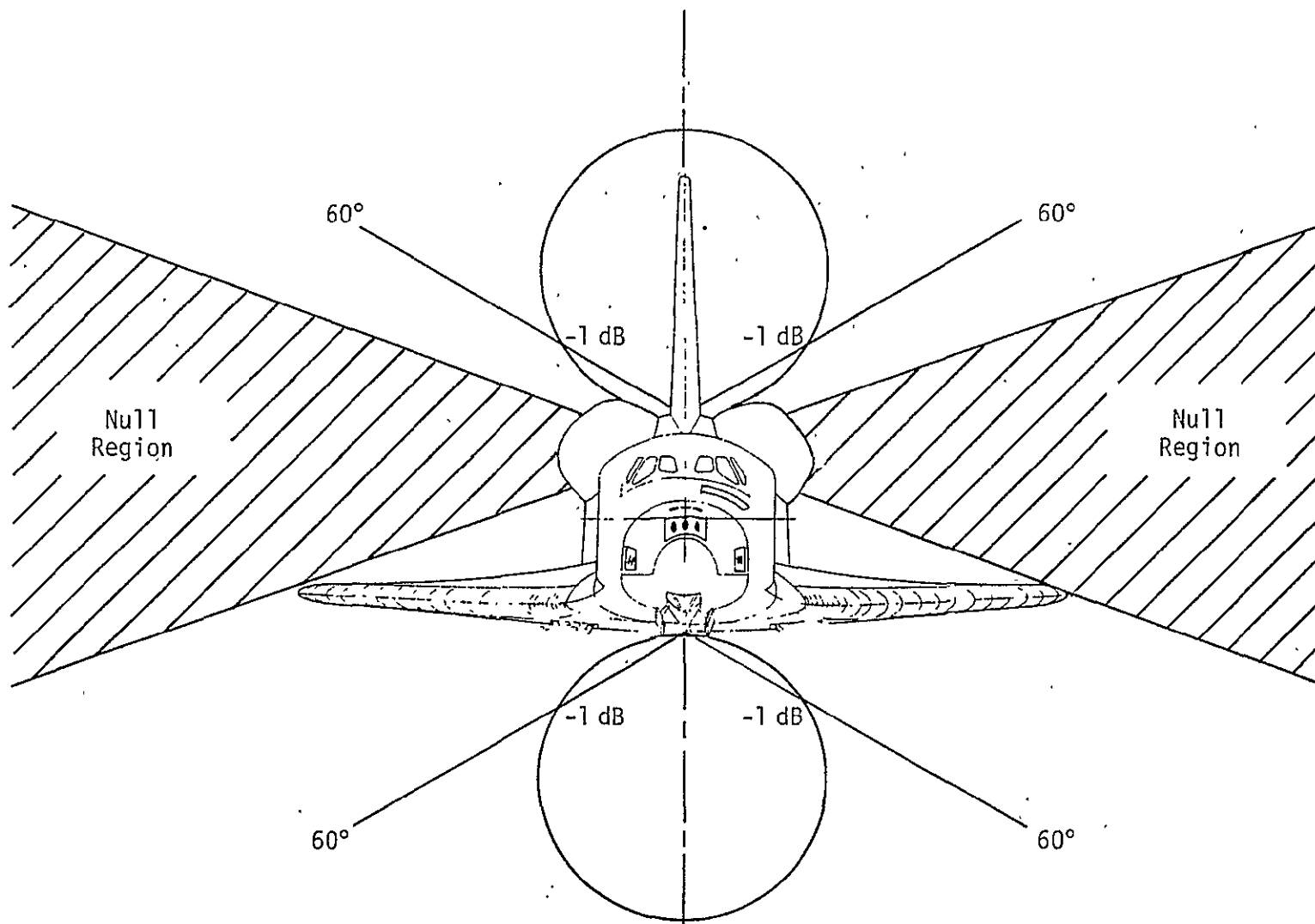
Figure 7-8. Approximate Antenna Coverage for Baseline Shuttle GPS System

the effective signal-to-noise ratio circuit loss. The effect of these losses on the effective signal-to-noise ratio circuit loss is shown plotted in Figure 7-9 for the 30 dB gain and 4 dB noise figure preamp. Using this curve, RI has determined the effective losses to be those values given in Table 7-2.

The link elements which have been discussed above have been factored into the Shuttle/GPS baseline system link budgets, which are given in Tables 7-3 through 7-6 for the P and C/A codes on both L1 and L2. Tables 7-7 through 7-14 are the baseline link budgets for carrier tracking and data detection. It should be noted that the C/N_0 requirement for the L2 links is based on a 7-ft 1-σ range error (70 ft for C/A). The explanation for this is discussed in Section 7.4.

7.3   Summary of Link Performance

In Section 7.2, the detailed link budgets for the baseline system studied during the contract were presented. These results are summarized in Table 7-15, and the meaning of the results is discussed. In addition, the link budget summary for a system called the test or experimental system that was examined prior to definition of the baseline system is presented in Table 7-16. A block diagram and conceptual drawing of the test system are presented in Figures 7-10 and 7-11, respectively.

The following conclusions can be drawn from examining these results:

1. For the baseline configuration, the lower antenna provides the limiting performance. This is due to the increased RF cable loss.

2. The ranging function is the most critical of the three basic receiver functions.

3. The L2 margins are all less than the L1 margins (due to lower satellite EIRP). However, the L2 link margins should not be used as an assessment of link performance, as discussed in Section 7.4.

4. The limiting performance is thus for the lower antenna, L1-P for ranging, and results in a link margin of 4.3 dB.

5. On link L2, the P and C/A margins are identical because, on L2 only, P and C/A codes are not transmitted simultaneously, as they are on L1. The L2 ranging and carrier
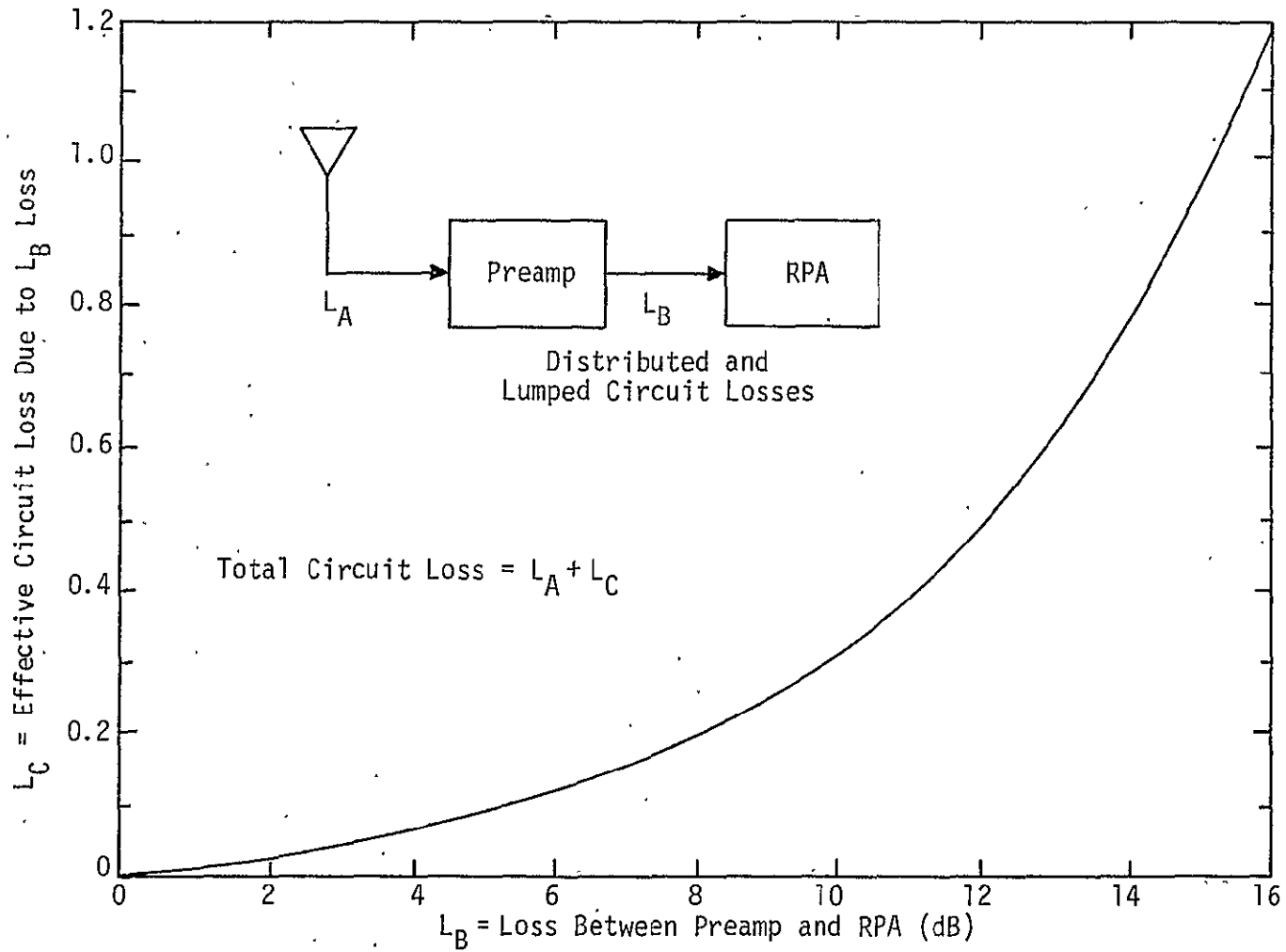
Figure 7-9. Effects of Circuit Loss on Margin

Table 7-3. Baseline Link Budget for Range Measurement, L1-P

Link L1-P, Range
Lower Antenna
Orbital Geometry: Path Tangential to Orbit

PARAMETER	VALUE	EXPLANATION
Satellite EIRP	23.8 dBw	EOE, Spec. CID-SV-10H
Space Loss	-184.6 dB	Path Tangent to Orbit
Pointing Loss	- 0.4 dB	
Polarization Loss	- 0.4 dB	
Atmospheric Loss	0	
Shuttle Antenna Gain	- 1.0 dB	
Circuit Loss	- 2.6 dB	Table 7-2
Received Power	-165.1 dBw	
System Noise Temperature	27.5 dBK	$T_{sys} = 563°K$; $T_{ant} = 125°K$
Boltzmann's Constant	-228.6 dB-W/K/Hz	
Noise Spectral Density	-201.1 dB-W/Hz	
C/N_0	35.9 dB-Hz	———
Required C/N_0 (Theoretical)	29.6 dB-Hz	$\sigma_{Range} = 5'$ Eq. (7-4)
Implementation Loss	2.0 dB	Table 7-1
Required C/N_0	31.6 dB-Hz	
LINK MARGIN	4.3 dB	

Table 7-4. Baseline Link Budget for Range Measurement, L1-C/A

Link L1-C/A, Range
Lower Antenna
Orbital Geometry: Path Tangential to Orbit

PARAMETER	VALUE	EXPLANATION
Satellite EIRP	26.8 dBw	EOE, Spec. CID-SV-10H
Space Loss	-184.6 dB	Path Tangent to Orbit
Pointing Loss	- 0.4 dB	
Polarization Loss	- 0.4 dB	
Atmospheric Loss	0	
Shuttle Antenna Gain	- 1.0 dB	
Circuit Loss	- 2.6 dB	Table 7-2
Received Power	-162.1 dBw	
System Noise Temperature	27.5 dBK	$T_{sys} = 563°K; T_{ant} = 125°K$
Boltzmann's Constant	-228.6 dB-W/K/Hz	
Noise Spectral Density	-201.1 dB-W/Hz	
C/N_0	38.9 dB-Hz	
Required C/N_0 (Theoretical)	29.6 dB-Hz	$\sigma_{Range} = 50'$ Eq. (7-4)
Implementation Loss	2.0 dB	Table 7-1
Required C/N_0	31.6 dB-Hz	
LINK MARGIN	7.3 dB	

Table 7-5.   Baseline Link Budget for Range Measurement, L2-P

Link L2-P, Range
Lower Antenna
Orbital Geometry: Path Tangential to Orbit

PARAMETER	VALUE	EXPLANATION
Satellite EIRP	19.1 dBw	EOE; Spec. CID-SV-10H
Space Loss	-182.4 dB	Path Tangent to Orbit
Pointing Loss	- 0.4 dB	
Polarization Loss	- 0.4 dB	
Atmospheric Loss	0	
Shuttle Antenna Gain	- 1.0 dB	
Circuit Loss	- 2.5 dB	Table 7-2
Received Power	-167.6 dBw	
System Noise Temperature	27.5 dBK	$T_{sys} = 563°K$; $T_{ant} = 125°K$
Boltzmann's Constant	-228.6 dB-W/K/Hz	
Noise Spectral Density	-201.1 dB-W/Hz	
C/N_0	33.4 dB-Hz	
Required C/N_0 (Theoretical)	27.5 dB-Hz	$\sigma_{Range} = 7'$ Eq. (7-4)
Implementation Loss	2.0 dB	Table 7-1
Required C/N_0	29.5 dB-Hz	
LINK MARGIN	3.9 dB	

Table 7-6. Baseline Link Budget for Range Measurement, L2-C/A

Link L2-C/A, Range
Lower Antenna
Orbital Geometry: Path Tangential to Orbit

PARAMETER	VALUE	EXPLANATION
Satellite EIRP	19.1 dBw	EOE, Spec. CID-SV-10H
Space Loss	-182.4 dB	Path Tangent to Orbit
Pointing Loss	- 0.4 dB	
Polarization Loss	- 0.4 dB	
Atmospheric Loss	0	
Shuttle Antenna Gain	- 1.0 dB	
Circuit Loss	- 2.5 dB	Table 7-2
Received Power	-167.6 dBw	
System Noise Temperature	27.5 dBK	$T_{sys} = 563°K$; $T_{ant} = 125°K$
Boltzmann's Constant	-228.6 dB-W/K/Hz	
Noise Spectral Density	-201.1 dB-W/Hz	
C/N_0	33.4 dB-Hz	
Required C/N_0 (Theoretical)	27.5 dB-Hz	$\sigma_{Range} = 70'$ Eq. (7-4)
Implementation Loss	2.0 dB	Table 7-1
Required C/N_0	29.5 dB-Hz	
LINK MARGIN	3.9 dB	

Table 7-7. Baseline Link Budget for Carrier Tracking, L1-P

Link L1-P, Carrier
Lower Antenna
Orbital Geometry: Path Tangential to Orbit

PARAMETER	VALUE	EXPLANATION
Satellite EIRP	23.8 dBw	EOE, Spec. CID-SV-10H
Space Loss	-184.6 dB	Path Tangent to Orbit
Pointing Loss	- 0.4 dB	
Polarization Loss	- 0.4 dB	
Atmospheric Loss	0	
Shuttle Antenna Gain	- 1.0 dB	
Circuit Loss	- 2.6 dB	Table 7-2
Received Power	-165.1 dBw	
System Noise Temperature	27.5 dBK	$T_{sys} = 563°K$; $T_{ant} = 125°K$
Boltzmann's Constant	-228.6 dB-W/K/Hz	
Noise Spectral Density	-201.1 dB-W/Hz	
C/N_0	35.9 dB-Hz	
Required C/N_0 (Theoretical)	28.0 dB-Hz	$\sigma_{Jitter} = 15°$ Eq. (7-5) Fig. 7-3
Implementation Loss	1.5 dB	Table 7-1 (filtering and PN loss)
Required C/N_0	29.5 dB-Hz	
LINK MARGIN	6.4 dB	

Figure 7-8. Baseline Link Budget for Carrier Tracking, L1-C/A

Link L1-C/A, Carrier
Lower Antenna
Orbital Geometry: Path Tangential to Orbit

PARAMETER	VALUE	EXPLANATION
Satellite EIRP	26.8 dBw	EOE, Spec. CID-SV-10H
Space Loss	-184.6 dB	Path Tangent to Orbit
Pointing Loss	- 0.4 dB	
Polarization Loss	- 0.4 dB	
Atmospheric Loss	0	
Shuttle Antenna Gain	- 1.0 dB	
Circuit Loss	- 2.6 dB	Table 7-2
Received Power	-162.1 dBw	
System Noise Temperature	27.5 dBK	$T_{sys} = 563°K$; $T_{ant} = 125°K$
Boltzmann's Constant	-228.6 dB-W/K/Hz	
Noise Spectral Density	-201.1 dB-W/Hz	
C/N_0	38.9 dB-Hz	
Required C/N_0 (Theoretical)	28.0 dB-Hz	$\sigma_{Jitter} = 15°$ Eq. (7-5) Fig. 7-3
Implementation Loss	1.5 dB	Table 7-1 (filtering and PN loss)
Required C/N_0	29.5 dB-Hz	
LINK MARGIN	9.4 dB	

Table 7-9. Baseline Link Budget for Carrier Tracking, L2-P

Link L2-P, Carrier
Lower Antenna
Orbital Geometry: Path Tangential to Orbit

PARAMETER	VALUE	EXPLANATION
Satellite EIRP	19.1 dBw	EOE, Spec: CID-SV-10H
Space Loss	-182.4 dB	Path Tangent to Orbit
Pointing Loss	- 0.4 dB	
Polarization Loss	- 0.4 dB	
Atmospheric Loss	0	
Shuttle Antenna Gain	- 1.0 dB	
Circuit Loss	- 2.5 dB	Table 7-2
Received Power	-167.6 dBw	
System Noise Temperature	27.5 dBK	$T_{sys} = 563°K$; $T_{ant} = 125°K$
Boltzmann's Constant	-228.6 dB-W/K/Hz	
Noise Spectral Density	-201.1 dB-W/Hz	
C/N_0	33.4 dB-Hz	
Required C/N_0 (Theoretical)	28.0 dB-Hz	$\sigma_{Jitter} = 15°$ Eq. (7-5) Fig. 7-3
Implementation Loss	1.5 dB	Table 7-1 (filtering and PN loss)
Required C/N_0	29.5 dB-Hz	
LINK MARGIN	3.9 dB	

Table 7-10. Baseline Link Budget for Carrier Tracking, L2-C/A

Link L2-C/A, Carrier
Lower Antenna
Orbital Geometry: Path Tangential to Orbit

PARAMETER	VALUE	EXPLANATION
Satellite EIRP	19.1 dBw	EOE, Spec. CID-SV-10H
Space Loss	-182.4 dB	Path Tangent to Orbit
Pointing Loss	- 0.4 dB	
Polarization Loss	- 0.4 dB	
Atmospheric Loss	0	
Shuttle Antenna Gain	- 1.0 dB	
Circuit Loss	- 2.5 dB	Table 7-2
Received Power	-167.6 dBw	
System Noise Temperature	27.5 dBK	$T_{sys} = 563°K$; $T_{ant} = 125°K$
Boltzmann's Constant	-228.6 dB/W/K/Hz	
Noise Spectral Density	-201.1 dB-W/Hz	
C/N_0	33.4 dB-Hz	
Required C/N_0 (Theoretical)	28.0 dB-Hz	Jitter $= 15°$ Eq. (7-5) Fig. 7-3
Implementation Loss	1.5 dB	Table 7-1 (filtering and PN loss)
Required C/N_0	29.5 dB-Hz	
LINK MARGIN	3.9 dB	

Table 7-11. Baseline Link Budget for Data Detection, L1-P

Link L1-P, Data Detection
Lower Antenna
Orbital Geometry: Path Tangential to Orbit

PARAMETER	VALUE	EXPLANATION
Satellite EIRP	23.8 dBw	EOE, Spec. CID-SV-10H
Space Loss	-184.5 dB	Path Tangent to Orbit
Pointing Loss	- 0.4 dB	
Polarization Loss	- 0.4 dB	
Atmospheric Loss	0	
Shuttle Antenna Gain	- 1.0 dB	
Circuit Loss	- 2.6 dB	Table 7-2
Received Power	-165.1 dBw	
System Noise Temperature	27.5 dBK	$T_{sys} = 563°K$; $T_{ant} = 125°K$
Boltzmann's Constant	-228.6 dB-W/K/Hz	
Noise Spectral Density	-201.1 dB-W/Hz	
C/N_0	35.9 dB-Hz	——
Required C/N$_0$ (Theoretical)	26.6 dB-Hz	$BER = 10^{-5}$ Eq. (7-7) Fig. 7-4
Implementation Loss	2.0 dB	Table 7-1
Required C/N_0	28.1 dB	
LINK MARGIN	7.3 dB	

Table 7-12. Baseline Link Budget for Data Detection, L1-C/A

Link L1-C/A, Data Detection
Lower Antenna
Orbital Geometry: Path Tangential to Orbit

PARAMETER	VALUE	EXPLANATION
Satellite EIRP	26.8 dBw	EOE, Spec. CID-SV-10H
Space Loss	-184.6 dB	Path Tangent to Orbit
Pointing Loss	- 0.4 dB	
Polarization Loss	- 0.4 dB	
Atmospheric Loss	0	
Shuttle Antenna Gain	- 1.0 dB	
Circuit Loss	- 2.6 dB	Table 7-2
Received Power	-162.1 dBw	
System Noise Temperature	27.5 dBK	$T_{sys} = 563°K$; $T_{ant} = 125°K$
Boltzmann's Constant	-228.6 dB-W/K/Hz	
Noise Spectral Density	-201.1 dB-W/Hz	
C/N_0	38.9 dB-Hz	
Required C/N_0 (Theoretical)	26.6 dB-Hz	$BER = 10^{-5}$ Eq. (7-7) Fig. 7-4
Implementation Loss	2.0 dB	Table 7-1
Required C/N_0	28.6 dB-Hz	
LINK MARGIN	10.3 dB	

Table 7-13. Baseline Link Budget for Data Detection, L2-P

Link L2-P, Data Detection
Lower Antenna
Orbital Geometry: Path Tangential to Orbit

PARAMETER	VALUE	EXPLANATION
Satellite EIRP	19.1 dBw	EOE, Spec. CID-SV-10H
Space Loss	-182.4 dB	Path Tangent to Orbit
Pointing Loss	- 0.4 dB	
Polarization Loss	- 0.4 dB	
Atmospheric Loss	0	
Shuttle Antenna Gain	- 1.0 dB	
Circuit Loss	- 2.5 dB	Table 7-2
Received Power	-167.6 dBw	
System Noise Temperature	27.5 dBK	$T_{sys} = 563°K$; $T_{ant} = 125°K$
Boltzmann's Constant	-228.6 dB-W/K/Hz	
Noise Spectral Density	-201.1 dB-W/Hz	
C/N_0	33.4 dB-Hz	
Required C/N_0 (Theoretical)	26.6 dB-Hz	$BER = 10^{-5}$ Eq. (7-7) Fig. 7-4
Implementation Loss	2.0 dB	Table 7-1
Required C/N_0	28.6 dB-Hz	
LINK MARGIN	4.8 dB	

Table 7-14. Baseline Link Budget for Data Detection, L2-C/A

Link L2-C/A, Data Detection
Lower Antenna
Orbital Geometry: Path Tangential to Orbit

PARAMETER	VALUE	EXPLANATION
Satellite EIRP	19.1 dBw	EOE, Spec. CID-SV-10H
Space Loss	-182.4 dB	Path Tangent to Orbit
Pointing Loss	- 0.4 dB	
Polarization Loss	- 0.4 dB	
Atmospheric Loss	0	
Shuttle Antenna Gain	- 1.0 dB	
Circuit Loss	- 2.5 dB	Table 7-2
Received Power	-167.6 dBw	
System Noise Temperature	27.5 dBK	$T_{sys} = 563°K$; $T_{ant} = 125°K$
Boltzmann's Constant	-228.6 dB-W/K/Hz	
Noise Spectral Density	-201.1 dB-W/Hz	
C/N_0	33.4 dB-Hz	
Required C/N_0 (Theoretical)	26.6 dB-Hz	$BER = 10^{-5}$ Eq. (7-7) Fig. 7-4
Implementation Loss	2.0 dB	Table 7-1
Required C/N_0	28.6 dB-Hz	
LINK MARGIN	4.8 dB	

Table 7-15. Baseline System Configuration, On-Orbit Link Margin Summary

| Link | | Link Margin by Function | | |
		Ranging (dB)	Carrier (dB)	Data (dB)
Lower Antenna				
L1	P	4.3	6.4	7.3
	C/A	7.3	9.4	10.3
L2	P	3.9	3.9	4.8
	C/A	3.9	3.9	4.8
Upper Antenna				
L1	P	4.8	6.9	7.8
	C/A	7.8	8.9	10.8
L2	P	4.4	4.4	5.3
	C/A	4.4	4.4	5.3

Table 7-16. Experimental System, Antenna in Payload Bay, On-Orbit Link Margin Summary

| Link | Link Margin by Function | | |
	Ranging (dB)	Carrier (dB)	Data (dB)
Payload Bay Antenna			
P	6.9	9.0	9.9
C/A	9.9	12.0	12.9
Window Antenna			
P	4.9	7.0	7.9
C/A	7.9	10.0	10.9
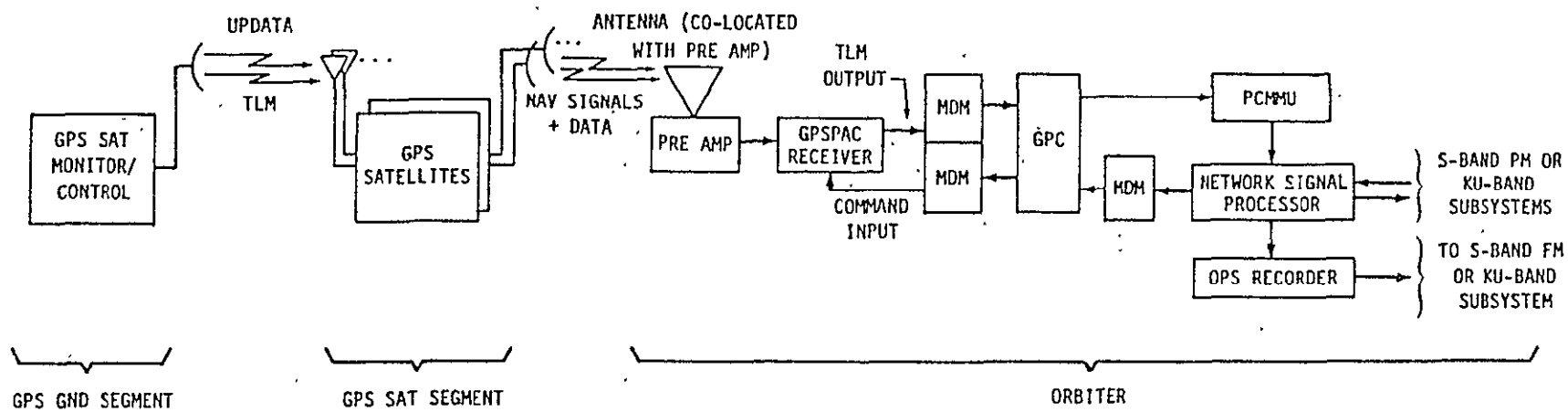
Figure 7-10. Functional Block Diagram of OFT Test/Demonstration System (Phase I)

PAYLOAD BAY LOCATION

ANTENNA AT   X = 1087
             Y = 44
             Z = 482.6

IECM
STACKED ANTENNA
DFI CONT NO. 1
PRE AMP UNIT
DFI CONT NO. 3
BOOM SUPPORT STRUCTURE
DFI CONT NO. 2
FWD
SUPPORT PNL
DFI PALLET STRUCTURE
HONEY COMB PNL
GPS PACKAGE
Yo 0.0

DFI PALLET INSTALLATION
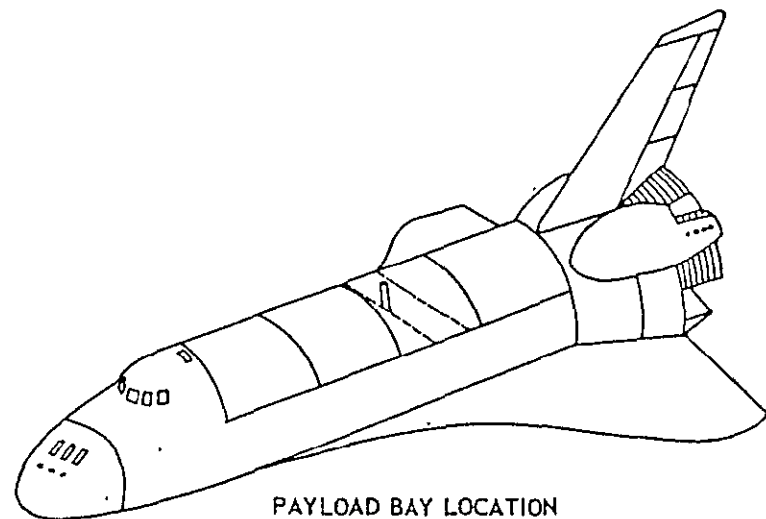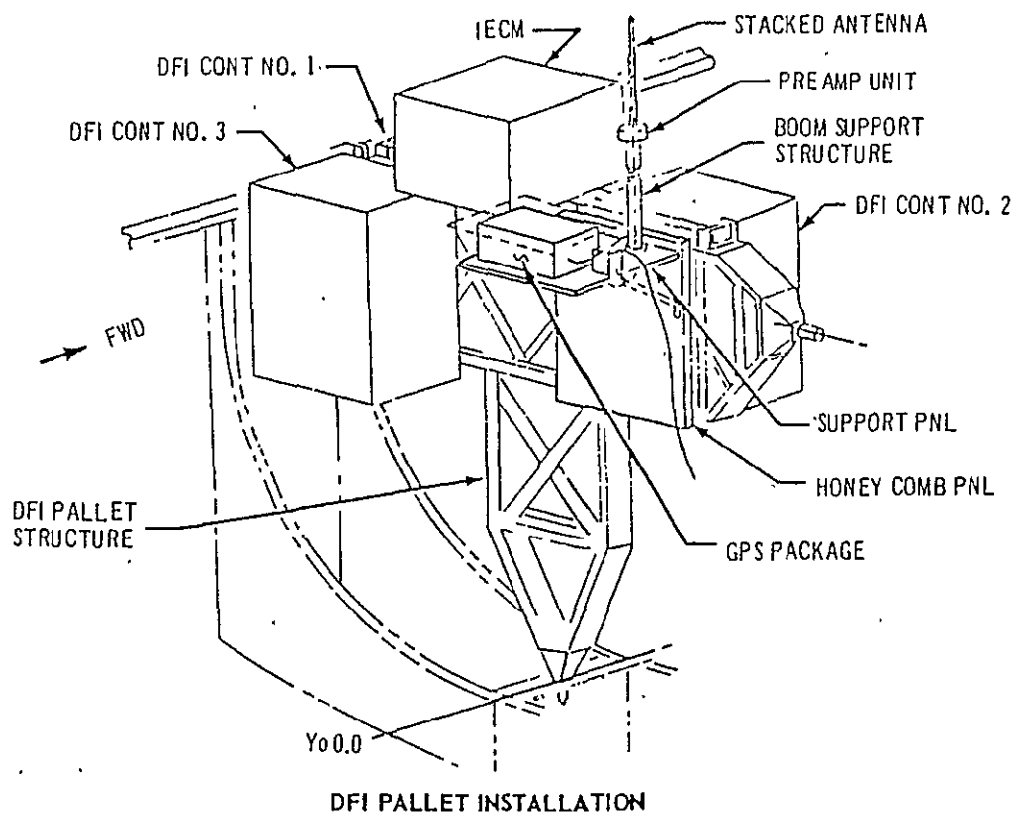
Figure 7-11.   OFT Test/Demonstration Installation Concept (Phase I)

tracking margins are the same only as a result of some
numerical coincidences.

. It is important to note that these margins are for on-orbit links, for
steady-state operation, i.e., they do not represent acquisition or
loss of lock (threshold) margins. These conditions will be studied
in detail for both on-orbit and ascent and entry operations.

The link margin summary for the test system studied for possible
early OFT operation is given in Table 7-16. This table includes margins
for both the payload bay-mounted antenna and the window-mounted antenna.
The basic reason for the superior link performance for the payload bay
antenna is the elimination of the feedline loss between the antenna and
preamp due to the mounting of the antenna integrally with the preamp.

7.4   L1 Versus L2 Measurement Accuracy Requirements

The GPS navigation signal design consists of a 1575.4 MHz, PN
modulated, carrier designated as L1 and a 1227.7 MHz, PN modulated,
carrier designated as L2. The satellite transmitter is designed so
that the L1 EIRP is 4.7 dB greater than the L2 EIRP. When the differ-
ence in path loss, due to the difference in frequency, is accounted for,
L1 has a net advantage of 2.5 dB over L2. This, of course, results in
poorer range, doppler, and data performance for the L2 link. The
reason the system is designed this way can be appreciated from con-
sideration of Figure 7-12: As can be seen the receiver processing
utilizes the L2 measurement to calculate an L1-L2 factor that is used
for ionospheric delay correction of the basic L1 measurement. Further-
more, the L1-L2 factor is averaged in a first-order filter for approxi-
mately 10 measurements, thus improving the effective L2 one-σ measure-
ment error by $\sqrt{10}$. Of basic importance is the fact that L2 exists only
as an ionospheric delay correction factor and that, if the link did not
propagate through the ionosphere, there would be no need for L2.

7.5   Analysis of Downlink Data Rate Requirements

The baseline system that was studied utilized the GPSPAC GPS
receiver. The output of this receiver is stored in 12 files which are
individually addressable for downlink telemetry. These files are listed
in Table 7-17. Since the GPSPAC was designed to be flown on an unmanned
satellite, having a mission design life of several years, the organization
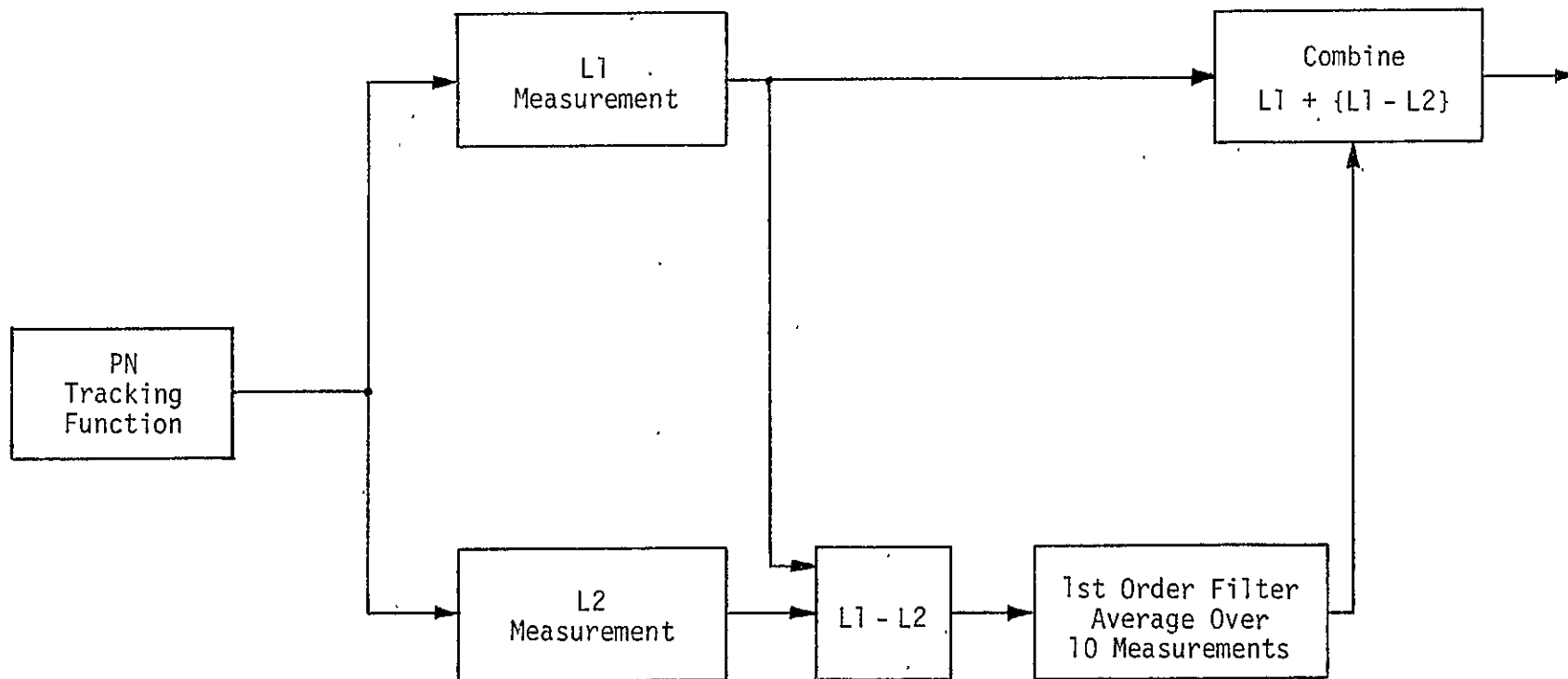
Figure 7-12.   L1/L2 Range Measurement Processing - Functional Block Diagram

Table 7-17. Baseline System Receiver Output Data File Organization

File Number	File Name	Size (bits)
0*	Command Echo Buffer	944
1**	Memory Load Bit Map	672
2*	R/PA Memory Contents	944
3	Current Operating Ephemeris	2832
4	System Status	688
5	NDS Almanacs	4720
6	Time Marks	912
7	Navigation Best Estimate	560
8	Kalman Input, Single Channel	432
9	Kalman Input, Dual Channel	816
10	Measurement Data	320
11	Compressed Measurement Data	896

*Output only when R/PA is in Command mode
**Output only when R/PA is in Boot Loader mode

of these data files and even some of the file contents are not efficient or, in some cases, at all useful to an on-orbit Shuttle mission. Furthermore, the baseline design depended on downlisting the navigation data for processing on the ground. Thus, it was necessary to study the file organization and eliminate all unnecessary data transmission to minimize the data rate. Of the files listed in Table 7-17, file numbers 5, 6, 8, 10, and 11 are not needed at all for the Shuttle/GPS mission. File numbers 0, 1, and 2 are outputted only when the receiver is loaded via uplink command to verify the correct loading of the receiver memory. This function would normally be performed prior to launch and would thus not impact the downlist data rate. File number 3, Current Operating Ephemeris, changes whenever the receiver acquires a new satellite. It was judged that the average frequency of update for this file would be approximately once every 10 minutes. Files number 4, 7 and 9 each contain data which changes every time a measurement cycle is completed, or once every 6 seconds. If all navigation filter processing is to be done on the ground, then file 7 could be eliminated. On the other hand, if all navigation filter processing is to be done on-board (not the baseline design), then file number 9 could be eliminated. The average data rate is calculated to be 698 bits per second, and the peak data rate is (4896/6) x 2 or 816 bits per second. The tabulation of these data rates is shown in Table 7-18.

It is important to realize that this discussion applies only to the baseline system configuration. The FY'78 study will determine what data should be processed in the GPS receiver, what data should be transferred to the Orbiter GPC for processing, and what data (if any) should be downlisted for ground processing.

Table 7-18. Baseline System Downlist Data Rate
Requirements (Two Receivers)

File I.D.	File Name	Size (Bits)	Update Period (sec)	Average Data Rate (bps)
3	Current Operating Ephemeris	5664	600	9.44
4	GPSPAC System Status	1376	6	229.33
7	Navigation Best Estimate	1120	6	186.66
9	Kalman Input, Dual Channel	1632	6	272.00
	Total Bits	9792	Average Data Rate	697.44

7.6 Shuttle Orbiter TACAN Transmitter Interference to Orbiter GPS Receiver

The TACAN transmitter on-board the Shuttle transmits RF pulses having a peak EIRP of approximately +60 dBm and a maximum possible carrier frequency of 1150 MHz. Since the GPS L2 carrier frequency is 1227.6 MHz, or less than 79 MHz away from the upper TACAN frequency, there is a potential for severe interference to the GPS receiver. Furthermore, unless suitable design precautions are observed, the TACAN signal has the potential for damaging the front end of the receiver preamplifier. Thus, it is necessary to analyze the interference situation and also examine possible operational or physical constraints (such as GPS antenna location relative to TACAN antenna location).

The analysis of the effects of pulses which saturate a receiver is complex, and depends to a great extent on the specific receiver and transmitter designs. However, it is possible to postulate generalized models and to determine some of the design considerations and tradeoffs which may ameliorate the severity of the problem. A more specific analysis is then more easily undertaken for specific receivers as their detailed characteristics are learned. Also, design specifications for new receiver developments or modifications of existing designs can be generated with the intent of minimizing the problem.

7.6.1 Receiver Saturation Model

A large amplitude pulsed carrier such as TACAN which is close in frequency to the receiver frequency will saturate the receiver preamplifier and possibly saturate following stages as well. The parameters which determine the degree of saturation include carrier frequency and amplitude, transmitted pulse shape, receiver filter characteristics, preamplifier linearity characteristics (i.e., 1 dB compression level), and gain. Once the TACAN energy has decayed to a level where it is in the receiver's linear operating range, the receiver processing gain inherent in the PN spread spectrum demodulation and tracking process determines the degradation of range measurement, range rate measurement, and data detection performance. The starting point for an analysis of this problem is the definition of a receiver model.

A generalized GPS receiver model for TACAN interference analysis is shown in Figure 7-13. The first point in the receiver that is affected by the TACAN pulse is the preamplifier. The preamplifier is modeled as a bandpass filter followed by a soft limiter. The soft limiter represents the transistor amplifier. The bandpass filter will affect the interference according to the relationship between the TACAN pulse spectrum (including center frequency) and the filter frequency response (including center frequency). Obviously, if the TACAN pulse is sufficiently outside the passband of the filter, the filter will attenuate the TACAN energy such that it will not saturate the receiver. On the other hand, if the TACAN pulse falls within at least a certain portion of the filter passband, the pulse energy may adversely affect the receiver. At this point, we will consider the more serious case, that is, when the TACAN center frequency is within the filter passband, as shown in Figure 7-14.

7.6.2 Pulse Spectrum Wider Than Filter Frequency Response

For purposes of understanding the problem, the problem can be considered in two phases. First, when the pulse spectrum width is approximately equal to or greater than the filter frequency response (i.e., a relatively narrow pulse), the filter "rings" or effectively spreads the TACAN pulse energy out in time. This is illustrated in Figure 7-15 for lowpass (equivalent) Butterworth filters. It can be seen that, as the filter order n is increased, corresponding to a filter with steeper skirts, the pulse energy is spread out longer in time. The implication here is that the filter design can significantly affect the recovery time, or the time it takes the receiver to function normally after a TACAN pulse. The recovery time period begins when the TACAN pulse voltage at the output of the filter exceeds the saturation level of the first transistor amplifier (modeled as a soft-limiter) and ends when the pulse voltage drops below this level, as illustrated in Figure 7-16. Of course, the longer the recovery time, the more serious will be the degradation to the GPS signal processing. The level at which the preamplifier saturates, or begins to generate significant intermodulation products, is determined largely by the preamplifier design. The parameter which relates this level to the input is the preamplifier 1 dB compression point. This point is where the preamp
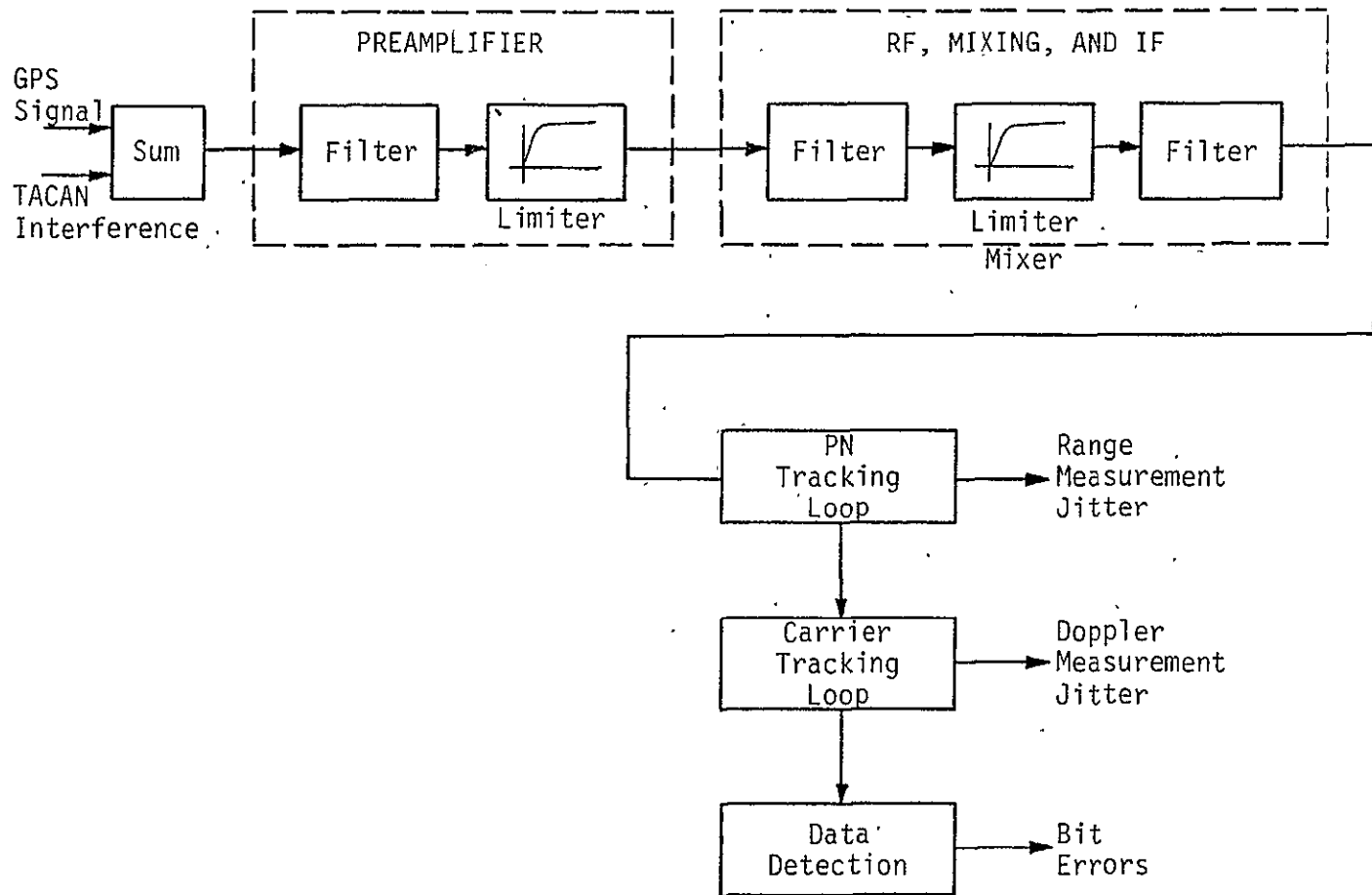
Figure 7-13. GPS Receiver Model for TACAN Interference Analysis
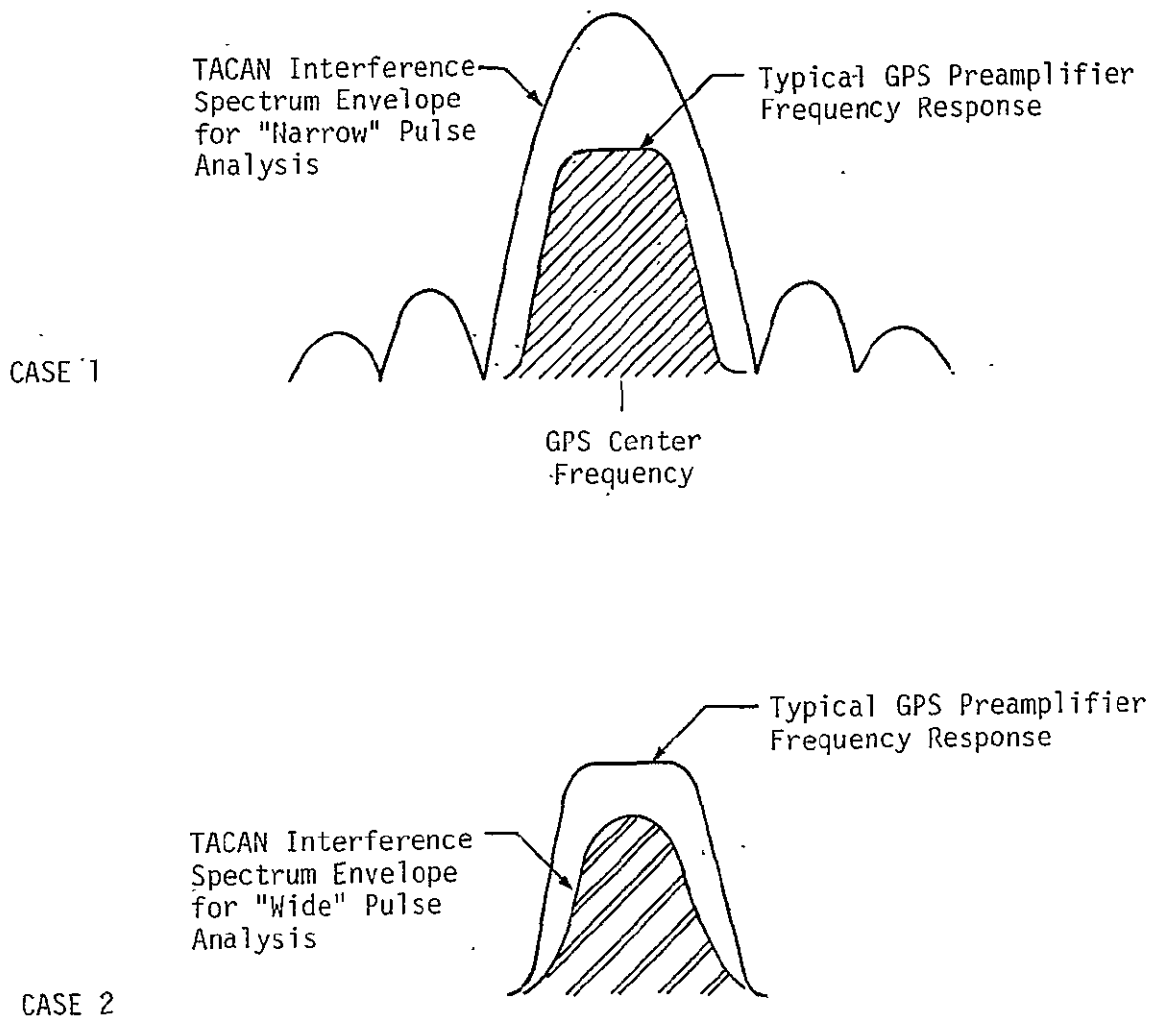
Figure 7-14.   Spectral Relationships for TACAN Interference Analysis
(Preliminary)
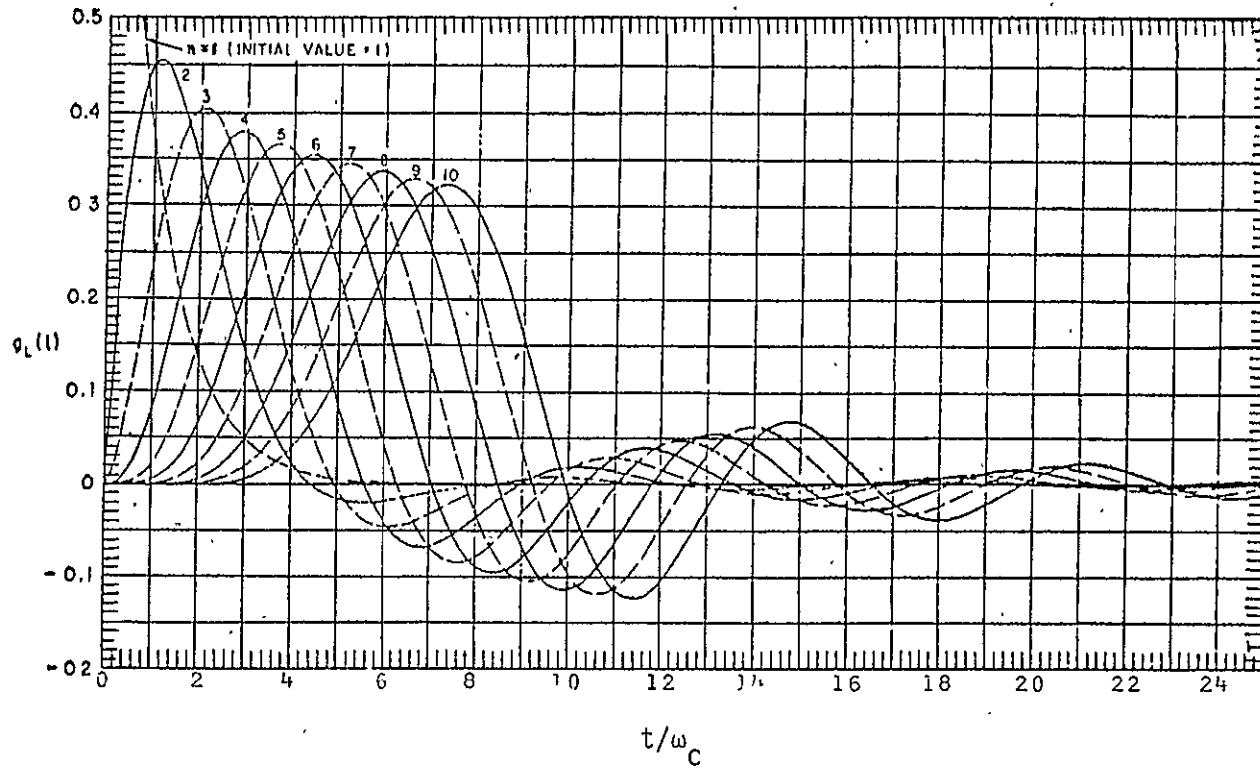
Figure 7-15. Approximate Transient Response of Butterworth Filter for Narrow Input Pulse
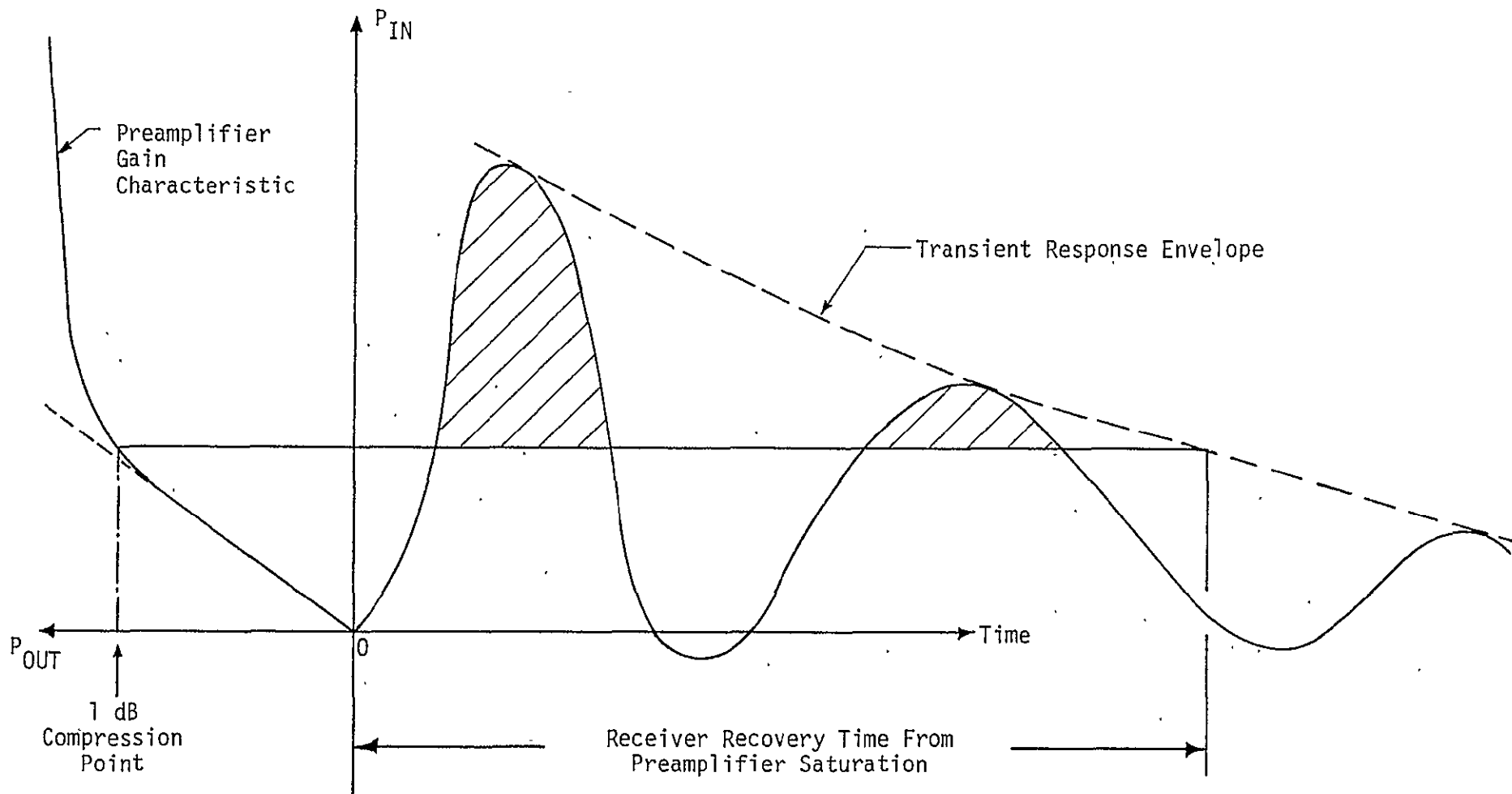
Figure 7-16.   Illustration of Receiver Recovery Time from Preamplifier Saturation by Narrow TACAN Pulse

output falls 1 dB below the output point if the preamp continued to operate linearly. It is traditionally used to define the point of the start of saturation for the preamp. Table 7-19 is a list of several typical low noise L-band preamplifiers and the input levels at which saturation occurs. From this table, it appears that a typical maximum input level for linear operations is approximately -17 dBm. Thus, as a first cut, the recovery time of the GPS receiver may be evaluated by computing the time required for the TACAN pulse energy at the preamplifier filter output to decay below -17 dBm. Considering the peak TACAN EIRP to be +60 dBm, and a realizable antenna isolation of 30 dB (first cut), the TACAN pulse energy must decay by 47 dB for the receiver to be operating in the linear region. We have discussed utilizing filter transient impulse response characteristics to determine the necessary decay time requirements for a relatively narrow pulse. Another similar approach which is less restrictive as to pulse width is to consider the filter step response as shown in Figure 7-17 for the Butterworth filter.

Using this approach, the recovery time is the time required to decay to within 1/224 (-47 dB) of the final value (unity). Thus, from Figure 7-17, approximately $t = 24/\omega$ is required for a filter of order 5 or more. For a 20 MHz-wide filter, the recovery time is on the order of 0.2 microseconds after the TACAN pulse is transmitted. In terms of blanking out the GPS signal, the filter ringing is thus seen to be insignificant. Consequently, of greater interest at this point is the case where the TACAN pulse is relatively long, or the pulse spectrum is narrow relative to the filter frequency response. During the FY'78 study, we will consider the filter ringing by a narrow pulse for a narrowband IF filter.

7.6.3 Pulse Spectrum Narrower Than Filter Frequency Response

We will now treat the case where the pulse spectrum is much narrower than the filter frequency response. In this case, the TACAN pulse appears at the filter output with little distortion, so that the filter does not prolong the receiver recovery time. Mathematically, this means that $F(\omega) \ll H(\omega)$, where $F(\omega)$ is the spectrum of the TACAN pulse, and $H(\omega)$ is the spectral response of the input filter. Consequently,

Table 7-19. Typical L-Band, Low-Noise Preamplifier Characteristics

Avantek Model No.	Gain (dB)	Noise Figure (dB)	Power Output for 1 dB Gain Compression (dBm)	Maximum Power Input for Linear Operation (dBm)
AMT-2014	25	4.0	+10	-15
AMG-2020	27	3.0	+10	-17
ABG-2012	27	5.0	+20	-17
ABG-2003	36	3.5	+20	-16
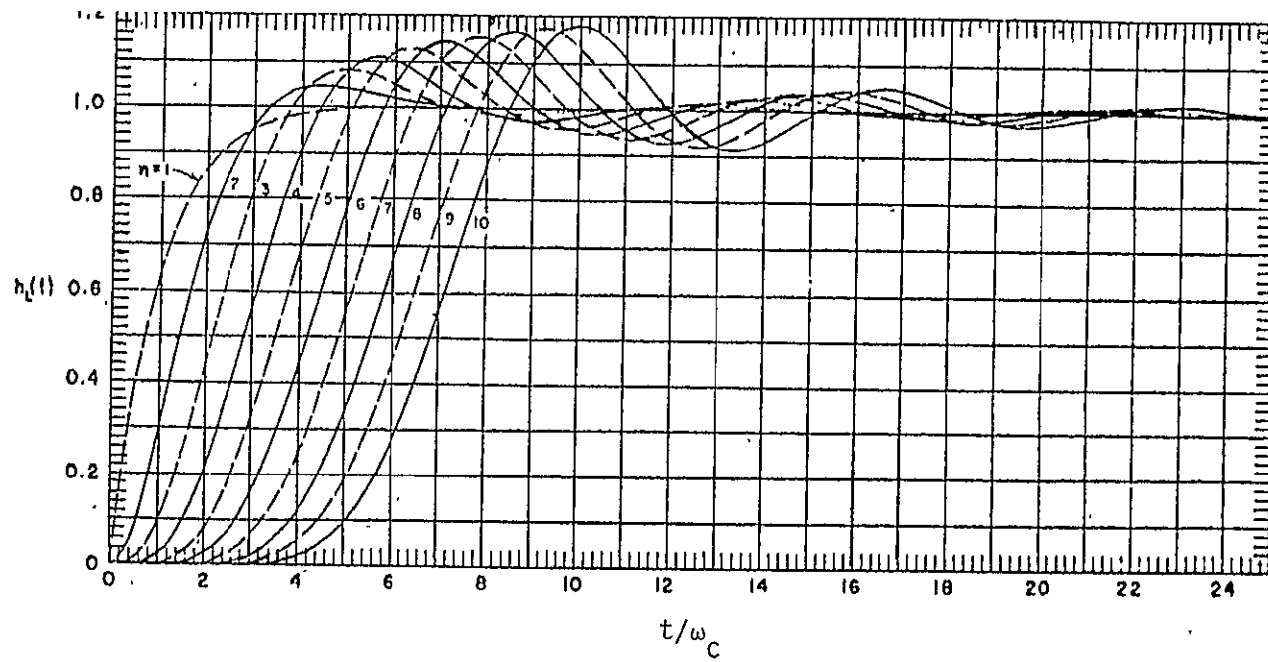
Figure 7-17.   Transient Response of Butterworth Filter for Step Input
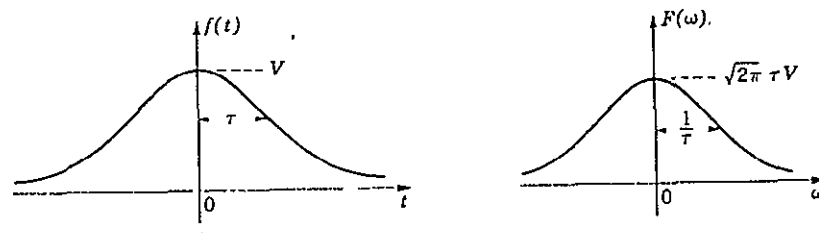
Gaussian Pulse
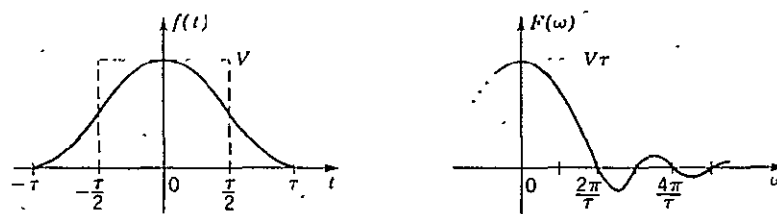
Raised Cosine Pulse

Figure 7-18. Gaussian Pulse and Raised Cosine Pulse Shapes
and Spectrum for "Wide" Pulse Saturation Analysis

$$g(t) = \int_0^\infty f(\tau) \, h(t-\tau) \, d\tau$$

$$\approx f(t), \tag{7-8}$$

where $f(t) \equiv$ time response of TACAN pulse

$\quad\quad h(t) \equiv$ impulse response of the filter as illustrated in Figures 7-15 and 7-16

$\quad\quad g(t) \equiv$ output of filter.

Provided that the GPS receiver bandwidths (RF and IF) are not chosen too narrow (to be dealt with more quantitatively during the FY'78 study), the above model is appropriate for the TACAN interference if we consider the TACAN pulse to be either a raised cosine pulse or a Gaussian pulse, as illustrated in Figure 7-18. The raised cosine pulse has a time response given by

$$f(t) = \begin{cases} \dfrac{V}{2}\left(1 + \cos\dfrac{\pi t}{\tau}\right); & |t| \le \tau \\[2em] 0; & \text{elsewhere}, \end{cases} \tag{7-9}$$

and a spectrum given by

$$F(\omega) = V\tau \frac{\sin \omega\tau}{\omega\tau[1 - (\omega\tau/\pi)^2]} \tag{7-10}$$

and the Gaussian pulse has a time response given by

$$f(t) = V e^{-t^2/2\tau^2} . \tag{7-11}$$

with a spectrum given by

$$F(\omega) = \sqrt{2\pi} \, \tau \, V \, e^{-\tau^2\omega^2/2} . \tag{7-12}$$

Preliminary information received from Rockwell International (RI) indicates that a good model for the TACAN pulse is a Gaussian pulse with a rise time of 2.5 ± 0.5 μsec between the 10% and 90% amplitude points. Thus, solving for τ,

$$0.10 \, V = V e^{-t_1^2/2\tau^2}$$

$$0.90 \, V \;=\; V \, e^{-t_2^2/2\tau^2}$$

$$\ln 0.10 \;=\; -t_1^2/2\tau^2$$

$$\ln 0.90 \;=\; -t_2^2/2\tau^2$$

and, since

$$|t_1 - t_2| \;=\; 2.5 \times 10^{-6} \, ,$$

$$|t_1 - t_2| \;=\; \left| \sqrt{(-\ln 0.1) \, 2\tau^2} \;-\; \sqrt{(-\ln 0.9) \, 2\tau^2} \right| \qquad (7\text{-}13)$$

$$\tau \;=\; \frac{2.5 \times 10^{-6}}{\sqrt{2} \, | \sqrt{(-\ln 0.1)} - \sqrt{(-\ln 0.9)} |}$$

$$=\; 1.48 \times 10^{-6} \, , \qquad (7\text{-}14)$$

so that, for the Rockwell TACAN pulse model,

$$f(t) \;=\; V \, e^{-t^2/4.38 \times 10^{-12}} \, . \qquad (7\text{-}15)$$

The receiver recovery time, or the time during which the TACAN pulse saturates the front end, is found by solving the above equation for the value of t for which $f(t)$ corresponds to -17 dBm. Since, as in the case of the narrow pulse previously considered, -17 dBm corresponds to a 47 dB decay (again assuming 30 dB antenna isolation), t is found by solving

$$20 \log e^{-t^2 \cdot 4.38 \times 10^{-12}} \;=\; -47 \text{ dB} \, ,$$

or

$$t \;=\; 4.87 \times 10^{-6} \, . \text{ seconds} \, , \qquad (7\text{-}16)$$

and, since the receiver is saturated for the first half of the pulse, i.e., the rising part of the pulse, as well as the falling part of the pulse, the total time the receiver is saturated by the Gaussian TACAN pulse is 9.7 microseconds. An appreciation for the effect of this saturation period is obtained by considering the duty cycle of the saturation period. The highest TACAN PRF is 150 pulse pairs per second, so the receiver saturation duty cycle is

$$\frac{2 \times 9.7 \times 10^{-6}}{1/150} = 0.291\% ,$$

which corresponds to a signal loss of approximately 0.01 dB. Thus, it can be concluded that, based on the assumptions made in the foregoing analysis, the time during which the GPS receiver is saturated is inconsequential.

The effects of the TACAN energy once the receiver is out of saturation will be to increase the receiver effective noise figure. This and other sources of receiver degradation due to the TACAN signal will be discussed next.

7.6:4 Receiver Degradation in the Nonsaturated Mode

The discussion above illustrated that the GPS receiver will saturate for only a relatively short period of time. However, during the remaining time when the receiver is operating in the linear mode, the TACAN pulse energy will appear as noise in the preamplifier input filter, as illustrated in Figure 7-19. This extra noise effectively increases the noise temperature of the preamplifier. Thus, it is necessary to calculate the integrated TACAN power that appears in the preamplifier filter. Preliminary results indicate that a Gaussian shaped pulse will cause no interference, while a rectangular shaped pulse without TACAN transmitter filtering will swamp out the GPS L2 signal, as shown in Figure 7-19. A detailed investigation of the TACAN pulse shape and transmitter filter will be undertaken during the FY'78 study.

Another aspect of the TACAN interference is that, due to the pulse nature, the interference spectrum consists of lines separated by the pulse repetition frequency. Thus, a single interfering spectral line will appear within the Costas tracking bandwidth (approximately 30 to 50 Hz). This line acts as a CW jammer and can cause the Costas loop to lock to it, rather than to the GPS carrier. This problem will be analyzed during the FY'78 study.

7.6.5 Summary

The effects of receiver saturation by a TACAN pulse have been considered for a worst-case situation, that is, the TACAN pulse falling within the receiver preamplifier bandwidth. It was shown that, for a

TACAN Signal = +30 dBm (including 30 dB antenna isolation)

Envelope of $(\sin x/x)^2$ spectrum for a rectangular pulse

Relative magnitude (not to scale)

Receive Filter

GPS Signal $(\sin x/x)^2$

1100   1150   1200   1227.6

Upper TACAN Frequency

Frequency (MHz)

GPS L2 Signal
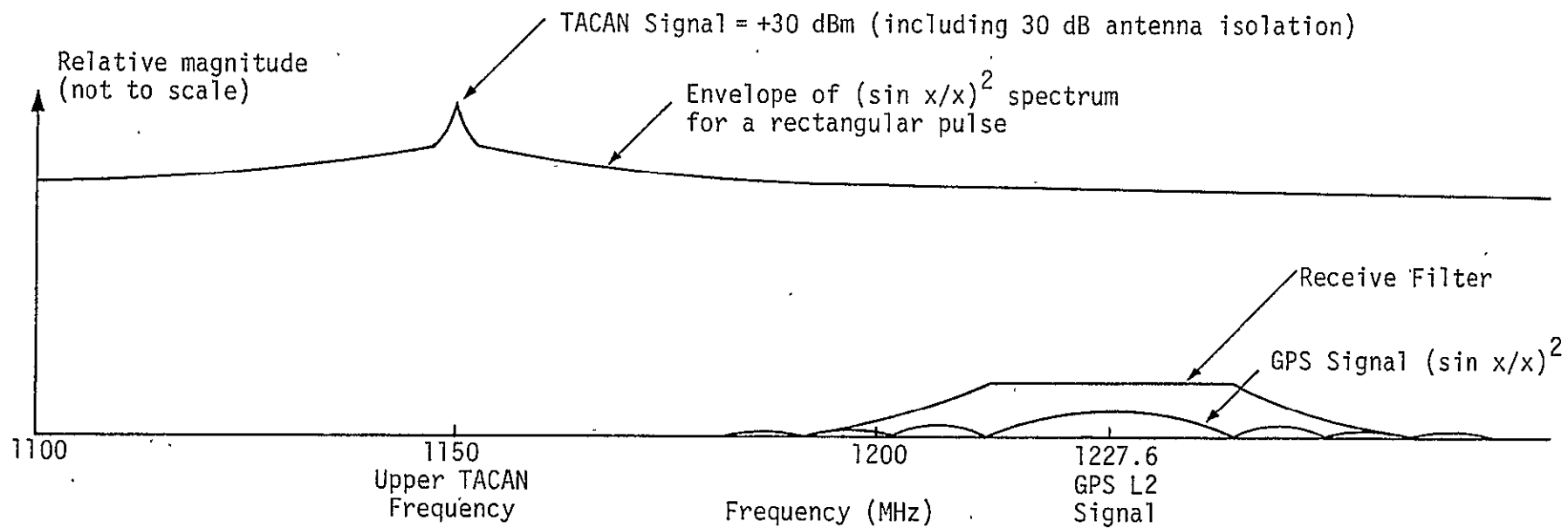
Figure 7-19. Spectral Interference Between the Upper TACAN Transmitter and GPS L2 Receiver

nominal 30 dB antenna coupling value and typical L-band preamplifiers, the receiver saturation time is on the order of 10 microseconds. This was for a Gaussian shaped pulse having nominal 2.5 microsecond rise and fall times. The receiver saturation for a sharp pulse (wide spectrum) was found to be on the order of the pulse width increased by a mere 0.2 microseconds (assuming a 20 MHz receiver filter). Thus, it has been concluded that

1. Saturation due to preamplifier saturation lasts a negligible time period.
2. Saturation effects for subsequent receiver stages wherein narrower bandwidths will be encountered must be analyzed.
3. The increase in effective receiver noise temperature due to TACAN energy spill-over for that time period when the receiver is not saturated must be evaluated.
4. The generation of intermods when the receiver is not saturated and their effects must be evaluated.

These additional analyses will be covered during the FY'78 study.

7.7   Atmospheric Attenuation of Shuttle/GPS Link Signals

Radio propagation through the atmosphere suffers attenuation at the GPS frequencies of 1575 MHz and 1227 MHz. The amount of attenuation depends on the local elevation angle of the line-of-sight path between the user antenna and the GPS satellite. The Applied Physics Laboratory (APL) of John Hopkins University has estimated the maximum attenuation to be 2 dB for the path labeled R_{max} for the geometry shown in Figure 7-20. This corresponds to a local elevation angle of 0° and, as such, represents an unrealistically severe case. In referring to Figure 7-20, the angle θ is seen to be the angle for which the line-of-sight path just clears the atmosphere, i.e., no atmospheric attenuation. This angle is calculated from the equation

$$\theta = \sin^{-1} \frac{H_A}{R_{GPS} \cos\left[\sin^{-1} \frac{R_E}{R_{GPS}}\right]} \tag{7-17}$$

where

Diagram labels: ORBITER, GPS, θ, R_{MAX}, $\propto$, H_A, R_E
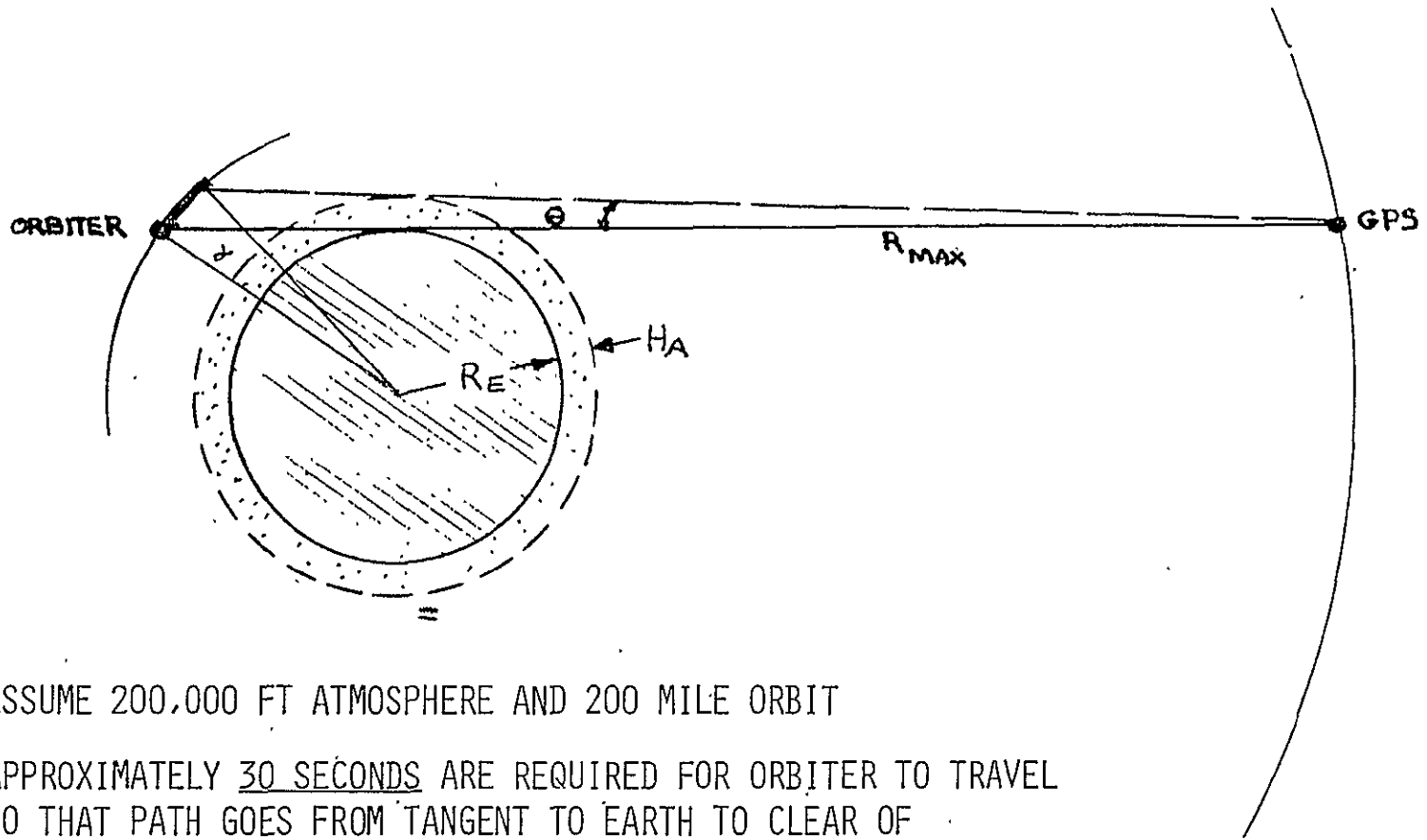
• ASSUME 200,000 FT ATMOSPHERE AND 200 MILE ORBIT

• APPROXIMATELY 30 SECONDS ARE REQUIRED FOR ORBITER TO TRAVEL SO THAT PATH GOES FROM TANGENT TO EARTH TO CLEAR OF ATMOSPHERE $\theta = 0.14°$ AND $\propto = 1.8°$

• CONCLUSION - ATMOSPHERIC ATTENUATION (2 dB IN BUDGET) IS NOT A FACTOR

Figure 7-20.   Orbiter Orbit Segment Eliminated by "No Viewing" Through Atmosphere

H_A = assumed atmospheric height

R_{GPS} = Semi major axis of GPS satellite orbit (26,650 km)

R_E = earth radius (6378 km)

For an atmosphere height that contributes to L-band attenuation assumed to be 200,000 feet, $\theta = 0.14$ degrees. This corresponds to an angular arc α for an Orbiter at 200 miles of 1.8 degrees, or approximately 30 seconds of time for the Orbiter to clear the atmosphere entirely. Another way to consider the on-orbit atmospheric viewing problem is to consider what GPS orbital arc is eliminated if there is. to be no propagation through the atmosphere. This geometry is illustrated in Figure 7-21, and the calculation for the angle which is eliminated (ϕ) is tabulated in the figure. Thus, for the 200,000 foot atmosphere case, approximately 1.7 degrees of viewing angle at the Orbiter is eliminated by the atmosphere. However, it is important to consider that this angle is eliminated for less than 30 seconds. Thus, the conclusion has been reached to not include atmospheric loss in the on-orbit link budget calculations.

The question as to what the atmospheric attenuation of the GPS signals is for the case when the Shuttle is within the atmosphere must be answered. The atmospheric attenuation of communication satellite signals has been carefully measured and documented and is shown plotted in Figure 7-22 as a function of local elevation angle at the earth's surface. This plot is for a frequency of 4 GHz and 6 GHz, typical communication satellite frequencies. The data may be scaled to the GPS frequencies by utilizing the atmospheric adsorption coefficient, plotted as a function of frequency in Figure 7-23. In doing this, the atmospheric attenuation for a 10 degree elevation angle at 1.6 GHz is found to be 0.16 dB. The right-hand ordinate of Figure 7-22 has been scaled from this calculation for attenuation at 1.6 GHz. From Figure 7-23, it can be seen that the atmospheric attenuation at 1.3 GHz will be slightly less than at 1.6 GHz. As a check on these calculations, reference to Figure 7-24, the atmospheric attenuation determined by JPL for the DSN at S-band, shows that at 10 degrees the attenuation is approximately 0.165 dB.
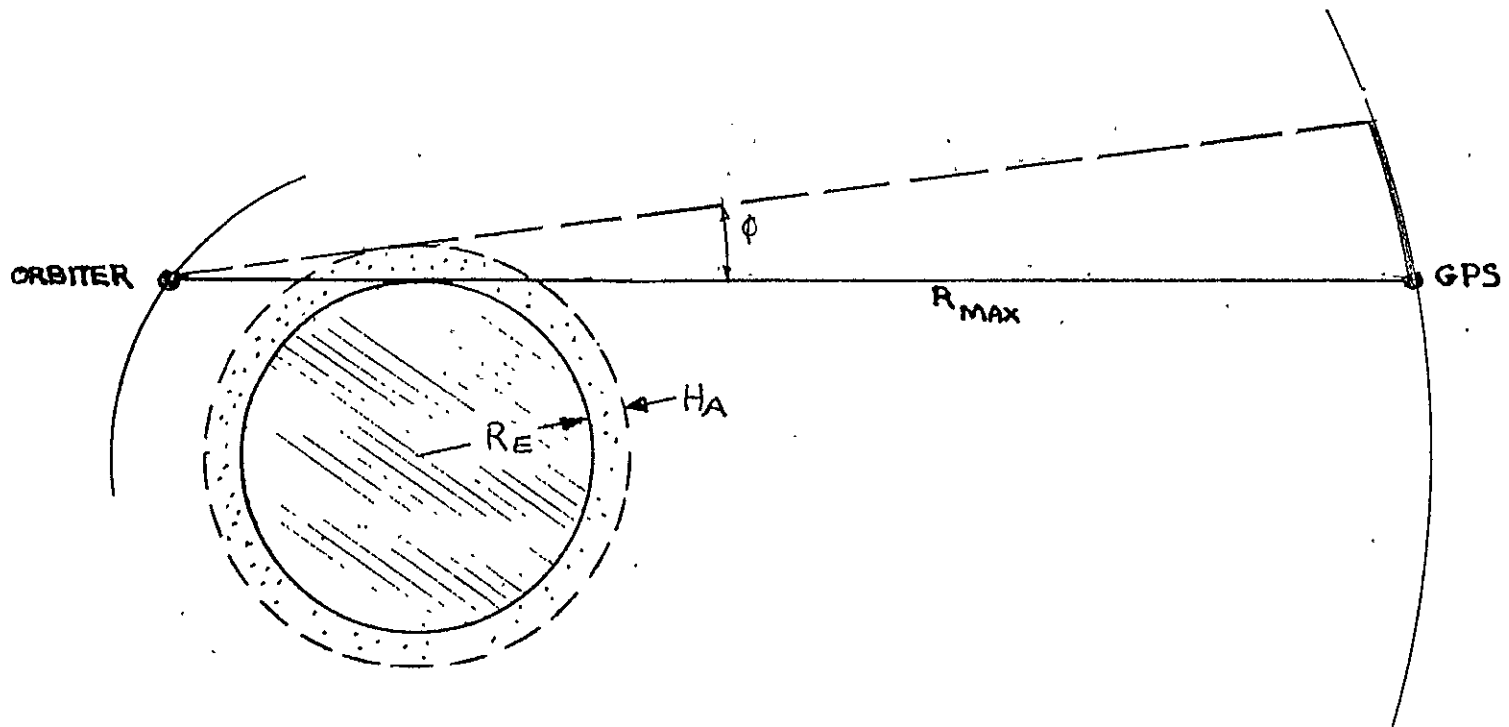
ATMOSPHERIC HEIGHT, H_A (FT)	ANGLE ELIMINATED, ϕ (DEGREES)
100,000	0.85
200,000	1.70
300,000	2.56

Figure 7-21. Orbiter Viewing Angle Eliminated if No Viewing Through Atmosphere

ATMOSPHERIC ABSORPTION

VS.

ELEVATION ANGLE

(4 AND 6 GHz)
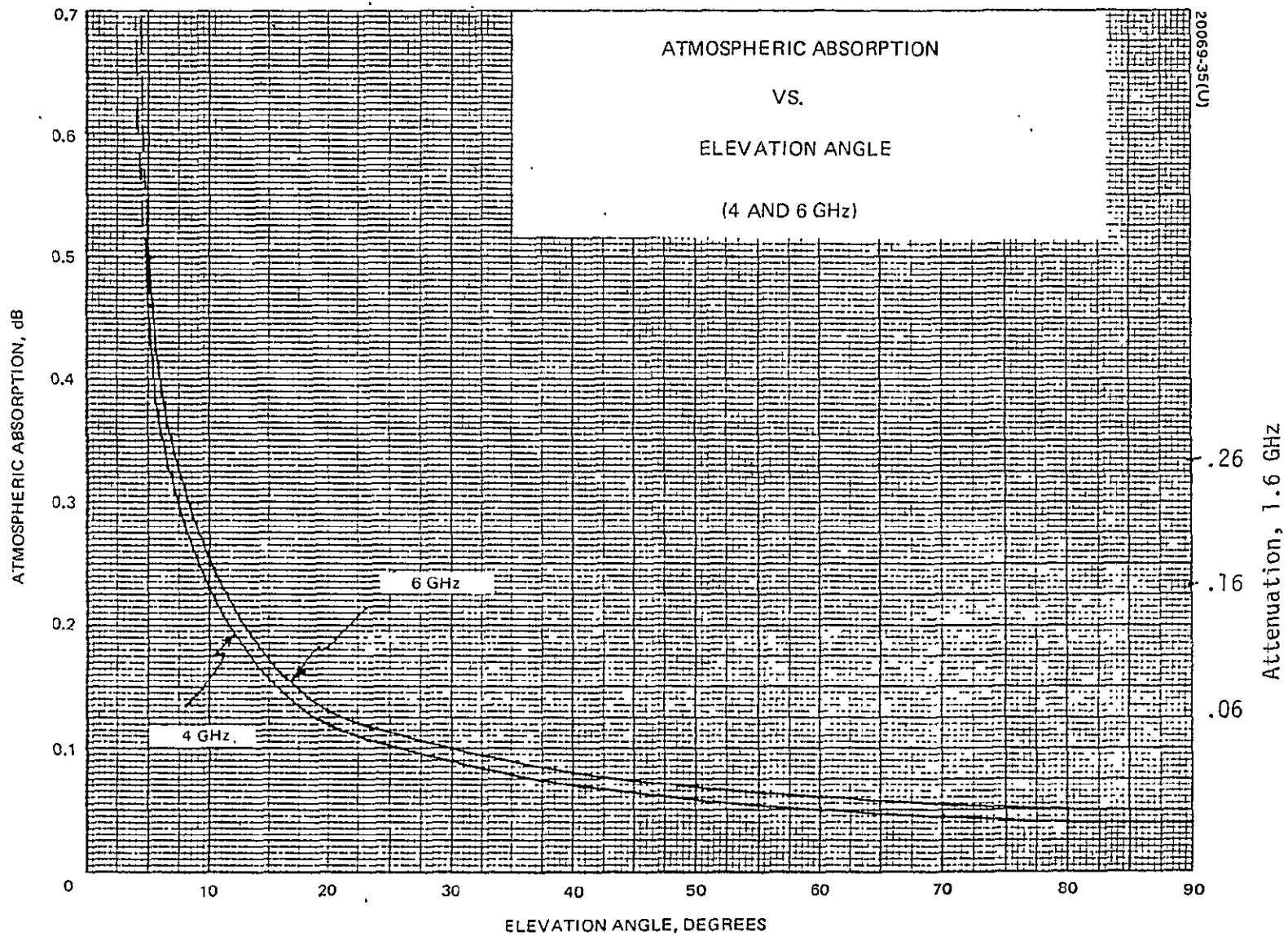
Figure 7-22. Atmospheric Attenuation Vs. Elevation Angle
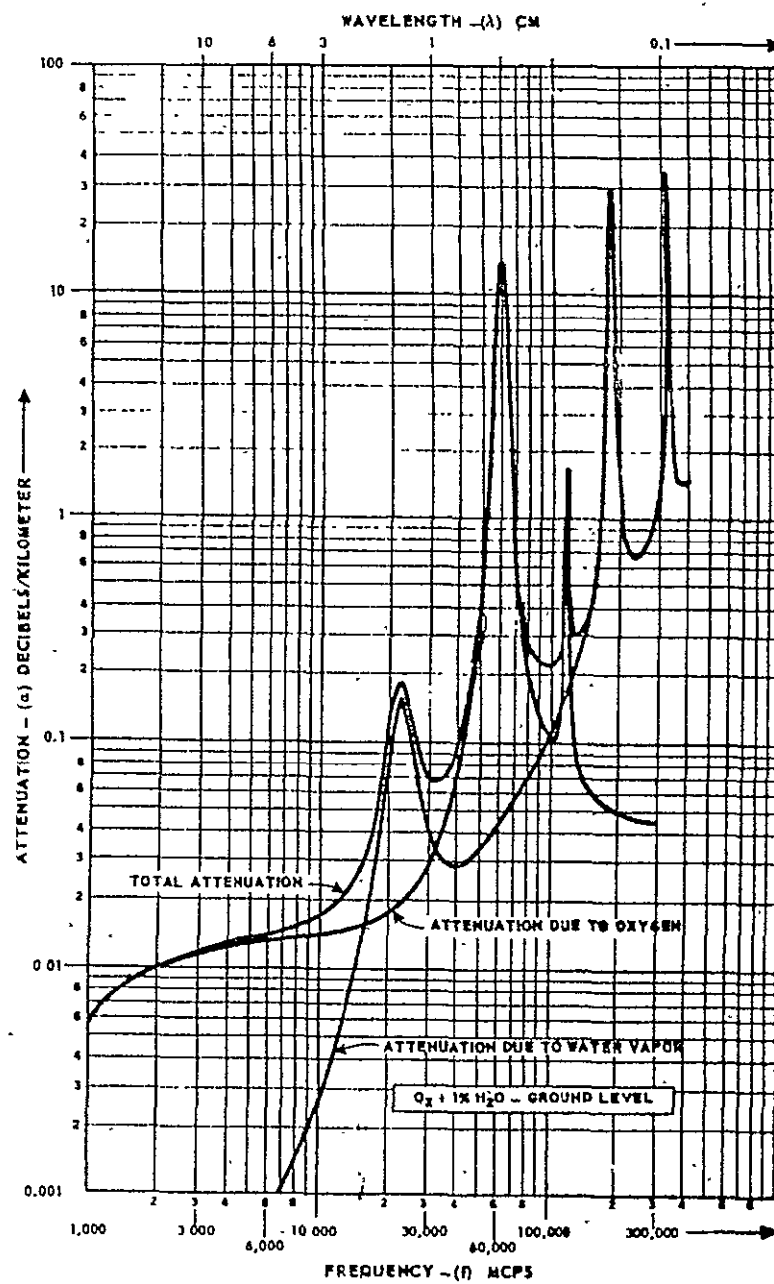
Figure 7-23. Calculated Total Atmospheric Adsorption
Coefficient Spectrum for the Centimeter-
Millimeter Region at Sea Level
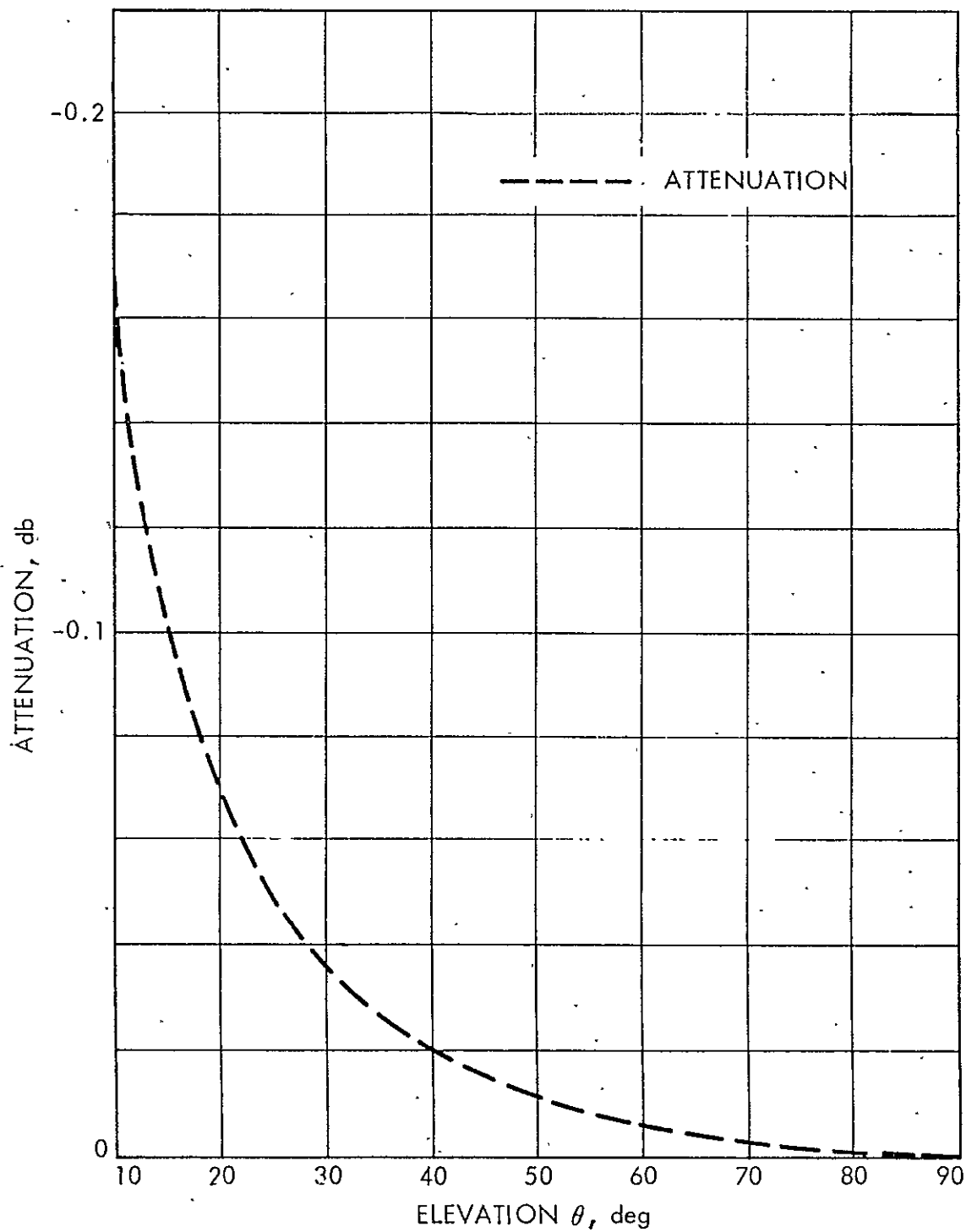
Figure 7-24. Atmospheric Attenuation for DSN 64-meter Antenna

7.8   Shuttle/GPS Anti-Jam Performance

The GPS signal design employs PN spread spectrum to achieve very precise range resolution while at the same time providing resistance to jamming. In an actual hostile jamming environment, additional code security equipment is designed to be added to the military GPS receivers to allow them to continue to use the P code which would be specially coded to deny use by unauthorized users during the time of crises. The C/A code would, however, remain accessible to the normal GPS receiver not equipped with the code security device. The necessity of providing the code security device to the Shuttle GPS receiver must be studied and, to a large extent, will depend on the adequacy of the navigation accuracy that can be derived from the C/A code. It is important to analyze what anti-jam protection the basic P code signal structure will provide the Shuttle GPS receiver. One can postulate a scenario in which the Shuttle GPS receiver is being intentionally jammed by an enemy intent on thwarting a Shuttle mission, and during which time no other overt hostilities have been demonstrated.

7.8.1 Types of Jamming Signals

The type of jamming signals that can be conceived are summarized in Table 7-20.

Table 7-20. Summary of Jamming Signals

Signal Category	Example or Description of Signal
Random Noise	Full Band - Continuous or Pulsed Partial Band - Continuous or Pulsed Narrowband - Continuous or Pulsed
Sinusoidal	Single CW Tone - Continuous or Pulsed - Coherent or Random Phase Multiple CW Tone - Continuous or Pulsed - Coherent or Random Phase
Modulated Carrier	AM, FM, PM, Radar, Carrier Sweep Pulse Modulation, On-Off Keying PSK, FSK, and ASK
Pseudonoise	Biphase, M-phase
Repeated Signal	Delayed and retransmitted Delayed, modulated, and retransmitted

The modulated carrier jam signals are often used to jam like-modulated signals, such as AM against AM, FM against FM, etc. If noise modulation is used, the resultant sideband bandwidth will occupy part or all of the spread bandwidth, depending on the modulation spectrum. Thus, neglecting whatever "wasted" power is in the carrier and the non-uniformity of the spectrum, modulated carrier, pseudonoise, and hence delayed repeated signals are regrouped into the random noise category.

Partial-band noise signal consists of Gaussian noise with a bandwidth less than the spread bandwidth, W, but greater than the baseband modulation bandwidth. Partial-band noise may be in single or multiple preselected channels or "bands" within the spread spectrum bandwidth. Partial-band noise jamming can possibly be more effective than full-band noise only against spread spectrum systems that do not continuously occupy the full spread band, such as frequency hopping systems. The same may be said of multiple CW tone signals. The jamming signals tabulated in Table 7-20 may thus be regrouped into eight basic jam types:

Continuous Full-Band Noise. The broadband continuous noise jamming signal is one which occupies the full bandwidth of the spread spectrum signal. Generally, it is assumed that such noise is Gaussian and white. Thus, the performance of spread spectrum systems in their stressed environment is essentially identical to that in thermal noise, with E_b/N_0 replaced by $E_b/N_j = SW/JR$.

Pulsed Full-Band Noise. The broadband burst noise jamming signal trades fractional-time operation for high peak power in an attempt to overcome a portion of the spread spectrum processing gain. The noise remains white and Gaussian but has noise power density J/BW, where B = pulse duty cycle.

Continuous Sinusoidal. The continuous CW tone signal places an unmodulated sinusoid having power J at the waveform carrier frequency. If the carrier phase is matched as well, a special case results called coherent tone jamming.

Continuous Partial-Band Noise. The continuous partial-band noise signal concentrates the total jam power J within a contiguous optimum bandwidth greater than that of narrowband noise, but less than W.

Pulsed Partial-Band Noise. The pulsed partial-band noise signal optimizes the effect of the jam power J in both time, frequency, duty cycle, and fractional band parameters.

Pulsed Sinusoidal. The pulsed tone signal bursts sinusoids having power J/α at the waveform carrier frequency. As in all cases of pulsed signals, the jammer randomizes the transmission epochs to prevent "gating out" of this jam signal.

Continuous Multichannel Narrowband Noise. The continuous narrowband noise signal concentrates the total jam power J within the baseband spectrum in the form of very narrowband Gaussian noise channels.

Pulsed Multichannel Narrowband Noise. The narrowband burst noise signal increases peak power by means of pulsed-duty-cycle operation. The signal concentrates peak jam power J/α within the baseband spectrum in the form of narrowband Gaussian noise channels.

7.8.2 Analysis of Baseline Shuttle/GPS Receiver Jam Protection

The parameter of primary interest is the anti-jam margin, AJ. This margin is given by

$$AJ \text{ (dB)} = PG \text{ (dB)} - S/N_{Required} \text{ (dB)}, \qquad (7-18)$$

where

    PG = receiver processing gain

    S/N = signal-to-noise ratio required for receiver function.

The processing gain is best understood from consideration of the signal modulation and demodulation. In the GPS signal structure, the message modulation m(t) is multiplied by the wideband PN signal PN(t). The signal is received with additive, uncorrelated interference n(t) of power N. At the receiver, correlation is performed by multiplying the received signal with a local version of the PN code to achieve

$$R(t) = [\sqrt{S} \, PN(t) \, m(t) + n(t)] \, PN(t), \qquad (7-19)$$

where S is the average power of the received signal. R(t) is averaged over a time period appropriate to the receiver function being performed. In the case of data detection, this is equivalent to passing R(t) through a filter B wide (where B is the data bandwidth) and, in the case of carrier tracking, the filter is merely $B_{L_{carrier}}$, where $B_{L_{carrier}}$ is the Costas loop bandwidth. For ranging (PN code tracking), the filter is the delay lock (or tau dither) loop bandwidth $B_{L_{code}}$. Thus, the filter output is given by

$$R(t)_{filter} = \overline{PN(t)^2} \sqrt{S}\, m(t) + n_0(t) , \qquad (7\text{-}20)$$

where

$\overline{PN(t)^2}$ = PN autocorrelation function

$n_0(t)$ = output noise.

The output noise power for tone jammer at the carrier frequency is

$$\overline{n_0(t)^2} = N_0 B_{filter} = J\left(\frac{B_{filter}}{B_{RF}}\right) , \qquad (7\text{-}21)$$

where

N_0 = white noise at the receiver input

J = tone jammer power

and $\quad B_{filter} = B_{data}$ for data detection

$\qquad = B_{L_{carrier}}$ for carrier tracking

$\qquad = B_{L_{code}}$ for code tracking.

Thus, we see that the tone jamming power is reduced by the ratio of the processing bandwidth to the spreading bandwidth, B_{RF}, so that the processing gain for the jammer is merely

$$PG = \frac{B_{RF}}{B_{filter}} . \qquad (7\text{-}22)$$

When the processed jammer power is much larger than the white noise component, then the AJ margin can be calculated directly from (7-18). Otherwise, the required (C/N_0) is

$$\left(\frac{C}{N_0}\right)_{req} = \frac{C}{N_0 + J/B_{RF}} = \frac{1}{N_0/S + (J/CB_{RF})} \qquad (7\text{-}23)$$

or $\qquad AJ = J/C = B_{RF}\left[\frac{1}{(C/N_0)_{req}} - \frac{1}{(C/N_0)}\right] , \qquad (7\text{-}24)$

where (C/N_0) is the available C/N_0 from the link budgets and $(C/N_0)_{req}$ is the C/N_0 required to meet the receiver performance criteria.

In applying these relationships to the baseline Shuttle/GPS system discussed in this report, we find the following:

$$AJ_{ranging} = 10 \log (10^7) + 10 \log \left[\frac{1}{10^{3.16}} - \frac{1}{10^{3.59}}\right]$$

$$= 36.4 \text{ dB} \tag{7-25}$$

$$AJ_{carrier\ track} = 10 \log (10^7) + 10 \log \left[\frac{1}{10^{2.95}} - \frac{1}{10^{3.59}}\right]$$

$$= 39.4 \text{ dB} \tag{7-26}$$

$$AJ_{data} = 10 \log (10^7) + 10 \log \left[\frac{1}{10^{2.81}} - \frac{1}{10^{3.59}}\right]$$

$$= 41.1 \text{ dB} . \tag{7-27}$$

The interpretation of these numbers is that a jammer must provide 36.4 dB more jamming power than the GPS signal at the Shuttle GPS antenna for the jamming to affect the range measurement accuracy of the GPS receiver. Likewise, the jammer must provide 39.4 dB and 41.1 dB more power at the Shuttle receiver to adversely affect the GPS carrier tracking and data detection, respectively. These results are tabulated in Table 7-21.

Table 7-21. Baseline AJ Margins

Receiver Function	P Signal AJ Margin (dB)
Ranging	36.4
Carrier Tracking	39.4
Data Tracking	41.1

A very difficult type of jamming to protect against is the repeat jammer. This type of jamming is illustrated in Figure 7-25. The operation of this jammer depends on the jammer "fooling" the GPS receiver into thinking it is a GPS satellite. The jammer receives a normal GPS satellite transmission, demodulates the data, and remodulates it on another PN modulated carrier. The jammer initially adjusts the phase of its PN code so that the Shuttle GPS receiver acquires it, thinking it to be a legitimate satellite. The jammer then starts to "pull" the phase of the PN code, thus causing an erroneous range to be measured. This type of jamming must be discriminated against by the navigation filter itself. This will be studied during the FY'78 study phase.
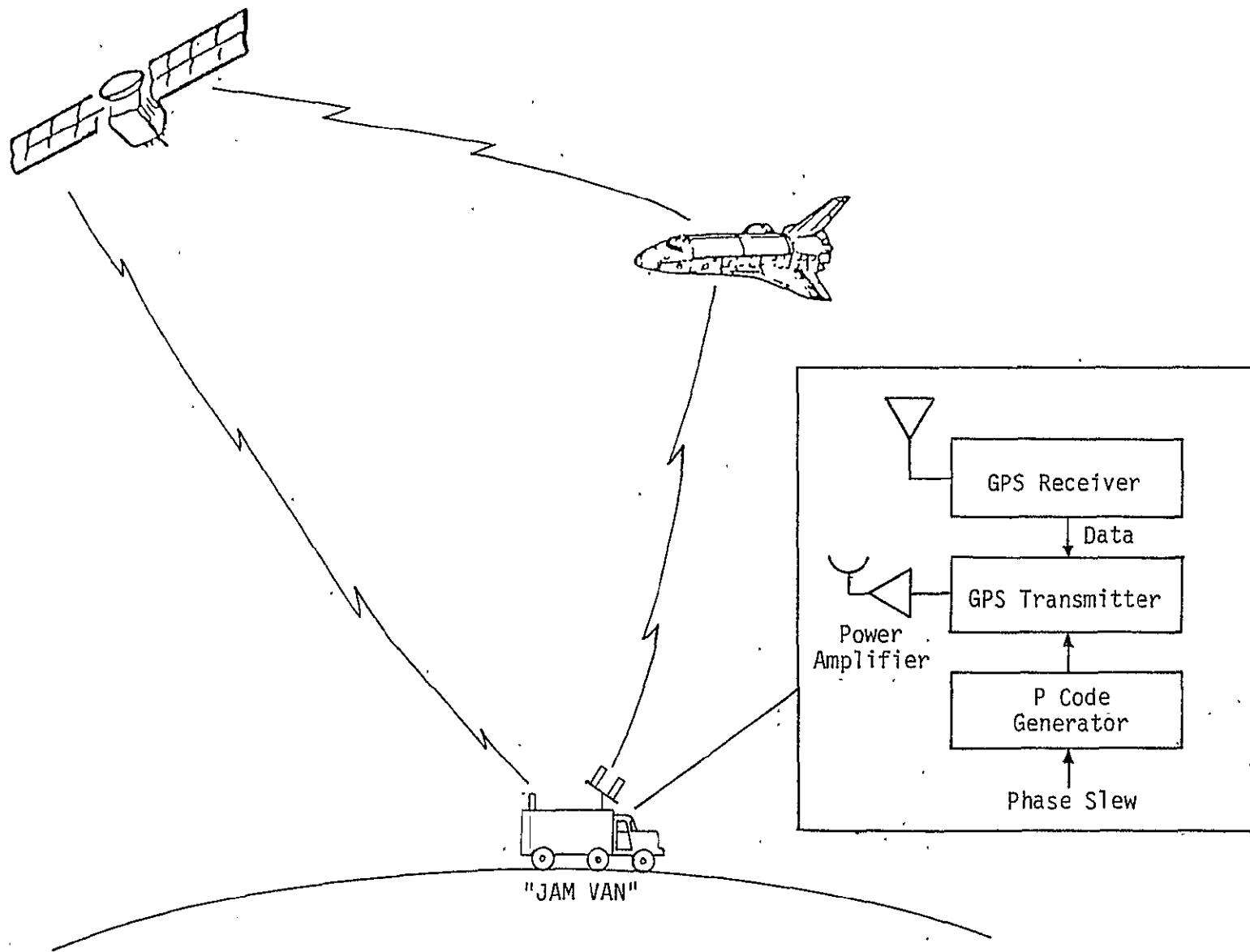
Figure 7-25. GPS Repeat Jammer Scenario

APPENDIX A

VARIATIONS IN GPS SATELLITE EIRP

The EIRP for the GPS satellites that has been used for the link analysis is the value specified in the Prime Item Development Specification for the Space Vehicle of the Space Vehicle Segment of the NAVSTAR Global Positioning System, CID-SV-101A, Volume 9. However, it is important to note that the spec value of 23.8 dBw (L1, P) is for the satellite end-of-life and includes eclipse operations. Furthermore, it is also for operation of the satellite at hot temperature extremes which does not necessarily represent typical operating conditions. Typically, at this temperature extreme, the solid state power amplifiers will have degraded performance relative to ambient operating condition. Also, these worst case conditions include operation of the power amplifier at minimum DC bus voltage conditions. This also contributes to lower power amplifier output power. These variations are shown in Table A-1, which is taken from functional test data for GPS satellite FSV #2. Thus, we see that there is a 1.3 dB variation between the nominal satellite condition and the worst case satellite condition.

Table A-1. Variation of Power Amplifier Output Power With Temperature and Voltage (L1, P Output, Watts)

DC Bus Voltage (Volts)	Output Power (Watts)		
	Base Plate Temperatures		
	0°C	23°C	56°C
25.5	12.1	11.9	11.0
26.9	12.6	12.3	11.3
27.5	12.8	12.4	11.4

☐ ≡ indicates nominal satellite condition

The variation in satellite antenna gain is indicated in Figure A-1, which is an elevation gain pattern for a functional test of the satellite antenna. The 12.8 dB gain value is just outside the edge of earth coverage and, as such, represents the gain value for a nominal Shuttle orbit. The 11.8 dB gain value represents the boresight gain.
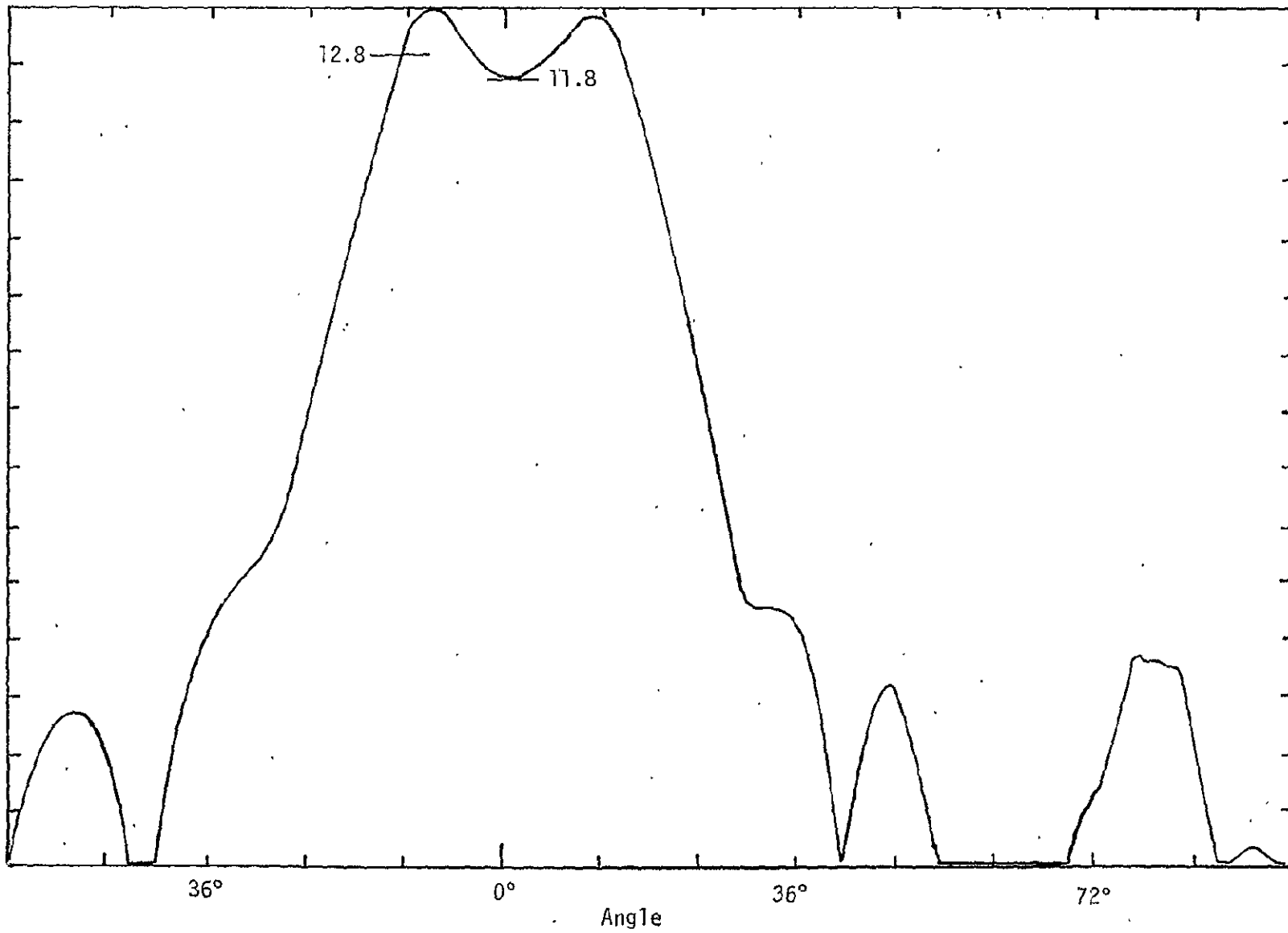
Figúre A-1. Typical Measured GPS Satellite Gain at L1

APPENDIX B

PN CLOCK TRACKING LOOP ANALYSIS

1.0   ANALYSIS OF THE DELAY LOCK LOOP

A block diagram of the delay lock tracking loop is shown in Figure B-1. Coherent demodulation to baseband will be assumed as it is more convenient to analyze a baseband loop, and the results apply directly to an IF loop. The receiver filter will be assumed to be an ideal bandpass filter which represents the bandlimiting accomplished by the IF filtering. The loop can be modeled mathematically as shown in Figure B-2 if the tracking error is small. In the analysis which follows, the variance of the tracking error $\Delta\tau$ and thus the rms tracking error will be found.

From Figure B-2, it can be seen that, by superimposition,

$$\tau_2 = \left[A K F(p) \frac{1}{p} \right] \Delta\tau + \left[K F(p) \frac{1}{p} \right] n(t) , \qquad \text{(B-1)}$$

where p is the operator notation for d/dt. Furthermore, in response to noise alone,

$$\Delta\tau = -\tau_2 , \qquad \text{(B-2)}$$

so that, by combining (B-1) and (B-2), we obtain

$$\Delta\tau = - \frac{\dfrac{K F(p)}{p}}{1 + \dfrac{A K F(p)}{p}} n(t) . \qquad \text{(B-3)}$$

Since it is more convenient to work with power spectral densities, (B-3) is written as

$$S_{\Delta\tau}(\omega) = \left| \frac{K F(j\omega)/j\omega}{1 + A K F(j\omega)/j\omega} \right|^2 S_n(\omega) , \qquad \text{(B-4)}$$

where $S_n(\omega)$ is the power spectral density of the noise and $S_{\Delta\tau}(\omega)$ is the power spectral density of the loop tracking error.

The noise density can be found from consideration of the process taking place in the loop "discriminator" shown in Figure B-3. From examination of the figure, it is seen that the equivalent noise, $n(t)$, for the mathematical model is related to the actual input noise by

$$n(t) = n_i(t) [a(t - \tau_d) - a(t + \tau_d)] , \qquad \text{(B-5)}$$
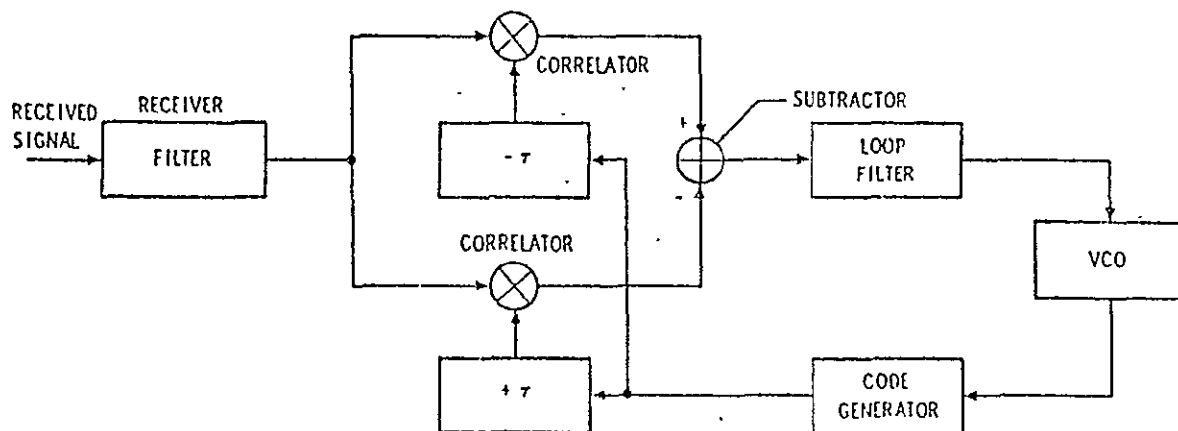
Figure B-1. Block Diagram of Delay Lock Tracking Loop
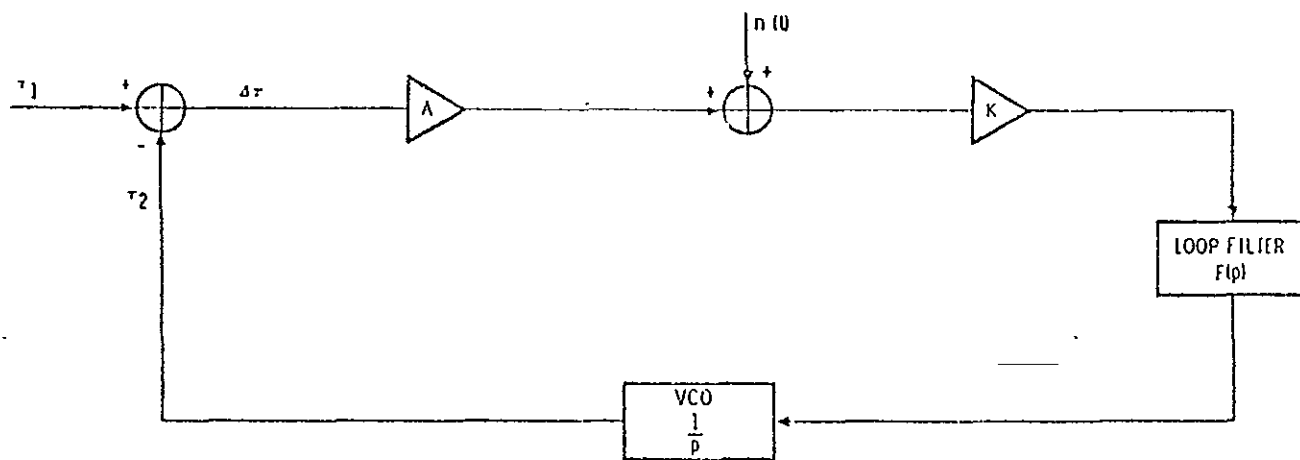
Figure B-2. Mathematical Model of Delay Lock Tracking Loop
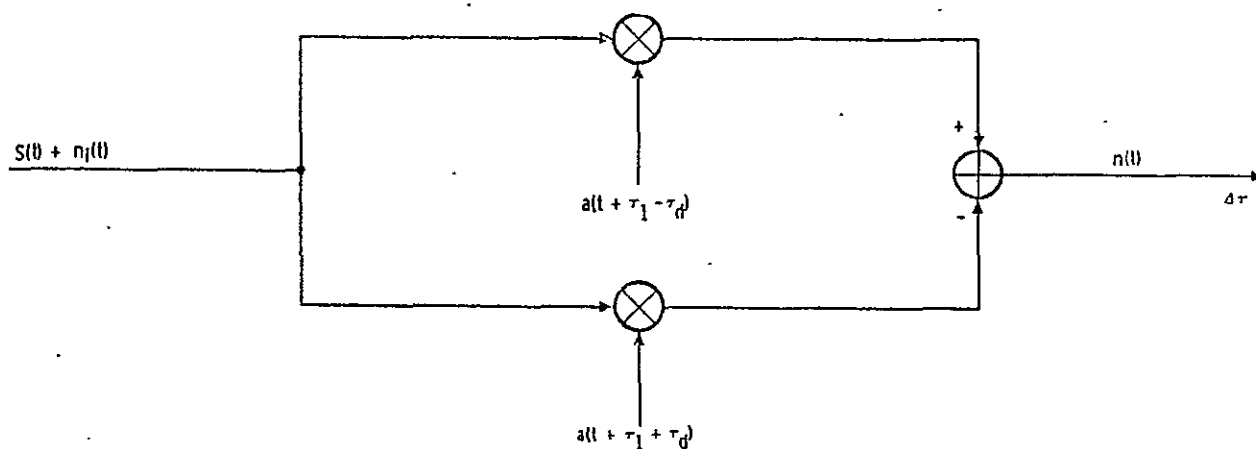
Figure B-3. Delay Lock Loop Error Discriminator

where

$n_i(t)$ = actual input noise $N(t)$ filtered by the receiver filter

$a(t - \tau_d)$ = reference PN code advanced by τ_d bits

$a(t + \tau_d)$ = reference PN code delayed by τ_d bits .

Since multiplication in the time domain is equivalent to convolution in the frequency domain, the power spectral density of the noise $n(t)$ is given by

$$S_n(\omega) = S_{n_i}(\omega) \otimes A(\omega) , \qquad (B\text{-}6)$$

where $A(\omega)$ = power spectral density of $a(t - \tau_d) - a(t + \tau_d)$ and $\otimes$ indicates convolution.

The power spectrum of $A(\omega)$ is given by

$$A(\omega) = a(\omega)\, a(\omega)^* \qquad (B\text{-}7)$$

where $a(\omega)$ = voltage spectrum for $a(t - \tau_d) - a(t + \tau_d)$,

$$a(\omega) = a_0(\omega) \left[e^{-j\omega\tau_d} - e^{+j\omega\tau_d} \right] \qquad (B\text{-}8)$$

so that

$$A(\omega) = A_0(\omega) \left[2 - e^{-j2\omega\tau_d} - e^{j2\omega\tau_d} \right] \qquad (B\text{-}9)$$

where $A_0(\omega)$ is the power spectrum of reference PN code with zero delay and the exponential terms account for the advance of the reference code by τ_d. The received noise spectral density $S_{n_i}(\omega)$ will be assumed to be white of value N_0 watts/Hz and limited to f_R, the bandwidth of the receiver filter.* Thus, from (B-9) and (B-6), the power spectral density of the equivalent noise is given by

---

*f_R = lowpass equivalent bandwidth.

$$N_0^{(out)} = S_n(0) = S_{n_i}(\omega) \otimes A(\omega)$$

$$= \frac{N_0}{2\pi} \int_0^{2\pi f_R} A_0(\omega)\left[2 - e^{-j2\omega\tau_d} - e^{j2\omega\tau_d}\right] d\omega$$

$$= \frac{N_0}{2\pi}\left[2\int_0^{2\pi f_R} A(\omega)\, d\omega - \int_0^{2\pi f_R} A(\omega)\, e^{-j2\omega\tau_d}\, d\omega - \int_0^{2\pi f_R} A_0(\omega)\, e^{j2\omega\tau_d}\, d\omega\right]$$

$$= N_0\left[2\,R(0)_{BL} - R(2\tau_d)_{BL} - R(-2\tau_d)_{BL}\right]$$

$$= 2N_0\left[R(0)_{BL} - R(2\tau_d)_{BL}\right], \tag{B-10}$$

where $R(x)_{BL} \equiv$ the bandlimited autocorrelation function for the PN code evaluated at x. The equivalent noise spectral density given by (B-10) may now be substituted into (B-4) to obtain the tracking error power spectral density, $S_{\Delta\tau}(\omega)$. Thus,

$$S_{\Delta\tau}(\omega) = \left|\frac{K F(j\omega)/j\omega}{1 + A K F(j\omega)/j\omega}\right|^2 2 N_0\left[R(0)_{BL} - R(2\tau_d)_{BL}\right] \tag{B-11}$$

Before proceeding further, it will be helpful to consider the term in the absolute value signs in hopes of simplifying (B-11). First, examining the mathematical model block diagram of Figure B-2, it is seen that the voltage transfer function may be written as

$$\frac{\tau_2}{\tau_1} = \frac{A K F(s)\frac{1}{s}}{1 + A K F(s)\frac{1}{s}} \tag{B-12}$$

and the power transfer function is given by

$$|H(j\omega)|^2 = \left|\frac{A K F(j\omega)\frac{1}{j\omega}}{1 + A K F(j\omega)\frac{1}{j\omega}}\right|^2 \tag{B-13}$$

Since the error signal gain A is independent of ω, (B-13) may be written as

$$\frac{|H(j\omega)|^2}{A^2} = \left|\frac{K F(j\omega)\frac{1}{j\omega}}{1 + A K F(j\omega)\frac{1}{j\omega}}\right|^2 \tag{B-14}$$

The quantity in the absolute value sign on the right side of (B-14) is recognized as being the same quantity in the absolute value signs in (B-11). Thus, substituting (B-14) into (B-11), we obtain

$$S_{\Delta\tau}(\omega) = \frac{|H(j\omega)|^2}{A^2} 2N_0 \left[R(0)_{BL} - R(2\tau_d)_{BL} \right].$$ (B-15)

Each term in (B-15) has been well defined with the exception of A. So far, A has been called the error signal gain. Referring again to the mathematical model of Figure B-2 and the loop "discriminator" of Figure B-3, it is seen that A:

1. Must convert to a time displacement, $\Delta\tau$, between the incoming code and the reference code to an error voltage.

2. Is solely a function of signal and not noise, i.e., is really the loop "discriminator" function for signal.

3. Has an output which is also proportional to the signal level $\sqrt{S}$.

4. Being a discriminator, has a transfer function given by the slope of the discriminator characteristic.

Thus, based on the above considerations,

$$A = \sqrt{S} \frac{d}{d\tau} \langle a(t+\tau_1) a(t-\tau_2-\tau_d) - a(t+\tau_1) a(t+\tau_2+\tau_d) \rangle_{\Delta\tau = 0} , \quad (B-16)$$

where

$$\langle X \rangle = \text{time average value of } X$$
$$X = \text{signal power}.$$

By making a simple change of variables, (B-16) may be written as

$$A = \sqrt{S} \frac{d}{d\tau} \langle a(t) a(t+\Delta\tau-\tau_d) - a(t) a(t+\Delta\tau+\tau_d) \rangle_{\Delta\tau = 0}$$ (B-17)

$$= \sqrt{S} \frac{d}{d\tau} \left[R(\Delta\tau-\tau_d)_{BL} - R(\Delta\tau+\tau_d)_{BL} \right]_{\Delta\tau = 0} ,$$ (B-18)

where the quantity $R(\Delta\tau-\tau_d) - R(\Delta\tau+\tau_d)$ is the discriminator characteristic for the delay lock tracking loop. Thus,

$$A = \sqrt{S} \left[R'(\Delta\tau-\tau_d)_{BL} - R'(\Delta\tau+\tau_d)_{BL} \right]_{\Delta\tau = 0}$$

$$= \sqrt{S} \, 2R'(\tau_d)_{BL} ,$$ (B-19)

where the bandlimited autocorrelation function is used since the signal
is first filtered by the receiver filter. By substituting (B-19) into
(B-15), we obtain

$$S_{\Delta\tau}(\omega) = |H(j\omega)|^2 \frac{2N_0 [R(0)_{BL} - R(2\tau_d)_{BL}]}{S [2R'(\tau_d)_{BL}]^2} . \qquad \text{(B-20)}$$

From noise theory,

$$\sigma_n^2 = \int_0^\infty S_n(\omega) \frac{d\omega}{2\pi} \qquad \text{(B-21)}$$

so that, by substituting (B-20) into (B-21), we obtain

$$\sigma_{\Delta\tau}^2 = \int_0^\infty |H(j\omega)|^2 \frac{2N_0 [R(0)_{BL} - R(2\tau_d)_{BL}]}{S [2R'(\tau_d)_{BL}]^2} \frac{d\omega}{2\pi}$$

$$= \frac{2N_0}{S} \frac{R(0)_{BL} - R(2\tau_d)_{BL}}{[2R'(\tau_d)_{BL}]^2} \int_0^\infty |H(j\omega)|^2 \frac{d\omega}{2\pi} . \qquad \text{(B-22)}$$

The noise bandwidth of a transfer function is defined as

$$B_L \equiv \int_0^\infty |H(j\omega)|^2 \frac{d\omega}{2\pi} , \qquad \text{(B-23)}$$

so that (B-22) reduces to

$$\sigma_{\Delta\tau}^2 = \frac{2N_0 B_L}{S} \frac{R(0)_{BL} - R(2\tau_d)_{BL}}{[2R'(\tau_d)_{BL}]^2} . \qquad \text{(B-24)}$$

Thus, the delay lock loop rms tracking error may be written as

$$\Delta\tau_{rms} = \frac{1}{\sqrt{\dfrac{S}{2N_0 B_L}}} \frac{\sqrt{R(0)_{BL} - R(2\tau_d)_{BL}}}{2R'(\tau_d)_{BL}} , \qquad \text{(B-25)}$$

where

B_L = one-sided loop noise bandwidth

N_0 = one-sided noise power density

S = average signal power.

2.0 DELAY LOCK LOOP TRACKING PERFORMANCE

It is desirable to plot the rms tracking error, $\Delta\tau_{rms}$, as a function of $S/N_0 B_L$, the loop signal-to-noise ratio, and several values of bandlimiting and displacement τ_d. The bandlimited autocorrelation functions used in (B-25) can be shown to be given by

$$R(X) = \frac{1}{\pi} \left[\frac{2}{B} \cos [BX] \left\{ \cos [B] - 1 \right\} - 2X \, si \, [BX] \right.$$

$$\left. + (1+X) \, si \, [B(1+X)] + (1-X) \, si \, [B(1-X)] \right] , \qquad (B-26)$$

where .

$$B = 2\pi f_R T_c$$

f_R = one-sided bandwidth of receiver filter

T_c = PN code bit width

X = time displacement in bits

and

$$si \, [X] = \int_0^X \frac{\sin y}{y} \, dy . \qquad (B-27)$$

The rms tracking error (B-25) is plotted in Figure B-4 as a function of $S/N_0 B_L$ and several values of B and τ_d. It is obvious that the larger B is, the smaller $\Delta\tau_{rms}$, and the smaller τ_d, the smaller $\Delta\tau_{rms}$. However, because of data transmission requirements and limited available spectrum, B is typically limited to 1.5π in a spread spectrum system. Thus, a plot of $\Delta\tau_{rms}$ versus τ_d for B = 1.5π, 3π, and ∞, as shown in Figure B-5 shows that for no bandlimiting the tracking error may be made infinitesimally small by making τ_d infinitesimally small. However, for practical values of bandlimiting, i.e., B = 1.5π, $\Delta\tau_{rms}$ changes very little as a function of τ_d.

The theoretical conclusion that an improvement is achieved by letting $\tau_d \to 0$ ignores the threshold behavior of the tracking loop, and actually an optimum τ_d exists for delay lock. To see this, assume a finite spacing for the delay lock tracking with an unfiltered signal having the ideal triangular autocorrelation function. Figure B-6 shows the error characteristics for a typical spacing $2\tau_d$, where the signal power is S and the PN clock interval is T_c. The output noise density
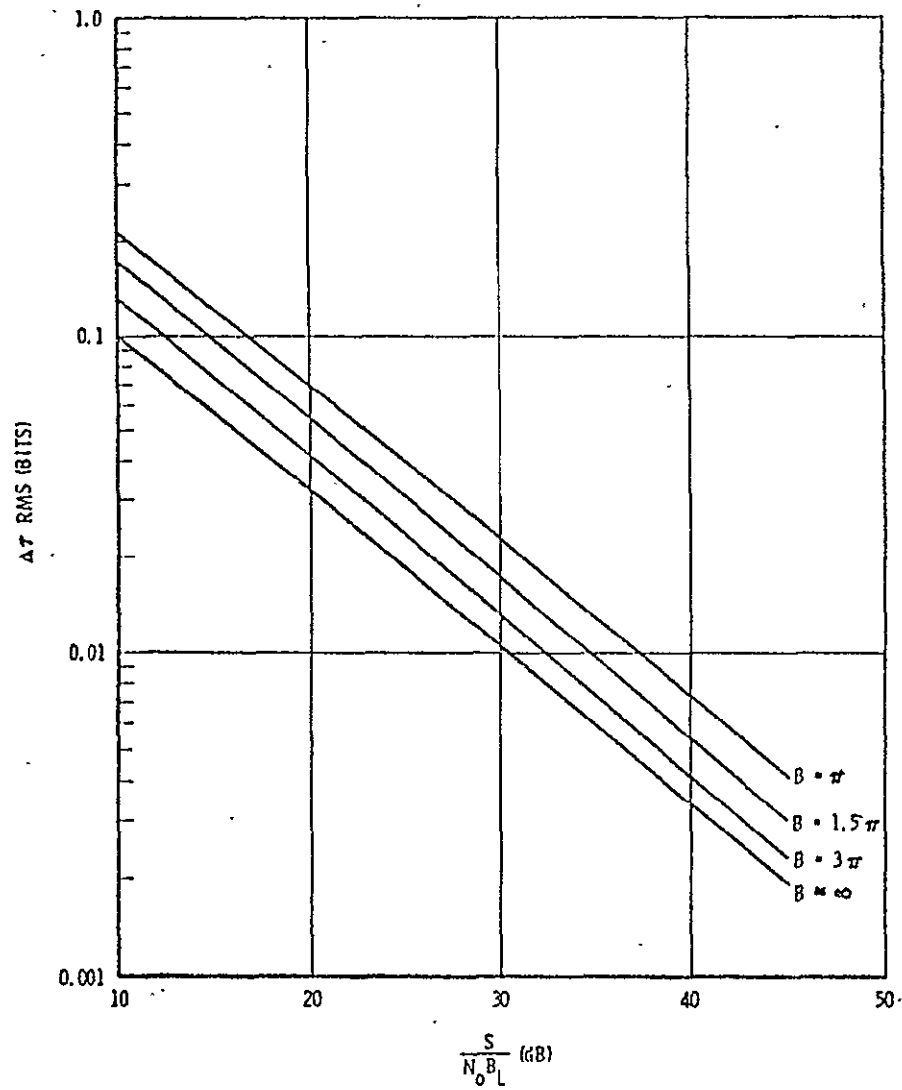
Figure B-4.   Delay Lock Loop rms Tracking Error vs. Loop Signal-
to-Noise Ratio; $\tau_d = 0.1$
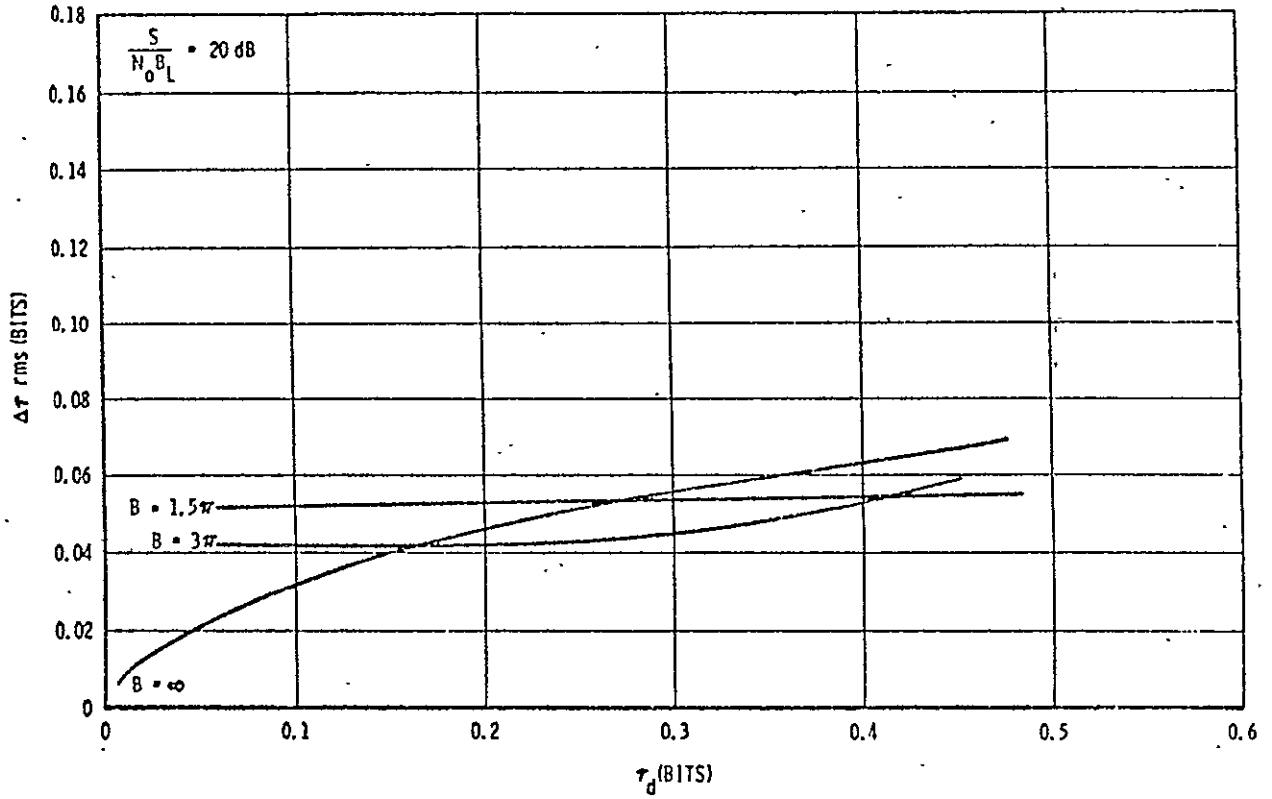
Figure B-5.   Delay Lock Loop rms Tracking Error as a Function of Displacement τ_d
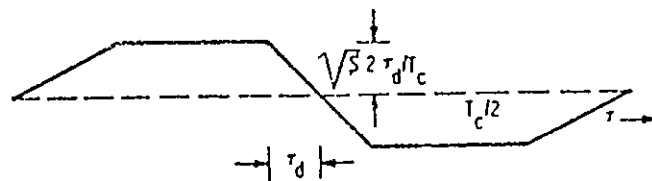
Figure B-6.   Error Characteristic for Delay Lock Tracking

for the delay lock tracker is given by (B-10) and, for the case of no filtering, reduces to

$$N_0^{(out)} = 4 N_0 \tau_d / T_c , \qquad (B-28)$$

where N_0 is the received noise density (one-sided). Since the slope of the error characteristic in the vicinity of zero error is

$$\text{Error slope} = \frac{\sqrt{S} \, 2\tau_d / T_c}{\tau_d} = \frac{2\sqrt{S}}{T_c} , \qquad (B-29)$$

the mean square tracking error is

$$\sigma_{\Delta\tau}^2 = \frac{N_0^{(out)} B_L}{[\text{Slope}]^2} = \frac{N_0 B_L}{S} \tau_d T_c , \qquad (B-30)$$

where B_L is the noise bandwidth of the linearized tracking loop.

The problem is now evident that a threshold exists. Note from Figure B-6 that τ_d is the limit of linearity, while (B-30) shows the rms time error due to noise is proportional to $\sqrt{\tau_d}$, other parameters being fixed. Thus, although (B-30) predicts a constantly decreasing error as τ_d is decreased, the region of linearity will be exceeded at some value of τ_d. Hence, an optimum choice for τ_d may be expected.

As an approximate first analysis, consider the quasi-linearization approach[*] which has been applied to demonstrate threshold in a phase lock loop. This approach replaces the nonlinear error characteristic by an equivalent gain (i.e., slope) for a linearized model, given by

$$\text{Equivalent slope} = \int_{-\infty}^{\infty} h'(\tau) \, p(\tau) \, d\tau , \qquad (B-31)$$

where

$h(\tau)$ = error characteristic

$p(\tau)$ = probability density of the time error, assumed to be Gaussian distributed.

With this equivalent slope, the closed loop bandwidth B_L can still be defined meaningfully. For the case of zero mean error and a variance

---

[*] J. A. Develet, Jr. "A Threshold Criterion for Phase-Lock Demodulation," Proc. of IRE, Vol. 51, February 1963, pp. 349-356.

$\sigma_{\Delta\tau}^2$, (B-31) is evaluated for the characteristic of Figure B-4 to be

$$\text{Equivalent Gain} \cong \int_{-\tau_d}^{\tau_d} (\sqrt{S} \, 2/T_c) \, \frac{1}{\sqrt{2\pi} \, \sigma_{\Delta\tau}} \, e^{-\tau^2/2\sigma_{\Delta\tau}^2} \, d\tau$$

$$= \frac{2\sqrt{S}}{T_c} \, [\Phi(\tau_d/\sigma_{\Delta\tau}) - \Phi(-\tau_d/\sigma_{\Delta\tau})] \tag{B-32}$$

considering, for simplicity, only the central portion of the error characteristics as significant. For $\sigma_{\Delta\tau} \to 0$, the expression reduces to the slope at $\tau = 0$. For larger $\sigma_{\Delta\tau}$, the equivalent slope is reduced, which increases the error using (B-30) with the equivalent slope substituted. This becomes

$$\sigma_{\Delta\tau}^2 \cong \left(\frac{N_0 B_L}{S}\right) \frac{\tau_d T_c}{[\Phi(\tau_d/\sigma_{\Delta\tau}) - \Phi(-\tau_d/\sigma_{\Delta\tau})]^2} \, . \tag{B-33}$$

Minimization of (B-33) by varying τ_d is now to be carried out. In normalized form, this is equivalent to maximizing the function

$$f(x) = [\Phi(x) - \Phi(-x)]^2/x \tag{B-34}$$

which occurs at $x = 1.4$. Thus, the optimum τ_d satisfies

$$\frac{\tau_d}{\sigma_{\Delta\tau}} = 1.4 , \tag{B-34}$$

which relates the optimum spacing to the tracking error, and the minimum rms error is computed to be

$$\left.\frac{\sigma_{\Delta\tau}}{T_c}\right|_{min} \cong 2 \, \frac{N_0 B_L}{S} \tag{B-36}$$

for the optimum τ_d given in (B-35). Equation (B-36) reflects the decrease in optimum τ_d as $S/N_0 B_L$ increases.

As an illustration, if $S/N_0 B_L = 20$ dB, the theoretical minimum tracking error is 0.02 of the PN bit interval, and the optimum separation is $\tau_d = 0.024$ of the PN bit interval.

In the bandlimited case, the performance varied much less (essentially not at all for $B = 1.5\pi$) with the separation τ_d. Thus, considering

practical filtering requirements, the choice of delay lock separation
is not critical. With saturation brought in again, the design tendency
should be towards large τ_d.

3.0 ANALYSIS OF THE TAU JITTER LOOP

A block diagram of a tau jitter tracking loop is shown in
Figure B-7. For analysis purposes, the equivalent math model for the
tau jitter tracking loop is the same as that for the delay lock loop,
with the exception of the error discriminator. Essentially, the error
voltage is generated by correlating the received code with a reference
code which is alternately advanced and delayed (jittered) by τ_d bits
and phase detecting the resultant signal with the square wave voltage
which jittered the reference code. This error discriminator is modeled
as shown in Figure B-8. By calculating the error signal gain, A, and
the output noise power for this discriminator, some of the results of
the delay lock loop analysis based on Figure B-2 may be used.

For the purpose of analysis, the jittering of the reference code
is accomplished by means of a switching function $U(t)$, which has the
following properties:

1. $U(t) = 0$

2. $\widehat{U(t)} = 1 - U(t)$

3. $\langle U(t) \rangle = \langle \widehat{U(t)} \rangle = 0.5$

4. $U(t)^N = U(t), \quad \widehat{U(t)}^N = \widehat{U(t)}; \quad N = 0,1,2,\ldots$

5. $U(t)\widehat{U(t)} = 0$.

The jittered reference PN code is denoted by

$$V_0(t) = a(t + \tau_2 - \tau_d)\,U(t) - a(t + \tau_2 + \tau_d)\,\widehat{U(t)}$$

so that the correlator output is given by

$$V_1(t) = [\sqrt{S}\,a(t + \tau_1) + n(t)][a(t + \tau_2 - \tau_d)\,U(t) - a(t + \tau_2 + \tau_d)\,\widehat{U(t)}].$$
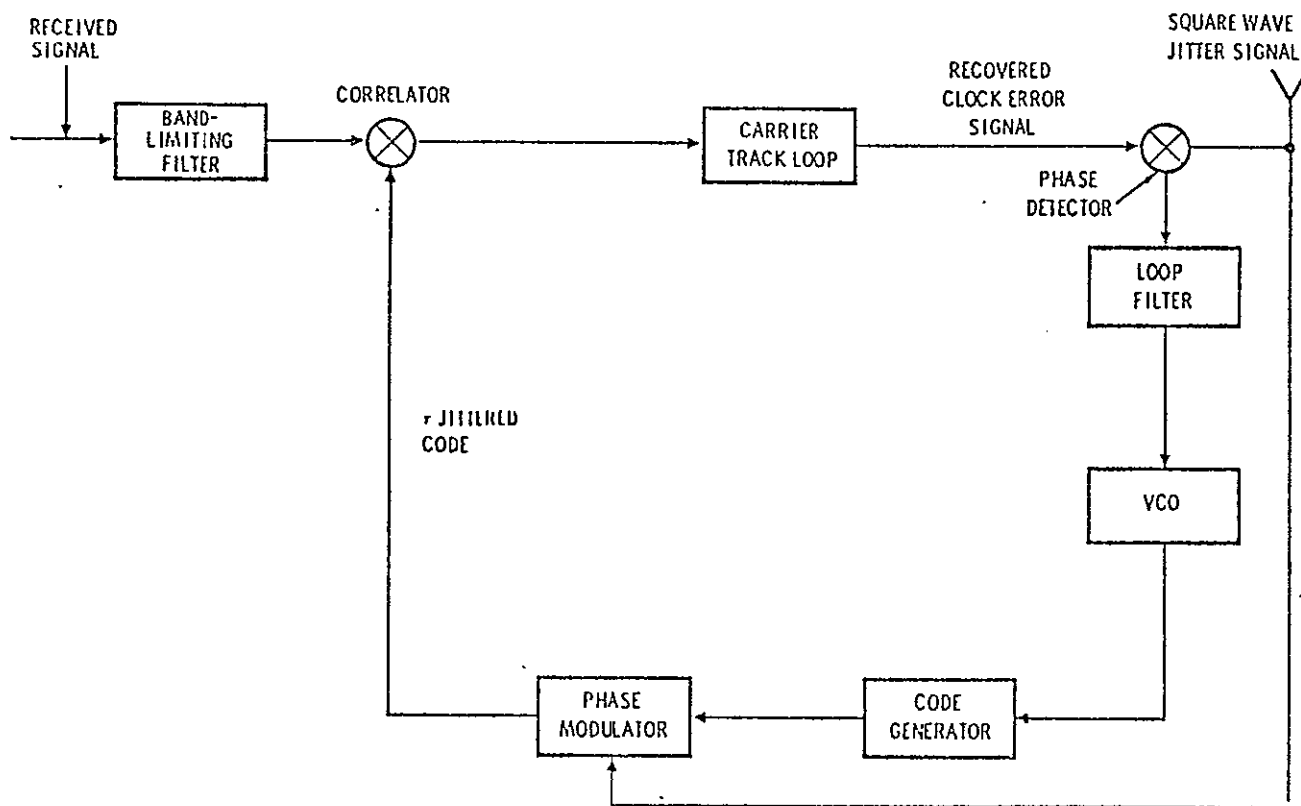
Figure B-7. Tau Jitter Tracking Loop
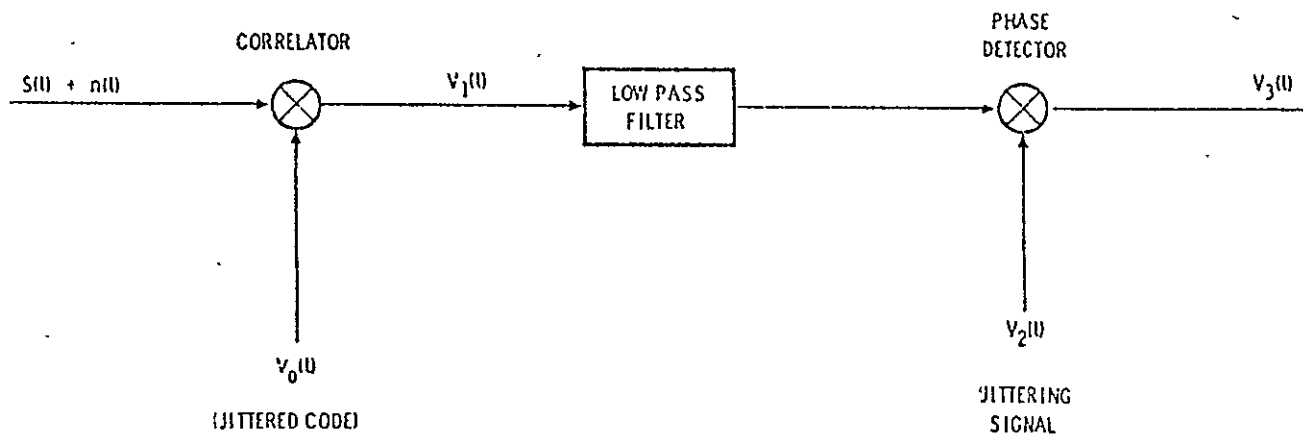
Figure B-8. Tau Jitter Error Discriminator Model

The reference for the phase detector is the jittering signal and is denoted by

$$V_2(t) = U(t) - \widehat{U(t)} \ .$$

The output of the phase detector is given by

$$V_3(t) = V_1(t) V_2(t)$$

$$= [\sqrt{S} \, a(t+\tau_1) + n(t)][a(t+\tau_2-\tau_d) U(t) - a(t+\tau_2+\tau_d) \widehat{U(t)}][U(t) - \widehat{U(t)}]$$

$$= \sqrt{S} \, a(t+\tau_1)[a(t+\tau_2-\tau_d) U(t)^2 - a(t+\tau_2+\tau_d) \widehat{U(t)}^2]$$

$$+ n(t) [a(t+\tau_2-\tau_d) U(t)^2 - a(t+\tau_2+\tau_d) \widehat{U(t)}^2] \ . \quad \text{(B-37)}$$

The average value of the phase detector output, $V_3(t)$, is the discriminator error voltage,

$$V_3(t) = \langle \sqrt{S} \, a(t+\tau_1)[a(t+\tau_2-\tau_d) U(t)^2 - a(t+\tau_2+\tau_d) \widehat{U(t)}^2] \rangle$$

$$= \frac{\sqrt{S}}{2} \left[R(\Delta\tau - \tau_d)_{BL} - R(\Delta\tau + \tau_d)_{BL} \right]. \quad \text{(B-38)}$$

The quantity inside the square brackets is recognized as being the same discriminator characteristic as the delay lock loop. Thus, as before, the error signal gain, A, for the math equivalent model is given by

$$A = \frac{d}{d\tau} \frac{\sqrt{S}}{2} \left[R(\Delta\tau - \tau_d)_{BL} - R(\Delta\tau + \tau_d)_{BL} \right]_{\Delta\tau = 0}$$

$$= \sqrt{S} \, R'(\tau_d)_{BL} \ . \quad \text{(B-39)}$$

Since the discriminator shown in Figure B-8 is a linear system, it is possible to find the relationship between the noise density at its input and at its output by finding the relationship between the input and output noise power. The noise power in the output is found by squaring $V_3(t)$ and averaging. Thus,

$$P_{N_{out}} = \langle V_3(t)_n^2 \rangle \quad \text{(subscript n indicates noise component of } V_3(t))$$

$$= \Big\langle n(t)^2 \Big[a(t+\tau_2-\tau_d)^2 U(t)^2 + a(t+\tau_2+\tau_d)^2 \widehat{U(t)}^2 $$

$$+ 2a(t+\tau_2-\tau_d) a(t+\tau_2+\tau_d) U(t) \widehat{U(t)} \Big] \Big\rangle$$

$$= \Big\langle n(t)^2 \Big[a(t+\tau_2-\tau_d)^2 U(t) + a(t+\tau_2+\tau_d)^2 \widehat{U(t)} \Big] \Big\rangle$$

$$= \langle n(t)^2 \rangle \langle a(t+\tau_2-\tau_d)^2 \rangle \langle U(t) \rangle + \langle a(t+\tau_2+\tau_d)^2 \rangle \langle U(t) \rangle \quad \text{(B-40)}$$

Since the noise is bandlimited by the receiver filter,

$$\langle a(t+\tau_2-\tau_d)^2 \rangle = \langle a(t+\tau_2+\tau_d)^2 \rangle = R(0)_{BL}$$

and (B-40) reduces to

$$P_{N_{out}} = \langle n(t)^2 \rangle R(0)_{BL} . \quad \text{(B-41)}$$

since

$$P_{N_{in}} = \langle n(t)^2 \rangle .$$

We find that the noise power out of the tau jitter discriminator is related to the noise power in by

$$P_{N_{out}} = P_{N_{in}} R(0)_{BL}$$

so that by considering the noise in the same bandwidth

$$N_0^{(out)} = N_0 R(0)_{BL} , \quad \text{(B-42)}$$

where N_0 is the input noise power spectral density. Thus, from (B-4), the spectral density for the tracking error for the tau jitter tracking loop is given by

$$S_{\Delta\tau}(\omega) = \left| \frac{K F(j\omega)/j\omega}{1 + A K F(\omega)/j\omega} \right|^2 N_0 R(0)_{BL} . \quad \text{(B-43)}$$

Upon substituting (B-14) into (B-43), the tracking error spectral density is found to be

$$S_{\Delta\tau}(\omega) = \frac{|H(j\omega)|^2}{A^2} N_0 R(0)_{BL} \tag{B-44}$$

and since A for the tau jitter loop is given by (B-39), (B-44) reduces to

$$S_{\Delta\tau}(\omega) = \frac{N_0 R(0)_{BL}}{S[R'(\tau_d)_{BL}]^2} |H(j\omega)|^2 . \tag{B-45}$$

Thus, the variance of the tracking error is found to be

$$\sigma^2_{\Delta\tau} = \int_0^\infty S_{\Delta\tau}(\omega) \frac{d\omega}{2\pi}$$

$$= \frac{N_0}{S[R'(\tau_d)_{BL}]^2} \int_0^\infty |H(j\omega)|^2 \frac{d\omega}{2\pi} \tag{B-46}$$

$$= \frac{N_0 B_L R(0)_{BL}}{S[R'(\tau_d)_{BL}]^2}$$

so that the rms tracking error for the tau jitter loop is given by

$$\Delta\tau_{rms} = \frac{1}{\sqrt{S/N_0 B_L}} \frac{R(0)_{BL}}{R'(\tau_d)_{BL}} . \tag{B-47}$$

4.0 TAU JITTER TRACKING LOOP PERFORMANCE AND COMPARISON WITH DELAY LOCK LOOP PERFORMANCE

The rms tracking error for the tau jitter tracking loop (B-47) is shown plotted in Figure B-9. A bandlimiting factor of $B = 1.5\pi$ was used since that value is typically used in PN systems. As can be seen, the error increases as τ_d, the jitter displacement, decreases. The dependence of $\Delta\tau_{rms}$ on τ_d is better illustrated by the plot of $\Delta\tau_{rms}$ versus τ_d shown in Figure B-10. This inverse relationship between τ_d and $\Delta\tau_{rms}$ is the opposite of the relationship for the delay lock loop, where $\Delta\tau_{rms}$ decreases for decreasing τ_d. This performance difference is obvious from comparing (B-25) and (B-47). However, a better understanding of the performance difference between the two loops is obtained from comparing what happens to the input noise in each of
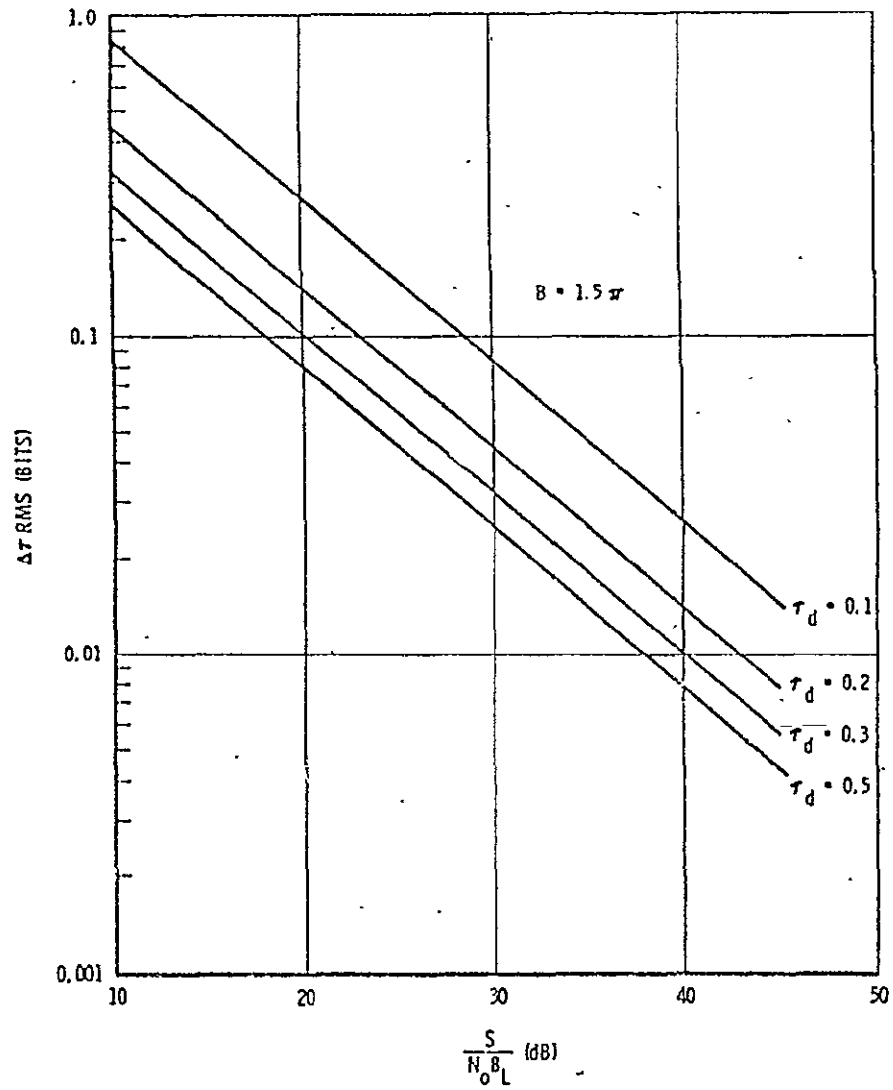
Figure B-9. Tau Jitter Tracking Loop Error as a Function
of Loop Signal-to-Noise Ratio
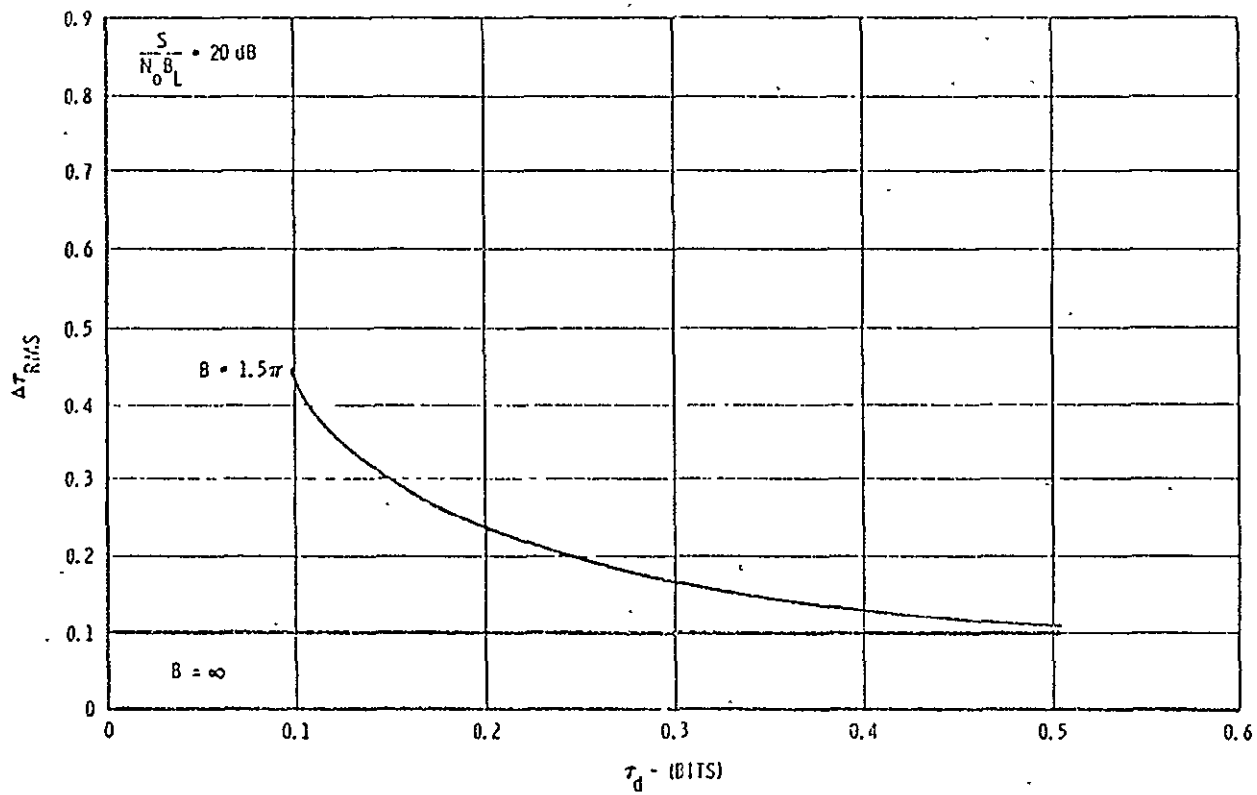
Figure B-10. Tau Jitter Tracking Loop Error as a Function of Jitter
Displacement τ_d

the "discriminators." In the delay lock loop, as τ_d becomes smaller, the noise at the output of each correlator becomes more correlated with the other channel's noise. Thus, as $\tau_d \rightarrow 0$, the noise in each channel becomes the same, so that the subtractor is subtracting the noise from itself and the noise output becomes zero. If the noise approaches zero, it is obvious that the tracking error also approaches zero. (However, due to bandlimiting and practical considerations, this does not actually happen in hardware loops.) The tau jitter loop, on the other hand, does not subtract noise from itself since it time-shares (time multiplexes) a common channel between the advanced and delayed signals. Furthermore, as τ_d becomes smaller, the slope of the bandlimited autocorrelation curve decreases and since the error signal gain is given by this slope, the performance of the loop decreases. The error signal gain for the delay lock loop also decreases as τ_d gets smaller; however, this is offset by the decrease in effective loop noise.

The degradation of tracking performance for a tau jitter loop relative to a delay lock loop and a conventional phase locked loop is shown plotted in Figure B-11. The plot is a function of τ_d, with $B = 1.5\pi$. Since it is sometimes the practice to make τ_d small (around 0.1 bit) so that the correlator output may also be used for data demodulation, it is obvious that much better tracking performance may be obtained from the delay lock loop.

5.0   EFFECTS OF CHANNEL UNBALANCE ON DELAY LOCK LOOP PERFORMANCE

In view of the superior tracking performance of the delay lock loop, it is worthwhile considering the effects of channel gains and time delay differentials on tracking error. Figure B-12 shows a delay lock discriminator model having a differential time delay of τ in one channel and a differential amplitude gain of K in the other channel.

This is merely the general case of the delay lock loop analysis given in Section B-1, where $\tau = 0$ and $K = 1$. Thus, it is easy to show that the rms tracking error for the loop having the discriminator shown in Figure B-12 is given by

$$\Delta\tau_{rms} = \frac{1}{S/N_0 B_L} \frac{(1 + K^2) R(0)_{BL} - 2 K R(2\tau + \Delta)_{BL}}{K R(\tau)_{BL} - R(-\tau + \Delta)_{BL}} . \tag{B-48}$$
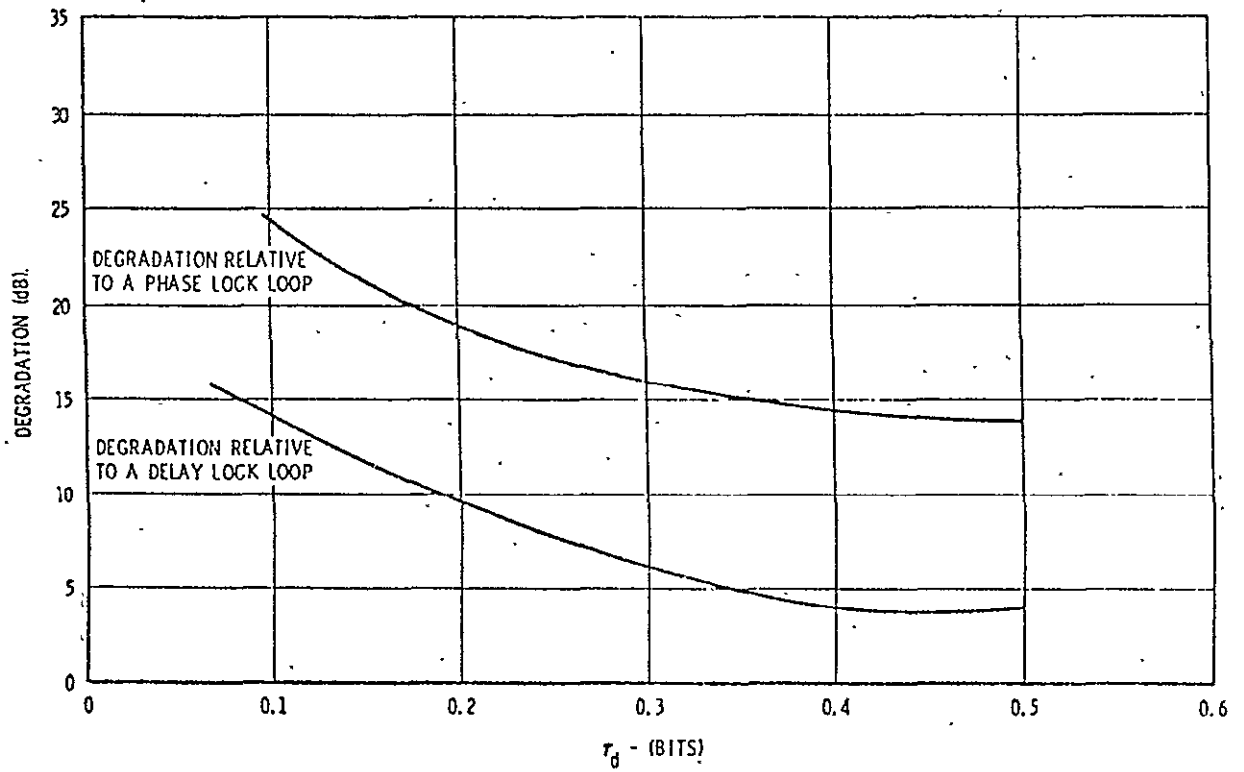
Figure B-11. Tau Jitter Tracking Degradation as a Function of τ_d
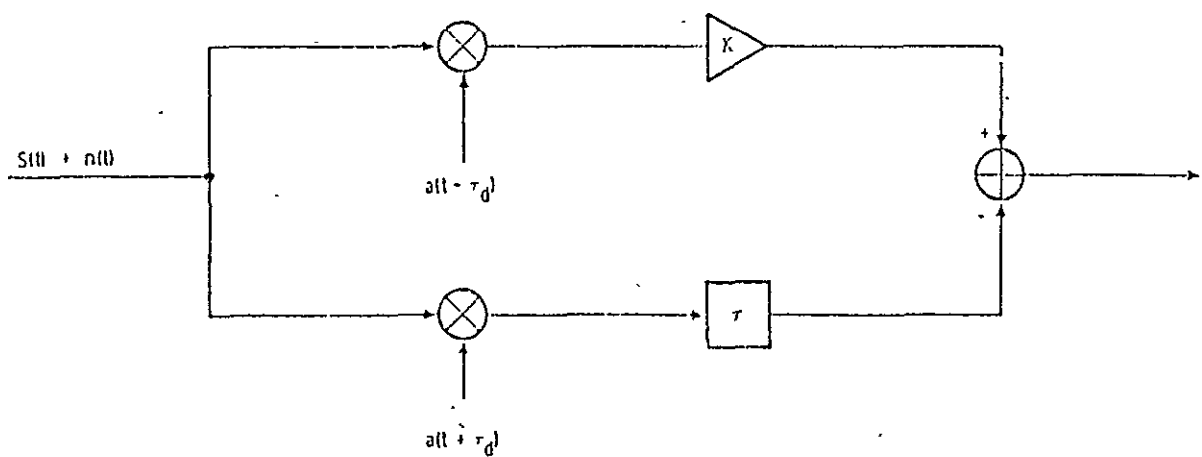
Figure B-12. Delay Lock Loop Discriminator with Gain and Time Delay Unbalances

By comparing the performance specified in (B-25) with that specified by (B-48), the effects of Δ and K may be evaluated. These effects are shown tabulated in Table B-1. It seems reasonable that, through good engineering design, the gain differential should be no greater than 1 dB and the time delay differential should be no greater than 10% of the time displacement of the reference code, τ_d. From Table B-1, it can be seen that this results in 10% increase in the rms tracking error or approximately 1 dB performance degradation.

Table B-1. Effect of Gain and Delay Differentials on Delay Lock Loop Tracking Error

K (dB)	τ (bits)	τ/τ_d (%)	Percent Change of $\Delta\tau_{rms}$
0.1	0.01	10	12
0.1	0.05	50	65
1.0	0.01	10	15
1.0	0.05	50	71

6.0 CONCLUSIONS

The analysis of clock tracking error in a pseudonoise spread spectrum system shows that a delay lock loop is preferred over a tau-jitter loop because the achieved error is smaller. An optimum correlator separation exists for the delay lock configuration, essentially equal to the magnitude of the noise-induced error for the wideband case. With a filtered signal, the choice of correlator separation is not critical, and a wider separation eases implementation problems associated with balance of the two correlator channels.

The tau jitter loop with large jitter is not practical because of the degradation of the carrier tracking loop, which was not included in this general analysis. With small jitter, the degradation compared with delay lock is substantial.

The clock tracking loop can be treated as a second order loop of specified bandwidth within the linear tracking range (or quasi-linear tracking range).

APPENDIX C

LOSS OF LOCK AND REACQUISITION PERFORMANCE
OF CARRIER TRACKING LOOPS

1.0   INTRODUCTION

In GPS navigation systems, the user must, in addition to measuring range, measure range rate and receive satellite ephemeris data. A carrier tracking loop enables range rate to be determined precisely by recovering carrier doppler. It also may be used to demodulate a phase shift keyed (PSK) data waveform. To successfully perform these functions, the carrier loop must retain lock with high probability and reacquire in a short time period with high probability.

The conditions under which the carrier tracking loop must reliably track include low signal-to-noise ratio and high user dynamics, i.e., high acceleration and acceleration rate (jerk). A typical acceleration profile is a ramp in acceleration, starting at zero acceleration at t_0 and leveling off at a constant value A at time t_1, i.e., a pulse in jerk $t_0 - t_1$ wide and of amplitude $A/t_0 - t_1$. Such dynamics require large loop bandwidths to retain loop lock, whereas the low signal energy-to-noise density ratio (E/N_0) requires narrow loop bandwidths to retain loop lock.

2.0   LINEAR MODEL

A linear theory model of a generalized phase lock carrier loop is first developed to determine an optimum bandwidth to minimize total loop tracking error, i.e., noise jitter error plus dynamic error. This bandwidth is a basis for the selection of bandwidths used in a digital computer Monte-Carlo simulation of the carrier tracking loop.

It is desirable to minimize the total loop error, defined here as

$$E = K\sigma_N + \theta_e(t) , \qquad\qquad (C-1)$$

where K equals statistical confidence factor, by proper selection of ω_n. The standard deviation of the noise error, σ_N, is given by the familiar expression

$$\sigma_N = \frac{1}{\sqrt{C/N_0 \, B_L}} \tag{C-2}$$

where

C = received carrier power (watts)

N_0 = noise power density (watts/Hz)

B_L = one-sided loop noise bandwidth (Hz).

     = $0.53 \, \omega_n$ (second order)

     = $0.843 \, \omega_n$ (third order).

The loop dynamic error, $\theta_e(t)$, is defined by the expressions

$$\frac{\theta_e(S)}{\theta_i(S)} = \frac{S^2}{S^2 + \sqrt{2} \, \omega_n S + \omega_n^2} \quad \text{(second order)} \tag{C-3}$$

$$\frac{\theta_e(S)}{\theta_i(S)} = \frac{S^3}{S^3 + 2\omega_n S^2 + 2\omega_n^2 S + \omega_n^3} \quad \text{(third order)}. \tag{C-4}$$

By differentiating E with respect to ω_n and setting the result equal to zero, the optimum bandwidth $\omega_{n_{opt}}$ for a given set of conditions may be found. By substituting $\omega_{n_{opt}}$ back into (C-1), the minimum loop error is found. If this is done for a pulse in jerk ($\dddot{R}$) input, it is appropriate to set $t = \infty$ for the second order loop and to set t equal to the value which maximizes $\theta_e(t)$ for the third order loop. When this is done, plots of E versus K for the second and third order loops are obtained, as shown in Figure C-1. These plots are for the specific case of $C/N_0 = 25$ dB, jerk = 10 G/s for 0.6 second and carrier frequency = 1.6 GHz. Since these plots are obtained from a linear model of an essentially nonlinear system, the statistical confidence factor K is chosen fairly large, i.e., $K = 3$. Then $\omega_{n_{opt}} = 31$ for the third order loop and $\omega_{n_{opt}} = 90$ for the second order loop. Thus, a starting point for the selection of bandwidths for a Monte Carlo simulation of the carrier tracking loop has been established.

3.0   MONTE CARLO SIMULATION

The carrier tracking loop is a nonlinear system during loss of lock and reacquisition. Therefore, the determination of its performance is not amenable to the usual analytic techniques. For this reason,

a Monte Carlo digital computer simulation of a Costas carrier tracking loop and a phase lock carrier tracking loop was performed. The Costas carrier tracking loop was considered first, since it offers the advantage of enabling a completely suppressed carrier waveform, such as bi-phase PSK, to be transmitted, thus wasting no power in the transmission of a phase reference. However, a Costas loop is essentially a squaring loop and thus is expected to give degraded performance at low signal-to-noise ratios. For this reason, a phase lock carrier tracking loop is also considered. Use of the phase lock loop, however, necessitates the transmission of an unmodulated carrier reference to enable data demodulation. A block diagram of the Costas loop as it was simulated is shown in Figure C-2.

The simulation was implemented on the computer by means of linear difference equations for 1/S and F(S) and the appropriate non-linear phase detector characteristics. Since the Costas and phase lock carrier tracking loops have identical linearized model transfer functions, the difference equations developed apply to either loop. To simulate the phase lock carrier loop, the inphase channel input to the third multiplier shown in Figure C-2 is merely set equal to 1.

If the carrier loop loses lock due to a loss of signal strength, it is desirable that it reacquire while in the track mode. It is necessary to know the maximum frequency (velocity) offset that can occur and still have the loop reacquire quickly. The Monte Carlo simulation discussed above was utilized to determine this. For this simulation, the loop was started with a random phase angle and the frequency offset in question. As before, the lock detector consists of making a threshold decision on the $\cos (\theta - \hat{\theta})$ term.

4.0   SIMULATION RESULTS

The loss of lock cumulative probability distribution curves for the third order Costas and phase lock loops which were obtained from the simulations are shown in Figure C-3. The input dynamics are also shown; C/N_0 is a parameter. It can be seen that the phase lock loop has approximately 6 dB better performance than the Costas loop. The loss of lock distribution curves for the second order loop are also shown in Figure C-3. It can be seen that the third order phase lock loop has approximately 4 dB better performance than the second order

loop for the dynamics considered. It is interesting to note that the optimum bandwidth found from the simple linear model agrees closely with the optimum bandwidth found by varying the simulation loop bandwidth, thus demonstrating the usefulness of the linear model bandwidth selection method.

The reacquisition time cumulative probability distribution curves for the third order phase lock loop are shown in Figure C-4. It can be seen that, as the input frequency offset becomes much larger than the loop bandwidth, the acquisition time in the track mode increases to an impractical value for a GPS navigation-satellite user.
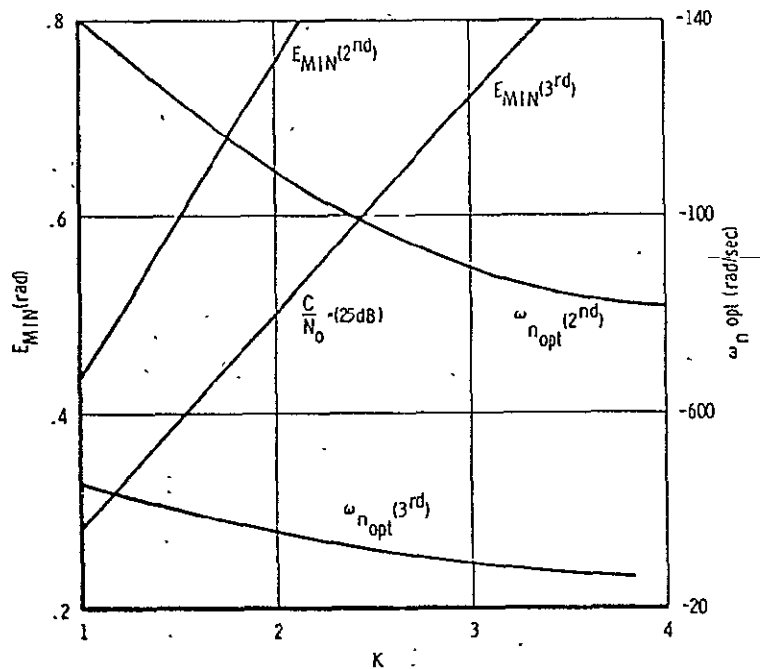
Figure C-1. Optimum Loop Bandwidth and Minimum Loop Error
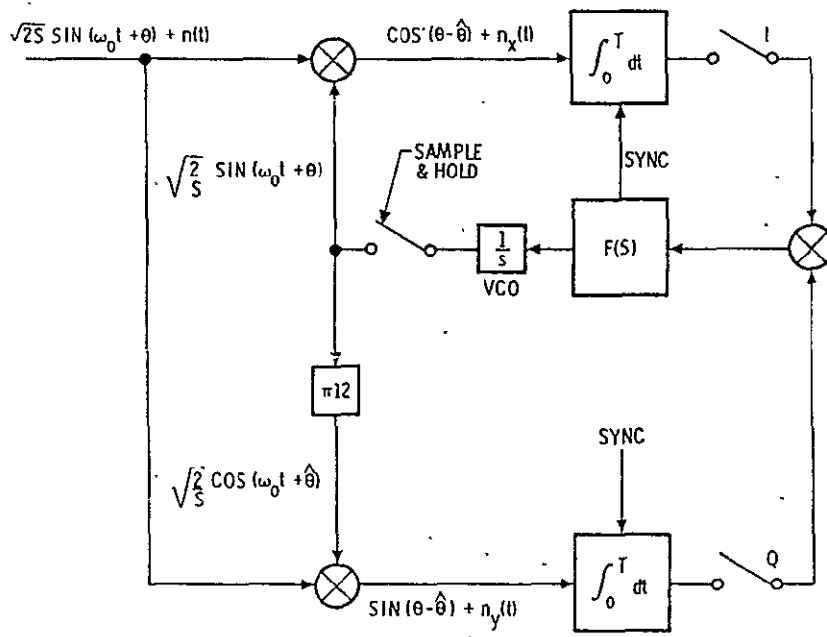
Figure C-2. Digital Costas Loop
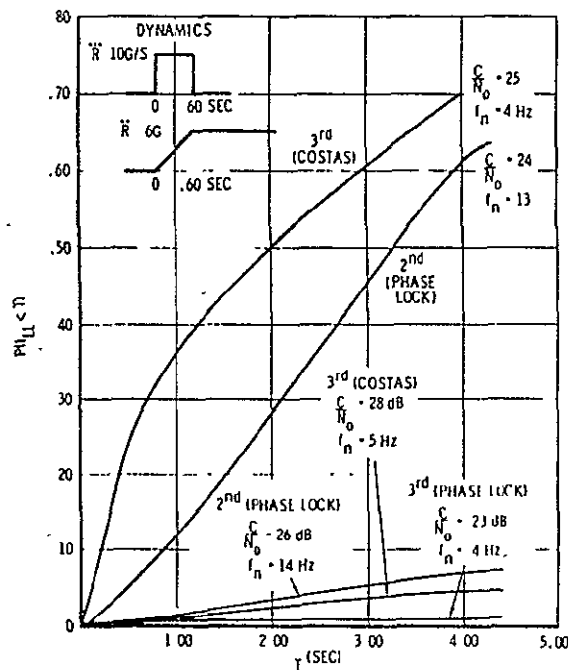
Figure C-3. Loss of Lock Cumulative Probability Distributions
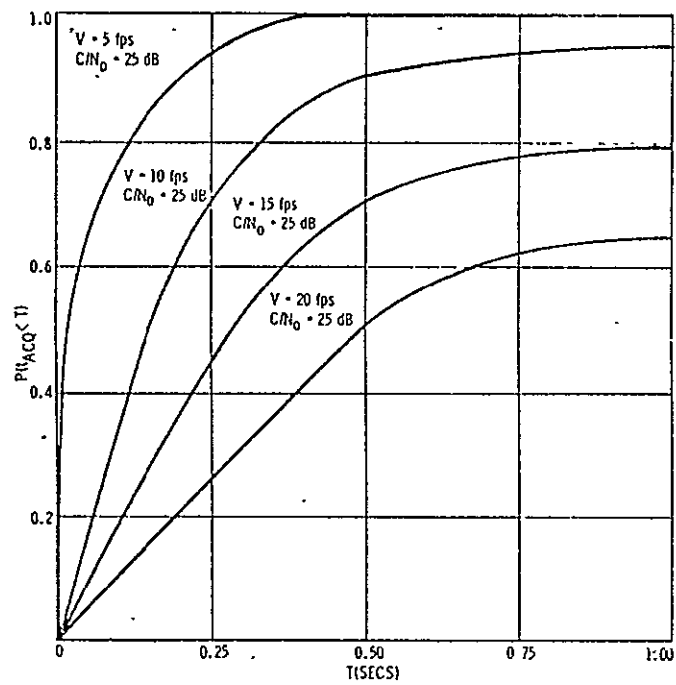
Figure C-4. Acquisition Time Cumulative Probability
Distribution Curves, 3rd Order Loop
$(\omega_n = 25$ rad/sec$)$

LinCom

·SHUTTLE GPS RECEIVER DEFINITION AND PERFORMANCE STUDY

‚Prepared by

LINCOM CORPORATION ·
P. O. BOX 2793D
Pasadena, CA 91105

for

AXIOMATIX
13900 Panay Way
Marina del Rey, CA 90291

‚Under

Subcontract No. AX770801GH ·

‚October 10, 1977

TR-1078-0178

LinCom

CONTENTS

1.0 INTRODUCTION

Preliminary studies concerning the application of the NAVSTAR Global Positioning System (GPS) to Shuttle navigation have determined that this system could significantly improve Shuttle navigation performance particularly during critical mission phases. This report addresses certain aspects of the problem of defining a Shuttle navigation receiver based upon the approach of taking advantage of current GPS Receiver Processor Assemblies (R/PA) presently under development. Figure 1-1 provides a summary of current GPS user equipment developments.

In order to baseline the Shuttle GPS navigation system characteristics several performance requirements must be defined. These include: (1) Shuttle Dynamics, (2) TTFF (Time-to-First-Fix), (3) Reacquisition Time, (4) Range and Range Rate Measurement Accuracy, (5) J/S Requirements, (6) Navigation Accuracy Requirements, and (7) Equipment Stabilization Time. In addition, the R/PA configuration, including size, weight and power requirements, must be defined. At present, there exists several receiver configuration options which must be considered in defining the baseline Shuttle GPS R/PA. These are summarized in Table 1-1. It is also noted that the key issues associated with the R/PA development are:

(1) Shuttle R/PA to be Developed from Existing GPS Equipments.

(2) Minimize R/PA Complexity to Fit Shuttle Configuration.

Figure 1-1. GPS USER EQUIPMENT DEVELOPMENTS

SET	DESCRIPTION	AUXILIARY SENSOR AIDING	OPERATING FREQUENCY L_1 and L_2	SIGNAL CODE P AND C/A	USER EQUIPMENT CONTRACTOR
XU	4 CHANNEL, HIGH PERFORMANCE		✓	✓	MAGNAVOX
YU	1 CHANNEL, MEDIUM PERFORMANCE	-	✓	✓	MAGNAVOX
XA	4 CHANNEL, HIGH PERFORMANCE	✓	✓	✓	MAGNAVOX
YA	1 CHANNEL, MEDIUM PERFORMANCE	✓	✓	✓	MAGNAVOX
HDUE	5 CHANNEL, HIGH PERFORMANCE		✓	✓	TEXAS INSTRUMENTS
MVUE	1 CHANNEL, MANPACK/ VEHICULAR		✓	✓	TEXAS INSTRUMENTS
AFAL/ GDM	5 CHANNEL, HIGH PERFORMANCE	✓	✓	✓	COLLINS RADIO
MP	1 CHANNEL,MANPACK		✓	✓	MAGNAVOX
Z	1 CHANNEL,LOW COST		L_1 only		MAGNAVOX
GPSPAC	2 CHANNEL, SPACE-BORNE		✓	✓	MAGNAVOX

LinCom

LinCom

Table 1-1.   SHUTTLE GPS RECEIVER CONFIGURATION OPTIONS

MAJOR FUNCTIONAL OPTIONS	PARAMETERS AFFECTED
SATELLITE CHANNELS TRACKED SIMULTANEOUSLY (1 or 4)	RECEIVER CHANNELS TTFF AND AJ
L_1 FREQ. ONLY	ACCURACY FOR
L_1/L_2 DUAL FREQ.	IONOSPHERE
USE OF C/A or P SIGNAL	ACCURACY, AJ, AND ACQUISITION TIME
IMU/BARO AIDED	INTERFACES AND
NO IMU AIDING	JAMMING MARGIN
NAV FUNCTION IN RECEIVER	RECEIVER COMPLEXITY
NAV FUNCTION IN CENTRAL COMPUTER	INTERFACES AND CABLING ,MEMORY

(3) Optimize Performance

 (a) TTFF

 (b) Reacquisition Time

 (c) Accuracy

 (d) J/S Capability

(4) Design R/PA to Fit Weight, Volume and Power Constraints
of Shuttle.

(5) Receiver Configuration Options

 (a) Single/Multiple Channel

 (b) Hardware/Software Receiver

(6) Cost

  In this report preliminary results are presented which
pertain to the performance analysis and requirements of the
R/PA's carrier and code tracking loops designed to track
the GPS signal characteristics received at the Shuttle
using current best estimates of the Shuttle signal dynamics.
Both aided and unaided loops are analyzed and their dynamic
tracking performance is compared with that of second and third
order loops. Design point loop parameters assumed in the
analysis are typical of those found in the Magnavox GPSPAC
and X set. The problem of Shuttle GPS R/PA oscillator
selection is considered and an oscillator mathematical model
is presented and parameterized in terms of vendor specifications.
In addition, a survey of current oscillator technology, applicable
to the Shuttle GPS application, is presented. Finally, the on-
orbit multipath problem is determined to be of no major concern.

It appears that further work must be performed before the Shuttle navigation requirements are complete. Once these are complete a baseline Shuttle navigation system can be defined that includes a R/PA selected from current available technology for use or modification.

2.0 THE SHUTTLE GPS NAVIGATION CONCEPT

The GPS concept requires accurate knowledge of the position of a satellite versus time and the transmit times of signals from these positions. Each satellite carries an atomic clock with stabilities on the order of 1 part in 10^{13} per day. This clock is used to generate timing for the dual frequency pseudorandom noise (PRN) spread spectrum UHF navigation signals

which the satellites radiate continually. These navigation
signals, see Table 2-1, contain information regarding the
satellite ephemerides and clock behavior. Geographically
dispersed monitor sets permit precise tracking of the satellites,
and a master control station (MCS) predicts their future
positions as well as the future behavior of the clock carried
by each satellite. The MCS insures that the satellite clocks
are synchronized within a few nanoseconds. The control segment
periodically uploads this information into each satellite's
memory. Each satellite can then continuously transmit its
position and system time. Assuming the Shuttle had an
accurate clock, synchronized to system time, it could
measure the precise time a signal from a satellite was
received and thus determine the time difference between
transmission and reception. By multiplying this time difference
by the speed of light, the Shuttle could determine the distance
or range from the satellite. By listening in this manner to
three satellites, the Shuttle position would be defined by the
intersection of three spheres of the determined radii .
centered at each satellite.

Unfortunately, equipping the Shuttle with a sufficiently
accurate clock and synchronizing it to the satellite's time
would be prohibitively expensive and cumbersome. To
circumvent this difficulty, it can be equipped with a
fairly inexpensive crystal clock. The satellite messages
continuously update information relating to the performance
of the clock. The Shuttle then listens to four satellites

Table 2-1. NAVSTAR GPS Satellite Signal Transmission.

Transmission Bands		Modulation Rates			RF Signal Levels* Phase I - Min Received	
Frequency	MHz	P-Code	C/A Code	Data	P-Signal	C/A Signal
L_1	1575.42	10.23 Mbs	1.023 Mbs	50 bps	-163 dBW	-160 dBW
L_2	1227.6	10.23 Mbs	N/A	50 bps	-166 dBW	N/A

*Referenced to an 0 dBiC antenna

(selected from those in view to optimize satellite-to-user geo-
metry) and essentially solves four equations in four unknowns
(three time-difference-of-arrivals for range and one time
correction factor) to compute this three-dimensional position
and system time.

To utilize the satellite clocks properly in determining
range to the Shuttle, and thereby its position, the refraction
effects on path length of the radio transmission must also
be known. Hence, two radio frequencies with different
propagation properties measure the ionospheric delay and
other medium effects. In addition, Shuttle velocity inform-
ation is extracted from the system by noting the doppler
frequency shift of the signals from each of the "tuned-in"
satellites.

The expected performance of a well designed system slated
for 1984 could be:

	Position (M)		Velocity	Time
	Horizontal	Vertical	M/S	nsec
50% of Time	5	7	0.10	11
90% of Time	9	10	0.22	27

Position and velocity "fixes" in three dimensions plus time
can be derived by the Shuttle equipments.

3.0 SHUTTLE GPS RECEIVER

The Shuttle GPS receiver is responsible for extracting the
pseudo range and range rate data from the GPS satellite trans-
mitted signals. The receiver concept used for this study has

been to consider the ultimate performance achievable with two types of GPS receivers. These include the sequential and non-sequential receivers.

A sequential receiver extracts ranging data from each. of four selected satellites in a sequential manner. The receiver actually breaks P-code lock from Satellite No. 1 and reacquires Satellite No. 2, then No. 3, and so on. Using a P-code fast time share or sequencing rate, the P-code generator can be positioned very close to the upcoming transmitted P-code position by taking advantage of "fly wheeling" action. If acquisition cannot be routinely performed, a P-code search is initiated and the signal found. The sequence of events required to acquire and track four satellites falls into five categories:

(1) Shuttle oscillator warm up.

(2) Estimate of time and position is fed into computer.

(3) Shuttle computer selects four satellites to navigate.

(4) Shuttle/GPS receiver searches, acquires and tracks the signals from the four satellites.

(5) Pseudo-range and range rate is measured by acquiring a full frame of valid data from each.

The time required to perform the above operations is called the "Time-to-First Fix" and is a performance measure of great concern.

It is important to keep in mind that the sequential concept is feasible and has been demonstrated to perform in recent hardware tests. The particular design features which will be of concern in the Shuttle/GPS application are those of:

(1) Incorporating the GPS signal design.

(2) Provide operational flexibility.

(3) Packaging.

The idea of employing a sequential tracking receiver is that performance can be for equipment costs, weight, volume, and power consumption; however, in this study cost constraints have not been a prime consideration. On the other hand, other requirements which must be accounted for in the design of the Shuttle/GPS receiver have been of great concern. In fact, key requirements which impact the design of the Shuttle/GPS receiver (and must be defined) are:

(1) TTFF's (Time to first fix).

(2) Accuracy.

(3) Operational Control of the Receiver.

(4) Power Consumption.

(5) Commonality of the Shuttle/GPS Receiver Design.

(6) Size and Weight.

(7) Modularity for Maintenance.

3.1 GPS Signal Characteristics

The GPS signal design is described in: "System Specification For the Navstar Global Positioning System" Phase I, April, 1974.* All GPS satellites will transmit two L-Band carriers L_1 and L_2. Each satellite transmits on the L_1 carrier a short clear acquisition PN code (C/A code) and L_2 a long length protected acquisition PN code (P-code). Each satellite transmits a unique C/A code from amongst a family of 511 bit Gold codes. A single P-code is transmitted from each satellite on both L_1 and L_2 carriers.

*Also see Table 2-1 of this report.

is modulo-2 added to the C/A code at 50 bits per second.

3.2   Shuttle GPS Receiver Functions

The Shuttle GPS receiver is required to receive and process the signals received from the satellite. It must perform the following functions during signal acquisition:

(1) Receive and Amplify both the L_1 and L_2 carriers.

(2) Acquire, demodulate and track the C/A code from a desired satellite selected by the computer.

(3) Maintain code track.

(4) Acquire and track the carrier after code demodulation.

(5) Obtain symbol sync.

(6) Detect data on the C-code and send data to computer.

(7) Transfer code demodulation from the satellite C/A code to the P-code using a priori information from the computer.

(8) Extract pseudo-range data from either the demodulated P-code or C/A code.

Implementation of the reciever to perform these functions depends greatly on the GPS signal design.

The requirement for receiving two L-band carriers dictates that the Shuttle GPS receiver must provide an RF processor capable of handling both carriers. The carrier is selected by the computer.

The C/A and P-codes are phase modulated onto two orthogonal carriers which fully suppress the L_1 carrier. The P-code is bi-phase modulated on the L_2 carrier. To reconstruct the carrier for tracking, the C/A or P-code must be demodulated by cross correlating the received signal with the locally generated reference code. A code tracking loop is required to acquire and track the code phase for range measurements.

Acquisition of the code is accomplished by searching for possible code correlation between the received and locally generated codes. A lock indicator will be needed to indicate when the two codes are synchronized. The code tracking loop will acquire and track the received code.

After the C/A and P-codes have been removed from the carriers, the carriers can then be acquired by some form of suppressed carrier tracking loop. Data will still remain on the C/A channel; therefore, the carrier is still suppressed. A suppressed carrier loop of the Costas type will be required for carrier recovery and data demodulation.

Once the carrier and code have been acquired and the carrier and code loops begin tracking, the encoded data may be detected. A symbol synchronizer is needed to establish and maintain bit sync and a integrate and dump circuit required to detect the data bits.

Since the data is differentially encoded at the satellite to overcome sign ambiguity in the receiver, the bit transitions

are provided to the computer; the computer will use this transition information to reconstruct the transmitted bits.

Since the P-code is encrypted by the satellite by a transec device to provide an additional measure of security against unauthorized users, the Shuttle GPS receiver must be able to accept a device which will encript the reference code prior to P-code demodulation. The receiver must then maintain the security of the information which is obtained after decoding the encryption.

The Shuttle, GPS receiver will be required to simultaneously or sequentially track at least four of the satellites. If the receiver is designed to operate in a sequential mode, it must provide storage for the state of the P-code for each of the four satellites being timeshared. This allows for rapid re-acquisition of a timeshared satellite.

The PN code clock rates establish the bandwidth of the Shuttle GPS receivers IF bandwidth; in particular, the P-code. Currently, the P-code clock rate is .10 MHz and is phase coherent with the transmitter frequency for both the L_1 and L_2 carriers. The receivers RF front end processor must have a sufficiently wide bandwidth to pass the 10 MHz P-code spectrum. The C/A code clock rate is approximately 1 MHz.

3.3 Shuttle GPS Receiver Operating Requirements

The received signal strength as well as the received signal-to-noise ratio, C/N_0 dB-Hz, is critical to the design

optimization of the Shuttle/GPS receiver. The receivers operational modes affected by the received signal strength include:

(1) Acquisition Mode

(2) Tracking Modes

(3) Data Acquisition Modes.

3.3.1 Acquisition Requirements.

The initial operations the receiver must carry out include:

(1) Power up oscillator.

(2) Input time and position estimate in computer.

(3) Computer must select appropriate satellites.

(4) Search and acquire codes and carriers.

(5) Detect a frame of data from each satellite.

(6) Track the codes and carrier and measure pseudo-range and range rate.

The time duration of this process is of primary interest and the C/N_0 acquisition threshold is of interest.

3.3.2 Data Acquisition Requirement.

The design point bit error probability is taken to be 10^{-5} or less. The energy per bit to noise ratio for coherent BPSK signal detection is approximately 9.6 dB. The data rate is 50 bits per second or 17 dB-Hz so the minimum C/N_0 required is 26.6 dB-Hz, without allowing for CNR degradations due to despreading, carrier noisy reference losses, hardware losses, etc. The margin estimated for the effects appears to

be on the order of 5.4 dB which leads to the C/N_0 requirement

for data acquisition of C/N_0 = 32 dB-Hz.

3.3.3 Shuttle Signal Dynamics.

Preliminary estimates for the Shuttle signal dynamics have

been obtained via the telephone. These are summarized in Fig.

3.3.3-1. Figure 3-3.3-2 summarizes the dynamics in terms of

frequency offsets. Most recently LinCom personnel held discussions

with Jim Kirkpatrick of JSC and new data will be made available

concerning worst case flight dynamics for OFT 1 during ascent,

on-orbit and during descent.

3.3.4 Shuttle, GPS Carrier Loop Static Phase Error Build Up in Second and Third Order Loops

During flight operation, the static phase error in the

receiver due to the orbit characteristics given in Fig. 3.3.3-1

and 3.3.3-2, is of great concern. The reason is that static phase

offsets reduce the receivers threshold characteristics and increase

the probability of losing phase lock. Figures 3.3.4-1 and 3.3.4-2

summarize results associated with the static phase error build up

during ascent and descent and on orbit. Both second and third

order loops have been considered. From these results we note

that a third-order loop without aiding is essentially as

effective as a second-order loop with aiding. Clearly an unaided

second-order loop will not provide adequate tracking performance.

3.3.5 Costas Loop Phase Jitter.

There are several factors which cause jitter in the carrier

recovery loops. Figure 3.3.5-1 summarizes the jitter arising in a

Figure 3.3.3-1. <u>SHUTTLE SIGNAL DYNAMICS*</u>

<u>DERIVATIVE</u>		<u>ASCENT**</u>	<u>ON ORBIT</u>	<u>DESCENT***</u>
DOPPLER	$\dot{R}$	± 7.6 km/sec	± 7.07 km/sec	± 7.5 km/sec
ACCELERATION	$\ddot{R}$	± 29.3 m/sec^2	± 10.2 m/sec^2	± 15.6 m/sec^2
JERK	$\dddot{R}$	± 0.011 m/sec^3	$\pm .011$ m/sec^3	$\pm .011$ m/sec^3

---

*KAMEN/HEATH/PORTER (JSC)

**WORST CASE ASCENT

***OFT-1 TRAJECTORY

Figure 3.3.3-2. SHUTTLE $\dot{R}$, $\ddot{R}$ AND $\dddot{R}$ TRANSLATED INTO FREQUENCY VARIATIONS

	$\dot{R}$	$\ddot{R}$	$\dddot{R}$
	DOPPLER	DOPPLER RATE	DOPPLER ACCELERATION
ORBIT	37,130 Hz	53.56 Hz/sec	.06 Hz/sec^2
ASCENT	40,015.67 Hz	153.66 Hz/sec	.06 Hz/sec^2
DESCENT	39,375.47 Hz	81.86 Hz/sec	.06 Hz/sec^2

Figure 3.3.4-1. STATIC PHASE ERROR BUILD UP DURING ASCENT AND DESCENT
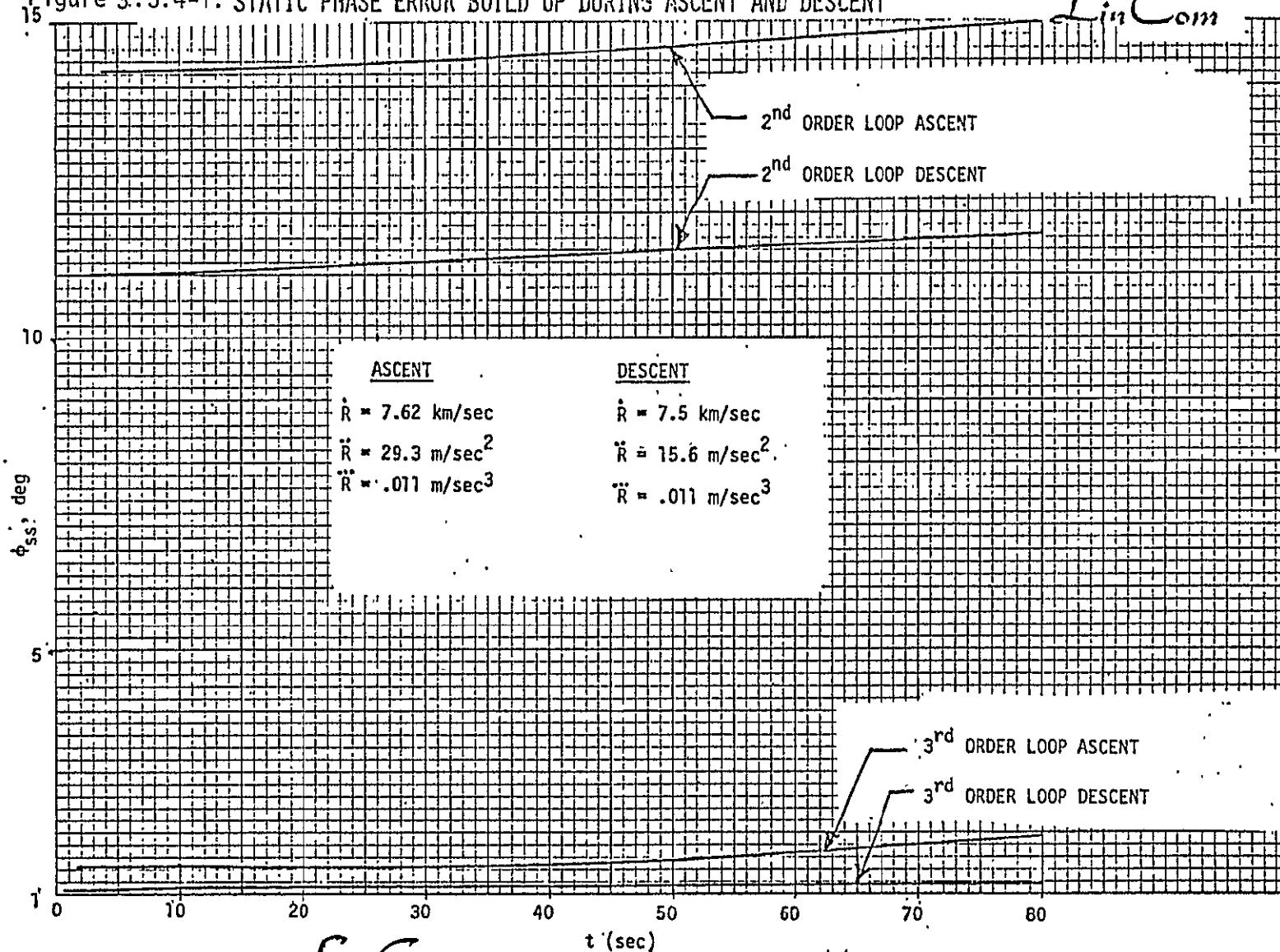
Figure 3.3.4-2. STATIC PHASE ERROR BUILD UP ON ORBIT
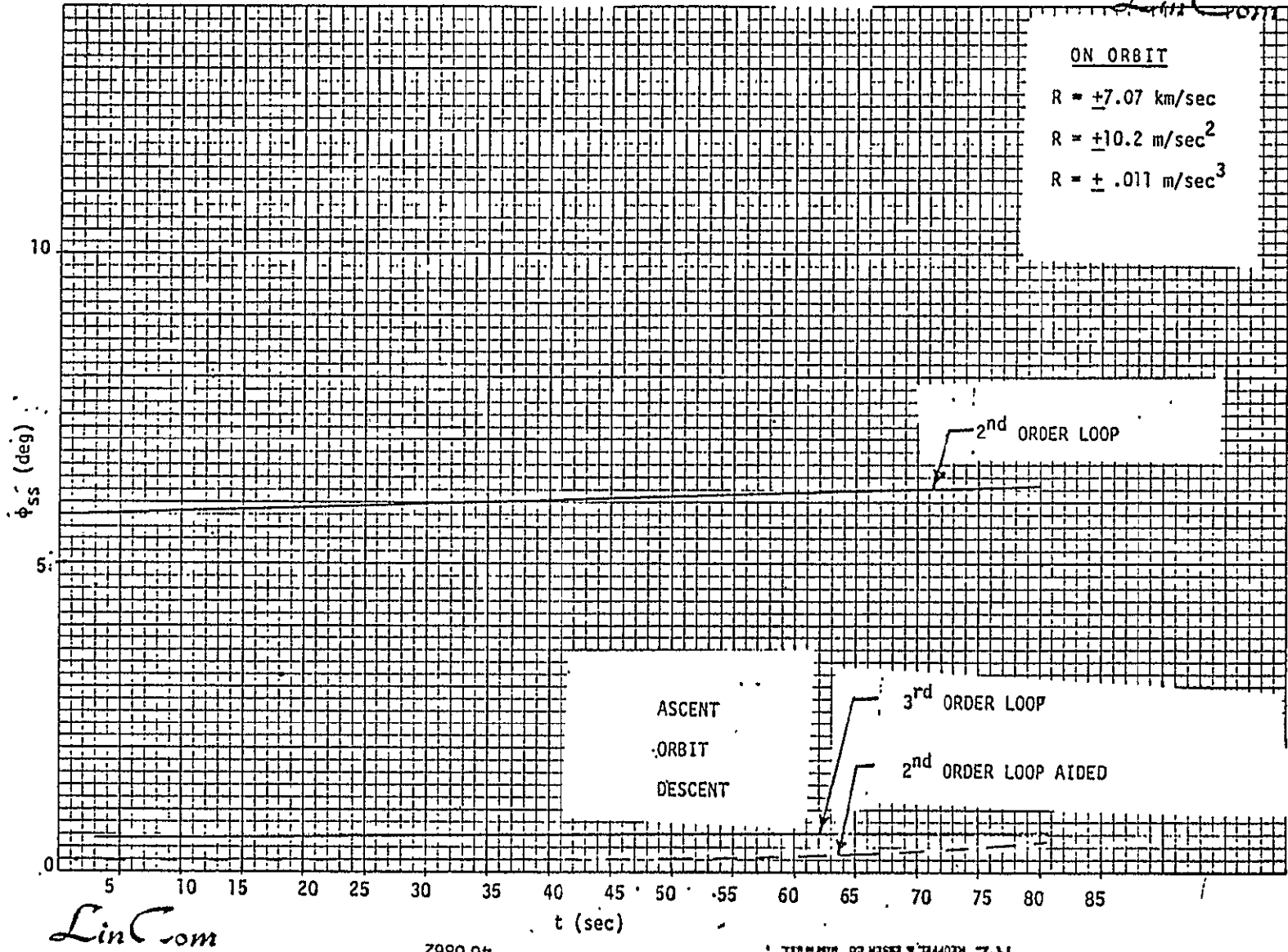
Figure 3.3.5-1. <u>PHASE JITTER</u>

JITTER	COSTAS	COSTAS/AFC	AFC THRESHOLD DEG.
10^0	32.2 dB-Hz	33.4 dB-Hz	1.2 dB
15^0	29.6 dB-Hz	30.5 dB-Hz	0.9 dB

35 Hz Costas loop when automatic frequency control (AFC) is provided and illuminated. It appears that the AFC degrades loop threshold by approximately one dB. In a loop with AFC, a C/N_0 of 29.6 dB-Hz gives 15 degrees of jitter. This value of C/N_0 is lower than the minimum required to give a 10^{-5} BER. The margin appears to be on the order of 2 to 3 dB.

3.3.6 Costas Loop Loss of Lock Characteristics.

Figure 3.3.6-1 summarizes the loss of lock characteristics of the Costas loop. Notice that for a mean slip time of 10 seconds the value of C/N_0 required is 29 dB-Hz when the static phase-error is zero. For 20 degrees of static phase error approximately 31.2 dB-Hz is required in order to provide a mean slip time of 10 seconds.

3.3.7 Shuttle GPS Code Loop Performance for 2nd and 3rd Order Loops.

In this section a summary of the PN code loop tracking performance is given. Figures 3.3.7-1 and 3.3.7-2 summarize the code loop static chip error versus time. Both second and third-order code tracking loops have been investigated. Notice that a second-order loop with aiding or a third-order loop will be required in order to minimize the effects of code loop static chip offset.

Figure 3.3.7-3 summarizes the mean time to first loss of code lock versus C/N_0 for two different code loop tracking bandwidths. From this figure one concludes that the loop bandwidth selected will be determined by code loop jitter as proposed to its loss-of-lock properties.

Figure 3.3.6-1. COSTAS LOOP THRESHOLD CHARACTERISTICS DURING ASCENT
AND DESCENT.
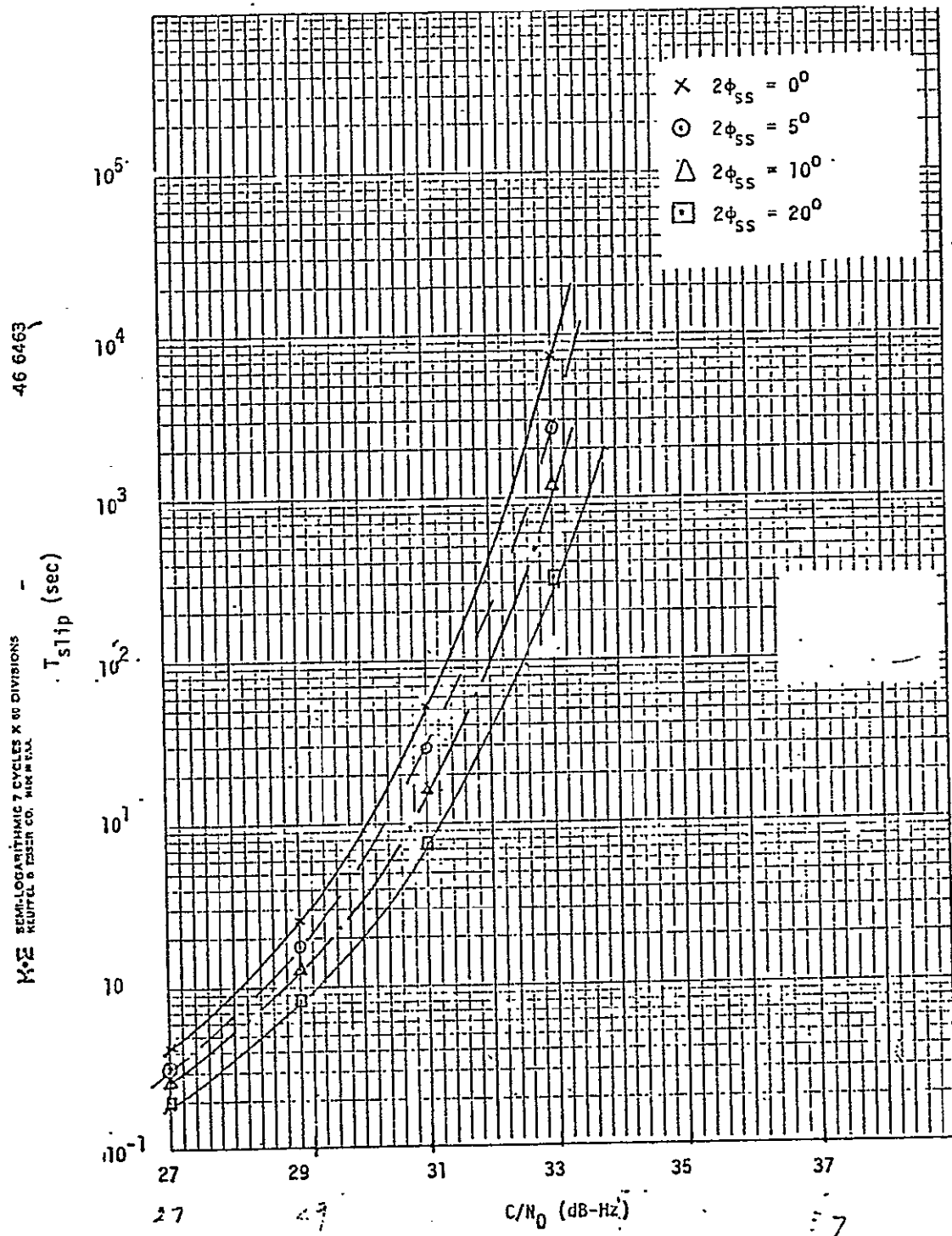
Figure 3.3.7-1. CODE LOOP STATIC CHIP ERROR VS TIME
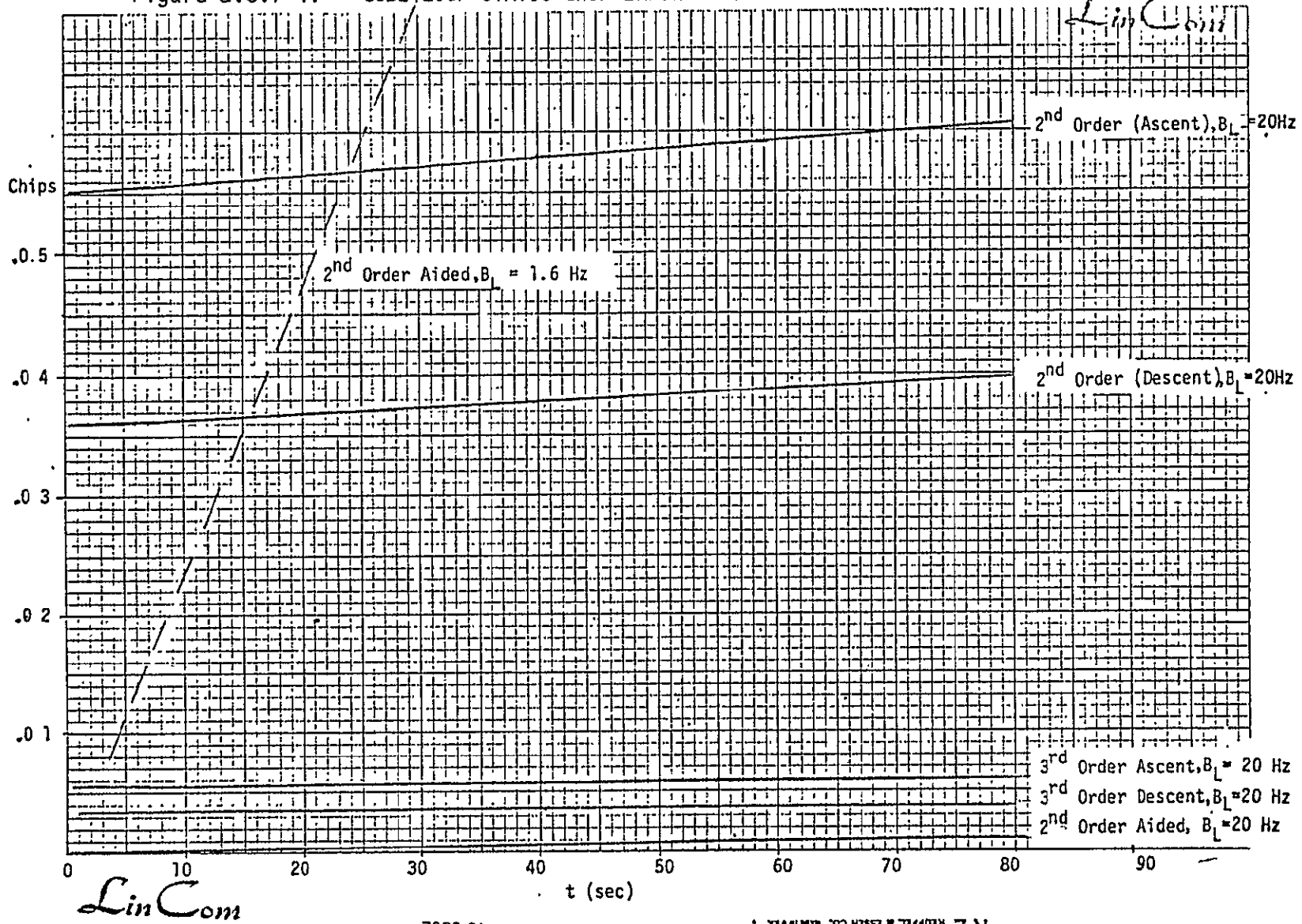
Figure 3.3.7-2. CODE LOOP STATIC CHIP ERROR VS TIME
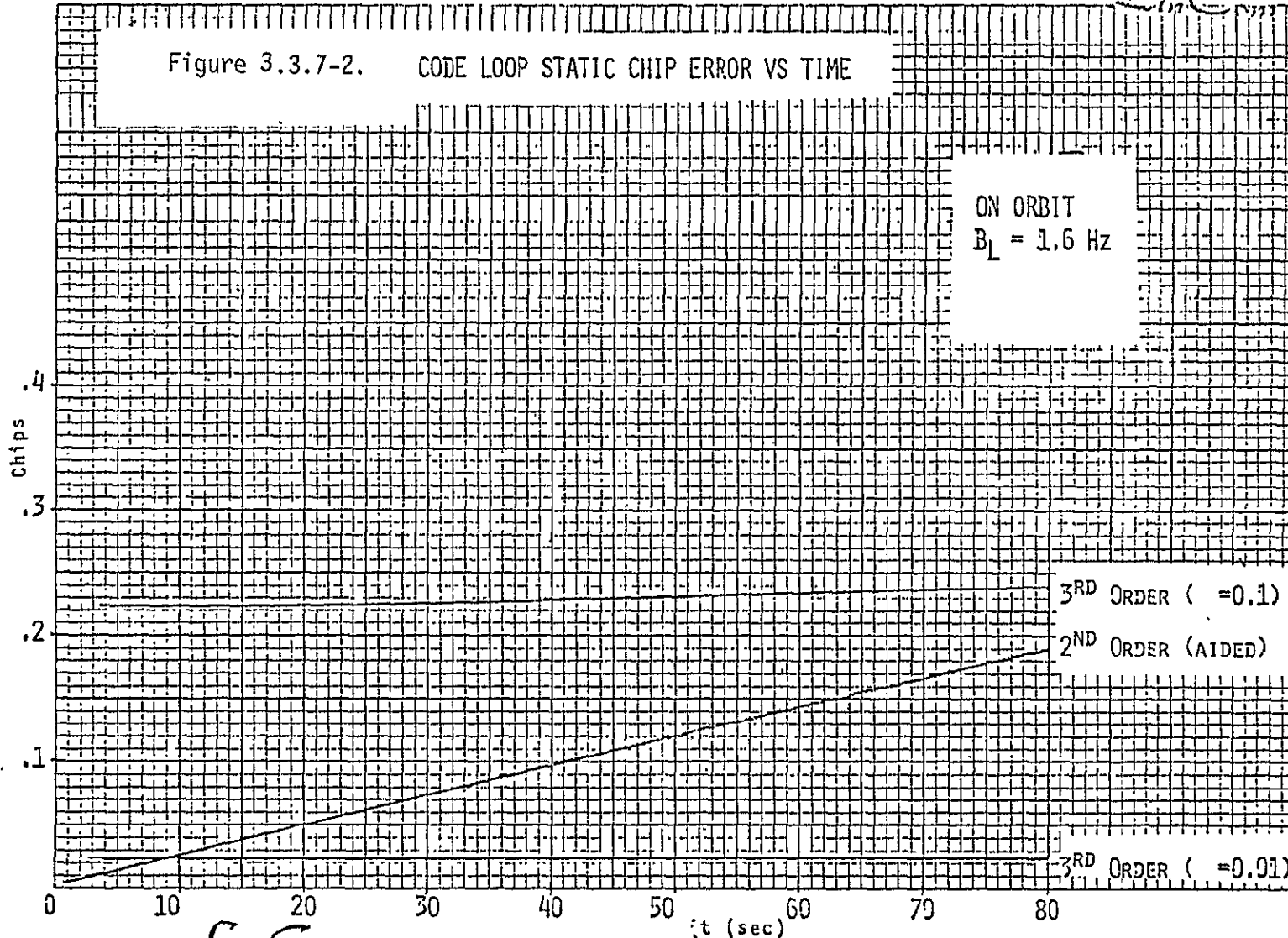
ON ORBIT
$B_L = 1.6$ Hz

3RD ORDER (=0.1)

2ND ORDER (AIDED)

3RD ORDER (=0.01)

chips

.4

.3

.2

.1

0   10   20   30   40   50   60   70   80

t (sec)

Figure 3.3.7-3. CODE LOOP MEAN TIME TO LOSS OF LOCK

$B_L = 1.6$ Hz

$B_L = 20$ Hz

C/N$_0$ (dB-Hz)

-25-
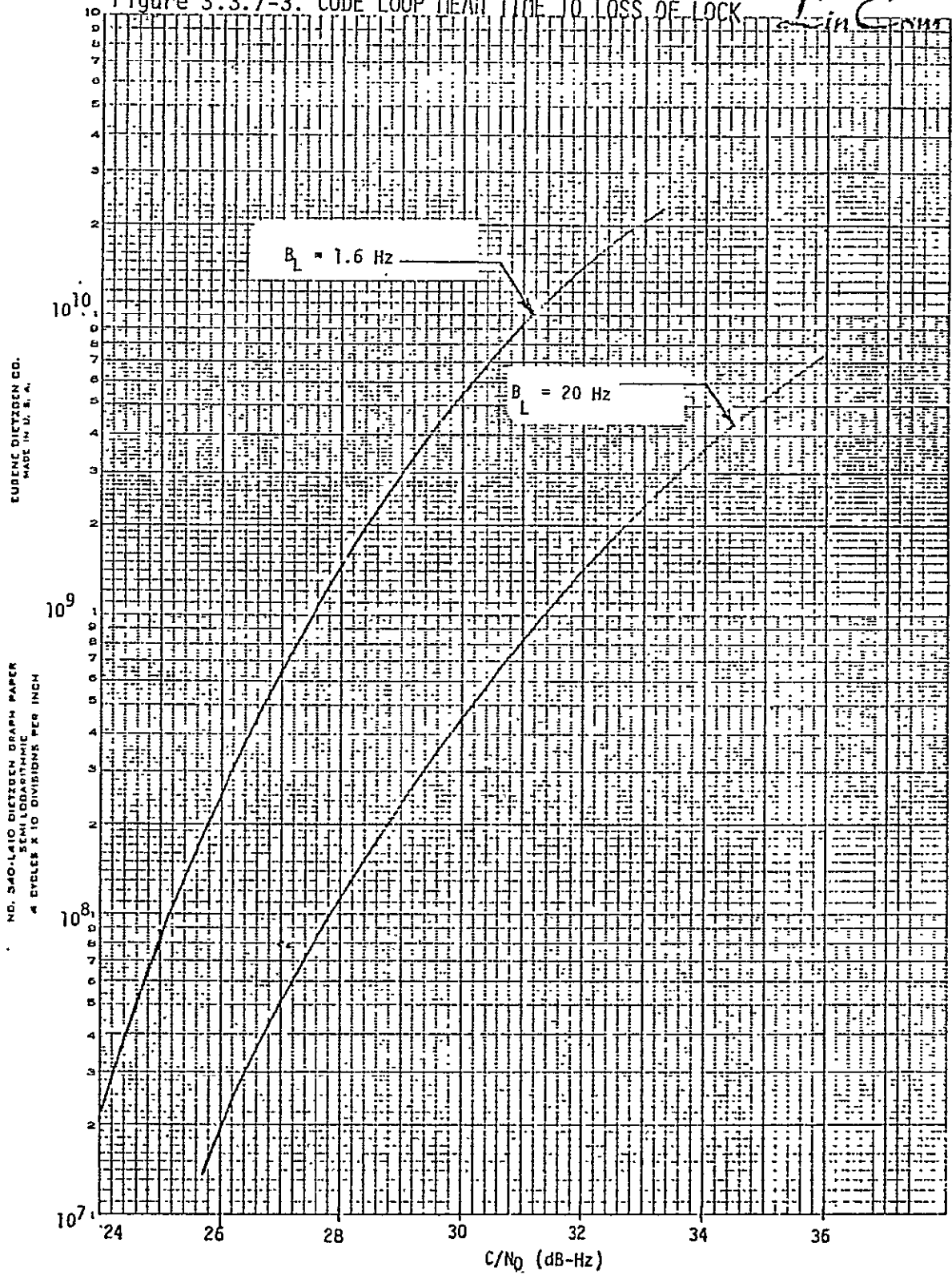
Figure 3.3.7-4. Range Error vs C/N$_0$.
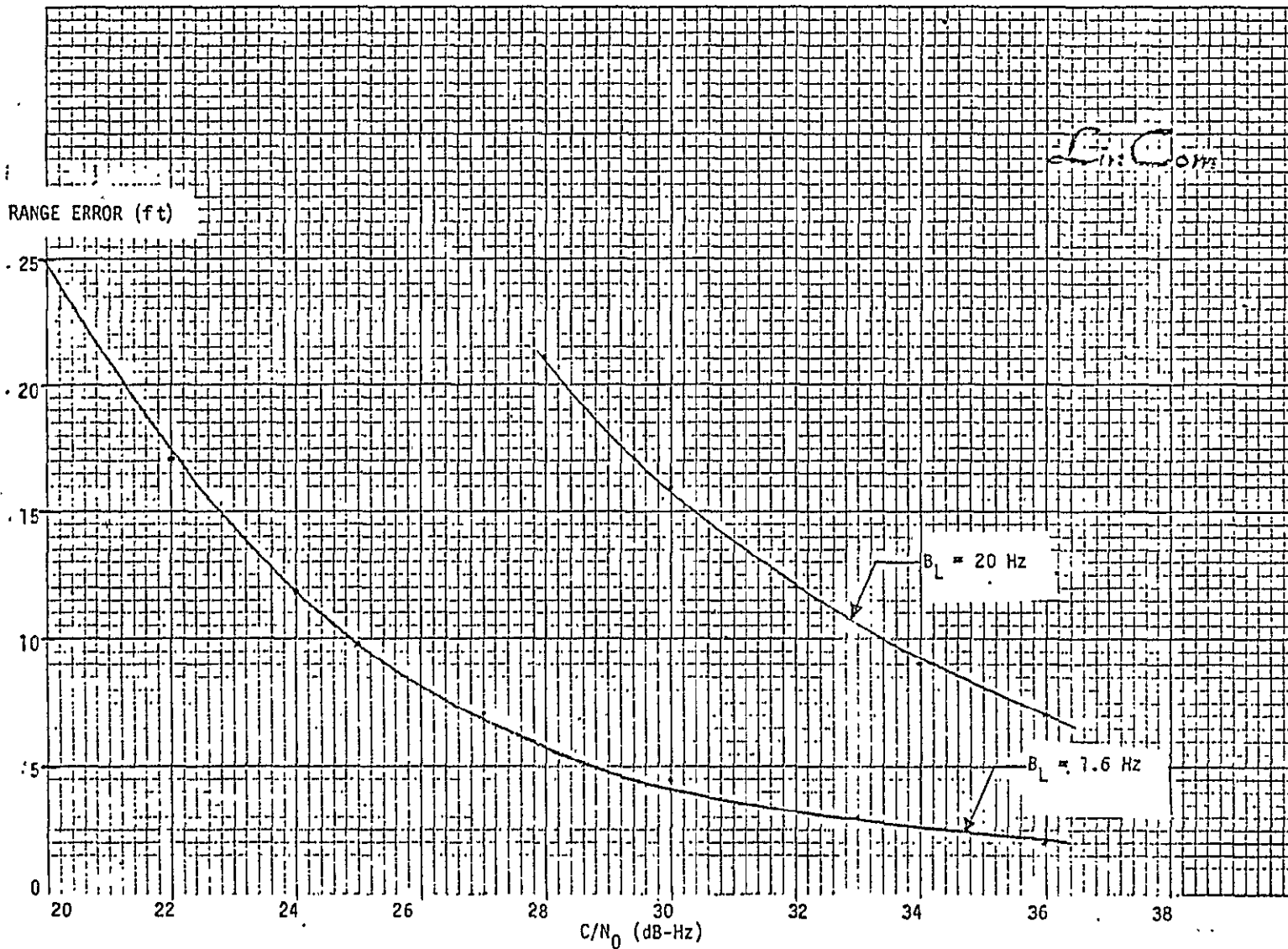
Figure 3.3.7-4 demonstrates code loop range error achievement with loop bandwidths of 1.6 and 20 Hz respectively. Notice for a loop bandwidth of 20 Hz the range error is approximately 15 at C/N_0 = 30 dB-Hz. The GPSPAC receivers code tracking loop bandwidth is 1.6 Hz and gives rise to a range error of approximately 4 feet when C/N_0 = 30 dB-Hz.

3.3.8 Aiding in the Shuttle GPS R/PA

Integration of other navigation sensors into the Shuttle GPS Receiver Processor Assembly (R/PA) can provide fruitful benefits relevant to receiver threshold reduction, signal acquisition and reacquisition performance limitations and antijam margins. The concepts used in current technology are to employ aiding to provide a priori knowledge of vehicle dynamics such that receiver tracking bandwidths can be reduced. The immediate benefit is to provide increased jamming immunity. Aiding provides augmented navigation capability which gives continuity during GPS outages and optimal performance with GPS. It also establishes a priori search domains in space and frequency to reduce acquisition time and for reacquisition. In summary, aiding auxiliary sensors provides the capability of narrowing all tracking and acquisition loop bandwidths providing improved jamming immunity and recovery. The significant Shuttle equipment parameters which are affected by aiding from an auxiliary sensor as summarized by Martin [ ] is provided in Tables 3.3.8-1, 3.3.8-2 and 3.3.8-3 along with functional dependency which governs the performance parameter and a description of what utility aiding would

Table 3.3.8-1. Primary Aiding Parameters

Parameter	Basic Functional	Utility for Aiding By Sensor
Jamming immunity	Receiver noise bandwidth	Narrow noise bandwidth to increase the signal-to-noise ratio by decreasing dynamics of signal
Range and range rate tracking accuracy	Receiver noise bandwidth	Same as above
Allowable vehicle dynamics	Receiver noise bandwidth and both tracking accuracy and jamming immunity as a function of receiver tracking threshold	Extension of maximum dynamics of vehicle without breaking receiver tracking

Table 3.3.8-2. Secondary Aiding Parameters.

Parameter	Basic Functional	Utility for Aiding By Sensor
Normal mode acquisition	Range and velocity domain uncertainty	A priori navigation and search window
Direct mode acquisition	Time domain uncertainty Range and velocity uncertainty same as for normal mode	A priori navigation and time, range, velocity search window indication
Time-to-First Fix	Acquisition time as defined by above parameters Dominating term is data word demodulation interval	Same as above
Reacquisition	Time, range, and velocity uncertainty	A priori navigation and time for range and velocity search window indication

Table 3.3.8-3. Restrictive Aiding Parameters.

Parameters	Basic Functional	Utility for Aiding By Sensor
Weight, size, power (including interfaces	Mechanical, electrical form and fit factors	Generally a penalty unless sensor is already available or predicated for other uese
Cost	Increasing dollars with increasing sensor complexity	No penalty if already predicated. Cost penalty if sensor must be added.
Reliability, redundancy	Decreased receiver hardware offers reduction in failures Secondary degraded navigational accuracy	Dead reckoning provided as degraded mode operation and reduction in basic receiver acquisition cost

provide relative to the particular parameter.

4.0 SHUTTLE GPS RECEIVER OSCILLATOR SELECTION

The selection of an oscillator for the Shuttle GPS receiver is constrained by many factors. Oscillator require-- ments are greatly affected by the operational scenarios of the Shuttle. The multitude of factors affecting the oscillator requirements include:

(1) Oscillator warm-up characteristics as they affect frequency accuracy required to meet initial signal acquisition.

(2) Specification of the required short-term stability and aging rate necessary to meet direct C/A or P subsequent fix performance accuracy and PN code tracking loop performance.

(3) Frequency stability degradation due to environmental factors and how this affects signal acquisition.

(4) Mechanical vibration induced frequency modulation of the crystal oscillator and the resultant system performance degradation.

(5) Oscillator phase noise as it effects carrier and code tracking loop rms phase errors.

(6) Oscillator phase noise as it effects cycle slips.

In what follows we examine oscillator technology available for Shuttle navigation system procurement; in particular, the many parameters such as warm-up time, fractional frequency stability, power, size and weight are summarized. Quantification of the effects due to oscillator phase noise

components is also presented.

4.1 Instantaneous Frequency Model

The deterministic component of instantaneous frequency f(t) at any time t can be modeled as

$$f(t) = f_0 + a f_r t \tag{1}$$

where f_0 is the nominal initial frequency, f_r is the reference frequency, a is the aging rate (rate of frequency shift). In the above equation, "a" describes the average rate of change of the oscillators output frequency, assuming that environmental parameters are constant. Since f(t) differs from f_r, the clock based on the oscillator model will gain or lose time because each cycle of the oscillation is shorter or longer with respect to the previous one. For the case when a is positive, f(t) is increasing with respect to f_r and each cycle of the oscillator is short by

$$\Delta = \left[\frac{1}{f_r} - \frac{1}{f(t)} \right] \tag{2}$$

For a short time period of Δt seconds there accumulates $f(t)\Delta t$ cycles of difference. The incremented time error can therefore be expressed as

$$\Delta \varepsilon = \left(\frac{1}{f_r} - \frac{1}{f(t)} \right) f(t)\Delta t \tag{3}$$

and in the limit

$$d\varepsilon = \left(\frac{f(t)}{f_r} - 1 \right) dt \tag{4}$$

so that the total accumulated error is found to be

$$\varepsilon \; = \; \varepsilon_0 + \left(\frac{f_0 - f_r}{f_r}\right) t + \frac{at^2}{2} \; . \tag{5}$$

where

ε_0 = initial time error

Δf = $f_0 - f_r$ = initial frequency error

a = oscillator aging rate

t = total elapsed time

Equation (5) can be expressed in terms of a fractional frequency stability $\Delta f/f_0$ via

$$\varepsilon \; = \; \varepsilon_0 + \frac{\Delta f}{f} t + at^2/2 \tag{6}$$

and when the random phase fluctuations $\psi(t)$ of the oscillator are added in we have the following model for the Shuttle oscillator phase accumulation, i.e.,

$$\Phi(t) \; = \; 2\pi[\varepsilon_0 + \frac{\Delta f}{f} t + at^2/2] + \psi(t) \tag{7}$$

Therefore to evaluate performance one only needs to specify ε_0, $(\Delta f/f)$, a, and the power spectral density of the stationary process $\psi(t)$. Such data is usually provided in the oscillator specification provided by the vendor.

4.1.1 Environmental Degradations of Frequency Stability.

Environmental effects on the Shuttle navigation system oscillator such as temperature variations, vibration, g-force loading, shock, load changes and voltage changes can all contribute to the fluctuations in the crystal oscillators output frequency. Usually these perturbations are modeled

as independent, normally distributed random variables.
Therefore the combined rms perturbation is the square root
of the sum of the variances of the individual perturbation.
The effects of the environmental factors tend to degrade
the fractional frequency stability according to the root
sum square law

$$\sigma_{\Delta f} = \sqrt{\sum_{n=1}^{M} (\sigma_{\Delta f_m})^2} \qquad (9)$$

Here $\sigma_{\Delta f_m}$ represents the standard deviation of the induced
change due to the mth degrading factor. For a particular
vendor oscillator, $\sigma_{\Delta f}$ can be evaluated using data provided
in the specification. A typical set of oscillator environmental
effects are summarized in Table 4.1.1-1. The resultant $\sigma_{\Delta f}$ deviation for
the parameters provided in Table 4.1.1-1 is easily found to be

$$\sigma_{\Delta f} = 24 \text{ Hz} \qquad (10)$$

at the L-Band frequency of 1.575 GHz. The three sigma value
is 72 Hz. This says that the environment will cause the
crystal oscillators output frequency to randomly change in
accordance with a Gaussian probability density of 3σ value
of 72 Hz worst case. The mean squared value of the phase jitter can
be evaluated when the power spectral density of the oscillator
instabilities is found. For both the carrier and code loops
the mean squared value of the phase noise jitter is easily
found from

$$\sigma^2 = \frac{1}{2\pi} \int_{-\infty}^{\infty} S_\psi(\omega) |1 - H(i\omega)|^2 d\omega \qquad (11)$$

Table 4.1.1-1. Environmental Effects Which Degrade
Oscillator Performance.

Parameter	Stability	Induced Change	$\sigma_{\Delta f}$ at L-Band (Hz)
Temperature Fluctuations	1×10^{-9}	$-20°C$ to $55°C$	1.6
Vibration	$2 \times 10^{-9}/G$	2.5	5.0
Shock	$2 \times 10^{-9}/G$	11 g	22.
G-Force Loading	$1 \times 10^{-9}/G$	2.5 g	2.5
Voltage Change	1×10^{-9}	5%	1.6
Load Change	1×10^{-9}	10%	1.6

where $H(i\omega)$ is the closed loop and $S_\psi(\omega)$ is the power spectral density of the oscillator phase fluctuations. For a second order loop this transfer function is given by

$$|1-H(i\omega)|^2 = \frac{\omega^4}{\omega^4+\omega_n^4} \qquad (12)$$

where ω_n represents the loop natural frequency. A typical GPS oscillator can be modeled by a power spectral density that decreases from 10^{-10} to 10^{-14} rad^2/Hz the frequency range of 2 Hz to 2 kHz. For frequencies greater than 2 kHz the power spectral density is flat at 10^{-14} rad^2/Hz. Substitution of this power spectral density into (11) and performing the integration leads to

$$\sigma^2 = \frac{4.65 \times 10^{-5}}{\omega_n^{1/3}} \int_0^\infty \frac{\omega^{2/3} d\omega}{1+\omega^4} \qquad (13)$$

which reduces to

$$\sigma^2 = 4.2 \times 10^{-5} \ rad^2 \qquad (14)$$

when use is made of the integral

$$\int_0^\infty \frac{x^{n-1}}{1+x^n} dx = \frac{\pi}{m \ sin(n\pi/m)} \qquad (15)$$

Assuming further an equivalent C/N_0 of 26 dB-Hz and a B_L = 20 Hz then the mean squared phase jitter due to noise is σ_n^2 = .052 rad^2. The total phase jitter in the carrier tracking loop therefore becomes

$$\sigma_\phi^2 = \sigma^2 + \sigma_n^2 = .053 \text{ rad}^2$$

4.1.2 Phase Noise Effects Due to Vibration

Mechanical vibration induces frequency modulation on the receivers reference oscillator crystal is of concern because of the error component induced into the Costas loop. The magnitude of the error signal which is induced by incidental frequency modulation can be related to an equivalent signal-to-noise degradation and loss-of-lock degradation.

Acceleration of a crystal oscillator in the Shuttle GPS receiver would cause its output frequency to change, for example, by $K(a/g)$ Hz. Here a/g is the acceleration relative to 32 ft/sec^2, K is the constant of proportionality. Typical values of K on any 3 axis X, Y and Z for a good crystal oscillator range from 10^{-9} per g to 3×10^{-9} per g. If one uses the maximum value of K and the GPS L_1 frequency $f_0 = 1.66$ Hz, we have $\Delta f \sim 5$ Hz/g. Vibration tests as applied to a receiver usually call for the test signal to be sinusoidal, random or shock and these have to be defined based upon Shuttle operating conditions. Generally speaking, a sinusoidal vibration environment causes a severe problem when the frequency lies in the vicinity of the loop natural frequency. The precise effects can be quantified once system performance requirements and specifications are made.

4.2 Effect of Oscillator Instabilities on Range Measurement and Carrier Phase Referencing

The GPS/Shuttle experiment is designed to perform a

one-way pseudo-range measurement from the GPS satellite to
the Shuttle. This is accomplished using the measurement
data provided, in part, by the range tracking delay-locked
loop. This measurement is degraded by transmitting and
receiving oscillator instabilities. The uncertainty
introduced in the range estimate due to oscillator instabilities
alone is related to the variance of the code tracking loop
error. To determine the limitation on range accuracy due to
oscillator instabilities one needs the GPS code-loop
oscillator instability data. The Allan variance versus
measurement time is usually provided; however, a spectral
plot of the oscillator instabilities is required in order to
determine the range accuracy. In addition, the GPS receiver
instabilities must also be established in order to provide
a complete account of the range accuracy. The phase noise
on the carrier recovery loop degrades the range rate
measurement and the bit error probability performance and
this degradation can be accessed once a particular oscillator
is chosen. We will now discuss candidate oscillators for
the Shuttle GPS R/PA.

5.0 SHUTTLE GPS R/PA OSCILLATOR SURVEY

In selecting an oscillator to be used for the Shuttle GPS R/PA oscillator several requirements must be considered. These include:

(1) Fast warm up or oscillator stabilization time.

(2) Minimum power consumption.

(3) Low spectral sidelobe phase noise properties.

(4) Small size.

(5) Required short and long term stability necessary to meet system performance requirements.

(6) Minimum cost.

During the course of this contract, five potential manufacturers have been identified and information pertaining to oscillator specifications has been summarized. These include:

(1) Collins Radio/ Development for ECOM of the high stability temperature.

(2) Frequency Electronics Corporation Model FE-22-D0313 modified.

(3) Austron Model 1120.

(4) Hewlett-Packard Corporation.

(5) Bendix Corporation's development for ECOM; fast warm-up tactical miniature crystal oscillator.

Specifications from the manufacturers for the oscillators listed are summarized in Table 5-1 and Figs. 5-1 and 5-2.

Table 5-1. Potential Oscillators for Use in Shuttle
GPS R/PA.

Description	Bendix	Hewlett-Packard	Frequency Electronics
Frequency	5 or 5.115MHz	5.0 MHz	5.0 or 5.115 MHz
Stabilization Time (at 25°C)	$\pm 3.3 \times 10^{-8}$ of abs frequency after 1 min.	$\pm 2 \times 10^{-9}$ of abs frequency after 30 minutes	$\pm 2 \times 10^{-8}$ of abs frequency after 6 minutes
Short Term Stability	$\pm 1 \times 10^{-11}$ for averaging time of 1 sec to 20 min.	$\pm 1 \times 10^{-11}$ for averaging times 1 sec to 100 sec	$\pm 1 \times 10^{-10}$ for averaging times of 1 sec
Aging Rate	$\pm 2 \times 10^{-10}$/week after 30 day stabilization	$\pm 5 \times 10^{-10}$/day $\pm 1.5 \times 10^{-7}$/year	$\pm 5 \times 10^{-10}$/day after one hour
Warm-Up Power	10 watt max for 0.1 min over -40°C to 75°C	8 watts max at 25°C	5 watts peak at 25°C (2 min)
Continuous Operating Power	250 mw over -40°C to 75°C	3.5 watts at 25°C	0.4 watts at 25°C
Temperature Stability	$\pm 1 \times 10^{-8}$ over -40°C to 75°C	$\pm 5 \times 10^{-9}$ over 55°C to 71°C	$\pm 1 \times 10^{-9}$ over -20°C to 40°C
Load Stability	$\pm 1 \times 10^{-9}$ for 5% load change at 50 ohms	$\pm 2 \times 10^{-10}$ for 10% load change at 50 ohms	$\pm 2 \times 10^{-10}$ for 5% load change at 50 ohms
Voltage Stability	$\pm 1 \times 10^{-9}$ for 5% voltage change at 12 VDC	$\pm 1 \times 10^{-10}$ for 10% voltage change at 20 VDC	$\pm 2 \times 10^{-10}$ for 10% voltage change at 12 VDC
Acceleration Sensitivity	$\pm 5 \times 10^{-9}$/g along any axis	$\pm 1 \times 10^{-9}$/g along any axis	$\pm 1 \times 10^{-9}$/g along any axis
Vibration Sensitivity	$\pm 5 \times 10^{-9}$/g during vibration without vibration isolators	$\pm 1 \times 10^{-9}$/g during vibration without vibration isolators	$\pm 1 \times 10^{-9}$/g during vibration without vibration isolators
Frequency Shock Stability	$\pm 5 \times 10^{-9}$/g after 50g, 11 msec	$\pm 1 \times 10^{-9}$ after 50g, 11 msec	$\pm 1 \times 10^{-9}$ after 50g, 11 msec
Spurious Output	Down 90 dB from rated output	Down 100 dB from rated output	Down 80 dB from rated output

Table 5.1 (Continued)

Description	Manufacturer		
	Bendix	Hewlett-Packard	Frequency Electronics
Harmonic Output	Down 30 dB from rated output	Down 30 dB from rated output	Down 40 dB from rated output
Phase Noise (measured in a 1Hz Bandwidth at an offset from 5 MHz)	10 Hz,-110dB 100 Hz,-130dB 10 kHz,-140dB	10 Hz,-120dB 100 Hz,-135dB 1 kHz,-145dB 10 kHz,-145dB	2 Hz,-108dB 20 kHz,-160dB
Volume (in^3)	1.0	30	6.5
Weight (oz)	8	20	5

Table 5-1. Potential Oscillators for Use in Shuttle GPS R/PA.

Description	Manufacturer	
	Austron	Collins Radio
Frequency	5.115 MHz	5.0 MHz
Stabilization Time (at 25°C)	$\pm 2 \times 10^{-8}$ of abs frequency after 5 minutes	$\pm 1 \times 10^{-8}$ of abs frequency after 1 minute
Short Term Stability	$\pm 3 \times 10^{-11}$ for averaging time of 1 sec	$\pm 1 \times 10^{-11}$ for averaging times of 1 sec
Aging Rate	$\pm 1 \times 10^{-9}$/day after 72 hours stabilization	$\pm 2 \times 10^{-10}$/day after 30 days stabilization
Warm-Up Power	5 watts peak at 25°C	10 watts max for 0.5 min over -40°C to 80°C
Continuous Operating Power	3 watts at 25°C	150 mw over -40°C to 80°C
Temperature Stability	$\pm 2 \times 10^{-8}$ over -20°C to +55°C	$\pm 5 \times 10^{-8}$ over -40°C to 80°C
Load Stability	$\pm 5 \times 10^{-9}$ for 5% load change at 50 ohms	$\pm 5 \times 10^{-9}$ for 5% load change at 50 ohms
Voltage Stability	$\pm 5 \times 10^{-9}$ for 10% voltage change at 28 VDC	$\pm 5 \times 10^{-9}$ for 10% voltage change at 12 VDC
Acceleration Sensitivity	$\pm 5 \times 10^{-9}$/g along any axis	$\pm 5 \times 10^{-9}$/g along any axis
Vibration Sensitivity	$\pm 5 \times 10^{-9}$/g during vibration without vibration isolators	$\pm 5 \times 10^{-9}$/g during vibration without vibration isolators
Frequency Shock Stability	$\pm 1 \times 10^{-9}$ after 50g, 11 msec	$\pm 5 \times 10^{-9}$/g after 50g, 11 msec
Spurious Output	Down 80 dB from rated output	Down 100 dB from rated output
Harmonic Output	Down 30 dB from rated output	Down 30 dB from rated output

Table 5.1 (Continued)

Description	Manufacturer	
	Austron	Collins Radio
Phase Noise (measured in 1 Hz Bandwidth at an offset from 5 MHz)	10 Hz,-110 dB 20 kHz,-145 dB	10 Hz, -110 dB 20 kHz,-140 dB
Volume (in^3)	19.5	2
Weight (oz)	9	10

Figure 5-1. <u>OSCILLATOR</u>

	<u>FEI</u>	<u>XSET</u>
TYPE	CRYSTAL	CRYSTAL
FREQUENCY	5.115,10.23 MHz	5.115 MHz
WARM UP TIME	30 MIN TO $\pm1\times10^{-8}$ (SEA LEVEL)	30 MIN TO $\pm2\times10^{-9}$ (SEA LEVEL)
FREQUENCY STABILITY	3×10^{-12} FOR 1 SEC 100 SEC	$\pm2\times10^{-12}$/SEC $\pm1\times10^{-19}$/24 HRS.
WEIGHT	26 oz	20 oz
TEMPERATURE RANGE	-20^0 TO 50^0C	-20^0 TO 65^0C
SIZE	30 IN^3	32 IN^3
PEAK POWER	3 MIN @ 10 WATTS	3 MIN @ 35 WATTS
AVERAGE POWER	1 WATT	3.5 WATT
PRESSURE	0 TO 30,000 FT.	0 TO 30,000 FT.

Figure 5:2.　　OSCILLATOR CHARACTERISTICS

OSCILLATOR (FEI DEVELOPMENT MID 78)

TYPE	CRYSTAL (DOUBLE ORIENTED SC CUT)
FREQUENCY	5.115 OR 10.23 MHz
TEMPERATURE RANGE	-20°C TO 50°C
WARMUP TIME	5 MIN (LOCK RANGE $\pm 3 \times 10^{-9}$)
FREQUENCY STABILITY	1.2×10^{-12} FROM .4 TO 1000 SEC
WEIGHT	8 OZ.
SIZE	9 IN^3
PEAK POWER	10 WATTS FOR 3 MIN
AVERAGE POWER	200 MW @ 50°C

REFERENCES

[1]   Martin, Edward, "Aiding GPS Navigation Functions,"
      NAECON-76, May, 1976, Dayton, Ohio.

[2]   System Specification for the NAVSTAR Global Positioning
      System, Phase I, April, 1974.